

UNIVERSITÀ
DEGLI STUDI
DI PADOVA

UNIVERSITÀ DEGLI STUDI DI PADOVA

DIPARTIMENTO DI INGEGNERIA INDUSTRIALE DII

CORSO DI LAUREA IN INGEGNERIA AEROSPAZIALE

**Position, velocity and time measurement with
multiple constellation data from GPS, Galileo,
GLONASS and BeiDou.**

Laureando:
Giulia SCHIEVANO

Relatore:
Ch. mo Prof. Alessandro
CAPORALI

24 Febbraio 2022

Anno Accademico 2021/2022

A Davide.

Contents

1	Introduction	1
1.1	The early satellite navigation	1
1.2	Positioning systems nowadays	3
2	The constellations	5
2.1	Global Navigation Satellite Systems	6
2.1.1	GPS	7
2.1.2	GLONASS	9
2.1.3	Galileo	11
2.1.4	BeiDou	13
2.2	Regional Navigation Satellite System	14
2.2.1	QZSS	14
2.2.2	IRNSS or NAVIC	16
2.3	Satellite Based Augmentation Systems	17
3	GNSS Signals	20
3.0.1	Modulation schemes	21
3.0.2	Multiple Access Techniques employed in GNSS	22
3.1	GPS signal plan	23
3.2	GLONASS signal plan	25
3.3	Galileo signal plan	28
3.4	BeiDou signal plan	30
4	Receiver Architecture	32
4.1	RINEX Files	35
5	The positioning	37
5.1	Ranging Measurements	38
5.2	Time reference frames and clocks	39
5.3	Source of errors and error mitigation	41
5.3.1	Signal propagation in refractive and dispersive media	41
5.3.2	Other types of delays and corrections	47
5.4	Pseudorange model	50
6	Position and Velocity Estimation	52
6.1	Pseudoranges positioning	52
6.1.1	The Least squares algorithm	52

6.1.2	Kalman filter	57
6.2	Velocity estimation	59
6.3	PVTZ multiGNSS algorithm	60
7	Software architecture	63
7.1	multiGNSS_v3 Suite programs	64
7.1.1	multiGNSS_v3 function	66
7.1.2	Modified versions of the multiGNSS_v3 function	67
7.2	multiGNSSvelocity code	68
8	Experimental tests and results	71
8.1	Static positioning	71
8.2	Dynamic positioning	78
9	PNT LEO satellite	83
9.1	PNT and rendering	83
9.2	Perturbation analysis	87
10	Conclusion	93
11	Misura della posizione, velocità e sincronismo con costellazioni GPS, Galileo, GLONASS e BeiDou	94
11.1	Introduzione	94
11.2	Principi di posizionamento multiGNSS	94
11.3	Risultati e conclusioni	96
12	List of figures	98
13	Acknowledgements	103
	References	104

Abstract

This work intends to outline the theory and the methods for the computation of position, velocity and time (**PVT**) of a user on the surface of the Earth or of a LEO satellite (*Low Earth Orbit*). An integrated software written in MATLAB and PERL has been used; it processes all the signals transmitted by all the constellations visible in that precise moment and in that precise place.

The software's core uses the *Weighted Least Squares* algorithm, which permits the efficient computation of position, speed, timing and tropospheric delay in a few iterations.

In this thesis, signals from GPS, Galileo, BeiDou and GLONASS have been used, specifically for the computation of the speed, which is calculated from the Doppler Effect. These signals were detected through a receiver STONEX Cube-a S580 provided by the University of Padua.

A good precision in determination of both positioning and speed has been achieved and also the PNT of a LEO satellite (Sentinel 3A) has been determined successfully, using data also to study J_2 perturbations on the orbit.

The principal aim of this thesis is to provide an efficient and precise software able to process pseudorange and Doppler shift multi-constellation data, to enhance, in its future evolutions, the precise positioning of a receiver on Earth's surface and in orbit, with interesting applications in many different fields such as defence, transportations and automotive, attitude determination in space and many others.

Chapter 1

Introduction

A **satnav** (satellite navigation system) permits the computation of the geo-spatial position velocity and time synchronization, and possibly an estimate of the Total Electron Content and Tropospheric zenith delay using visible satellites in that moment: more precisely, a user can determine at any time and position at or near the Earth's surface its location in terms of longitude, latitude and altitude with high precision (within a few centimeters to meters) by detecting signals transmitted along a line of sight by radio from satellites. The signals are also used by the receiver to calculate the current local time with high precision, allowing time synchronization. These functions are collectively known as **Positioning, Navigation and Timing (PNT)**. [1] Ultra-precise satellite navigation relies on the same basic principle as counting the seconds after a lightning flash before the accompanying thunder is heard, in order to estimate a storm's remoteness: **a time value is converted into a reckoning of distance**. [2]

Concerning the satellites communications, the signal emitted from each satellite is a radio wave containing the time it was transmitted and the satellite's current orbital position. As signals travel at the speed of light, by calculating the signal's Time Of Flight, it is possible to derive the precise distance between the satellite and the receiver. The user's speed can be computed by deriving with respect to time by the position acquired or by using the **Doppler effect**: the relative motion between the user and the satellite generates a shift (i.e. the *Doppler Shift*), that can be detected, obtaining the user's speed. The physical model will be described in Chapter 6.2,

Nowadays the fully operational satellite navigation systems are the United States' Global Positioning System (GPS), Russia's Global Navigation Satellite System (GLONASS), China's BeiDou Navigation Satellite System (BDS) and the European Union's Galileo. Japan's Quasi-Zenith Satellite System (QZSS) is a regional system (i.e. with a limited coverage) and the Indian Regional Navigation Satellite System (IRNSS), which plans to expand to a global version in the long term.

These are generally known as **GNSS** (even though literally refers to global coverage system).

1.1 The early satellite navigation

In the past the positions of points on the Earth's surface had been determined using observations of distant objects: for example celestial navigation using observations of



Figure 1.1: Transit 2A during launch preparations

the Sun, stars, and planets. However, it was only during the **Space Race** in the Cold War that the necessary technologies were developed and enhanced to design and deploy a global system for high accuracy positioning and navigation.

Several radio systems were developed for satellite tracking and orbit determination: in the United States, these systems included radar, the Goddard Space Flight Center Range and Range Rate (GRARR) system, NASA's Minitrack system and the US Army's Sequential Collation of Range (SECOR) system that was specifically created for positioning purposes. But the most successful satellite-based positioning system was **Transit** that partially overlapped the development of GPS.

Also known as the US Navy Navigation Satellite System (NAVSAT or NNSS), Transit was the world's first satellite-based positioning system to operate globally. It evolved from the efforts to track the Soviet Union's Sputnik I, then it was deployed by the U.S. Navy to provide accurate location information to its Polaris ballistic missile submarines, and by the Navy's surface ships, as well as for hydrographic survey and geodetic surveying. The satellite units of the system (known as **OSCAR** or **NOVA**) were placed in low polar orbits, at an altitude of about 1100 km, with an orbital period of about 106 min. By measuring the Doppler frequency shift of the 20 MHz radio signals received from the satellite at a known location, the orbit of the target could be determined. And shortly thereafter, researchers realized that if the orbit of a satellite was known, then the position of a receiver could be computed from the shift. These studies led to the development of Transit, with the first experimental unit (Transit 1A) being launched in 1959.

Initially defined as "classified", the system was made available to civilians in 1967 and was widely used for navigation and precise positioning until it was shut down in 1996.

The Soviet Union developed a similar system called *Tsikada* and a special military

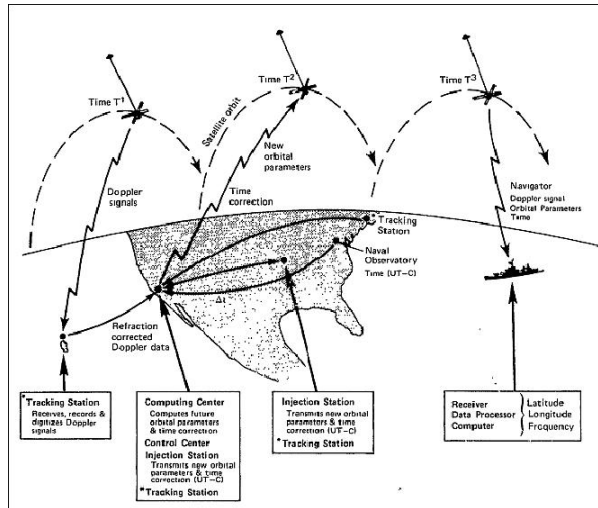


Figure 1.2: Fix with Transit's satellite passing.

version called *Parus*.

A Transit acquisition required the measurements of the satellite signal's Doppler shift for a complete pass, that could take up to about 18 min from horizon to horizon. At the conclusion of the pass, the latitude and longitude of the receiver, the position fix, could be determined. With five satellites in operation, the mean time between fixes at a mid-latitude site was around 1 h. Eventually, as the orbits of the satellites became better determined, two-dimensional position fix accuracies of several tens of meters were possible from a single satellite pass. By recording data from a number of passes over a few days from a fixed site on land, three-dimensional accuracies better than one meter were possible. The Transit satellites used signals on *two different frequencies* (150 and 400 MHz) to cancel out ionospheric delays, a concept that was later inherited by GPS and the other GNSSs. Besides its main use as a navigation system, Transit also provided early contributions to geodesy and helped to establish a new global reference frame. Transit was decommissioned at the end of 1996 with the advent of GPS and its superior performances. The equivalent Russian satellite Doppler systems have essentially been replaced by the *Global'naya Navigatsionnaya Sputnikova Sistema* (Russian Global Navigation Satellite System, GLONASS), which was the second fully operational GNSS. These new systems were based on the **concept of range measurements** rather than Doppler observations and used a different constellation design offering continuous coverage. These new concepts enabled a notable increase in accuracy as well as instantaneous positioning around the globe. [1]

1.2 Positioning systems nowadays

GPS was the first of a new generation of navigation satellite systems to become operational. The success of GPS has inspired the development of similar Global Navigation Satellite Systems (GNSS), Regional Navigation Satellite Systems (RNSS) and Space-Based Augmentation Systems (SBAS).

This increasing interest in satellite navigation and precise positioning gave rise to

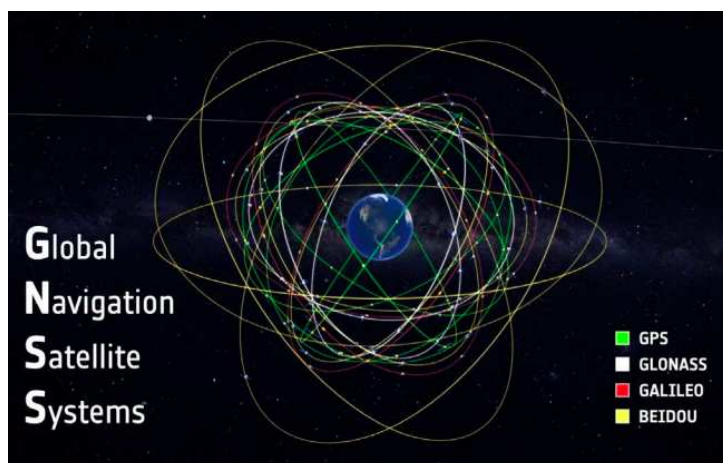


Figure 1.3: Orbits of GPS, BeiDou, GLONASS and Galileo.

more direct and more efficient solutions. Satellites broadcast a signal that contains orbital data (from which the position of the satellite can be calculated) and the precise time of transmission. Orbital data include a rough almanac for all satellites to aid in finding them, and a precise ephemeris for that specific SV. An atomic clock is used to maintain mutual synchronization in the constellation; the receiver compares the time of broadcast encoded in the transmission of four (or more) different satellites, measuring the Time Of Flight to each. Several measurements can be made at the same time to different satellites, allowing a continuous fix to be generated in real time thanks to **adapted version of trilateration algorithm**.

Global coverage for each system is generally achieved by a satellite constellation of 18–30 Medium Earth Orbit (MEO) SVs spread over several orbital planes. The actual systems use orbital inclinations of $> 50^\circ$ and orbital periods of approximately twelve hours (at an altitude of about 20'000 km). Each system's specifications and peculiarities will be better described in Chapter 2.

Chapter 2




The constellations

In this Chapter the peculiarities of satellite navigation systems are presented in terms of their system architecture with a short description of their space segment's design and the capabilities of their control segment.

Satellites constellations for the positioning and navigation services can be classified by the extension of their coverage:

1. Global Navigation Satellite Systems (GNSS): as the name says, they have global coverage; usually their orbital design consists in a certain number (≥ 24) of MEO (i.e. *Medium Earth Orbit*) satellites and (for BeiDou) in some GEO (i.e. *Geostationary orbit*) satellites and some in IGSO (i.e. *Inclined Geo-Synchronous Orbit*). GPS, Galileo, GLONASS and BeiDou are considered GNSS.
2. Regional Navigation Satellite Systems (RNSS): they cover a specific area, providing a regional service using a constellation of satellites in GEO and IGSO. These are IRNSS, which provide an independent positioning, navigation, and timing service over India and surrounding areas and QZSS, which was originally planned to enhance GPS capability and performance in the area surrounding Japan.
3. Satellite Based Augmentation Systems (SBAS): they support wide-area or regional augmentation through the use of additional satellite-broadcast messages; SBASs improve the positioning accuracy by providing corrections for the largest error sources. They are EGNOS, WAAS, MSAS, GAGAN, SDCM, BDSBAS (formerly SNAS), while others are under feasibility studies; SACCSA, Malay, African and South Korean SBAS.

A brief description of constellations' characteristics and specifications is presented in Fig. 2.1 (GNSS and RNSS) and in Fig. 2.2 (SBAS).

System						
Orbit	MEO	MEO	MEO, IGSO, GEO	MEO	IGSO, GEO	IGSO, GEO
Nominal number of satellites	24	24	27, 3, 5	30	3, 1	4, 3
Constellation	6 planes 56° inclination	Walker (24/3/1) 64.8° inclination	Walker (24/3/1) 55° inclination	Walker (24/3/1) 56° inclination	IGSOs with 43° inclination	IGSOs with 29° inclination
Services	SPS, PPS	SPS, PPS	OS, AS, WADS, SMS	OS, CS, PRS	GCS, GAS, PRS, EWS, MCS	SPS, RS
Initial service	Dec 1993	Sep 1993	Dec 2012	2016/2017 (planned)	2018 (planned)	2016 (planned)
Origin	USA	Russia	China	Europe	Japan	India
Coverage	Global	Global	Global	Global	East Asia Oceania region	-30° < φ < 50° 30° < λ < 130°
Frequency (MHz)	L1 1575.42 L2 1227.60 L5 1176.45	L1 1602.00 L2 1246.00 L3 1202.025	B1 1561.098 B2 1207.14 B3 1268.52	E1 1575.42 E5a 1176.45 E5b 1207.14 E6 1278.75	L1 1575.42 L2 1227.60 L5 1176.45 E6 1278.75	L5 1176.45 S 2492.028

SPS: Standard Positioning Service; PPS: Precise Positioning Service; OS: Open Service; AS: Authorized Service; WADS: Wide Area Differential Service; SMS: Short Message Service; CS: Commercial Service; PRS: Public Regulated Service; GCS: GPS Complementary Service; GAS: GPS Augmentation Service; EWS: Early Warning Service; MCS: Message Communications Service; PS: Precision Service; RS: Restricted Service

Figure 2.1: An overview of the Global and Regional Satellite-based Navigation Systems.






					
System	WAAS	SDCM	EGNOS	MSAS	GAGAN
Orbit	GEO	GEO	GEO	GEO	GEO
Nominal number of satellites	3	3	4	1	3
Longitudes	133° W, 107° W, 98° W	16° W, 95° E, 167° E	15.5° W, 5° E, 25° E, 31.5° E	145° E	55° E, 83° E, 93.5° E
Date of being operational	July 2003	–	October 2009	September 2007	February 2014
Origin	USA	Russia	Europe	Japan	India
Service area	CONUS, Alaska, Canada, Mexico	Russia	Europe	Japan	India
Frequency (MHz)	L1 1575.42 L5 1176.45	L1 1575.42	L1 1575.42 L5 1176.45	L1 1575.42	L1 1575.42 L5 1176.45

Figure 2.2: An overview of the Satellite Based Augmentation Systems.

2.1 Global Navigation Satellite Systems

A Global Navigation Satellite System is usually composed by three units, having different tasks and independent functions:

- Space segment: it comprises the in orbit satellite-units or satellite constellation and the uplink and downlink links.

- Control Segment: known also as ground segment, it enables management of a spacecraft, and distribution of payload data and telemetry among interested parties on the ground.
- User control segment: it consists of equipment for tracking GNSS signals and for determining position, velocity, and time.

4 GNSS CONSTELLATIONS

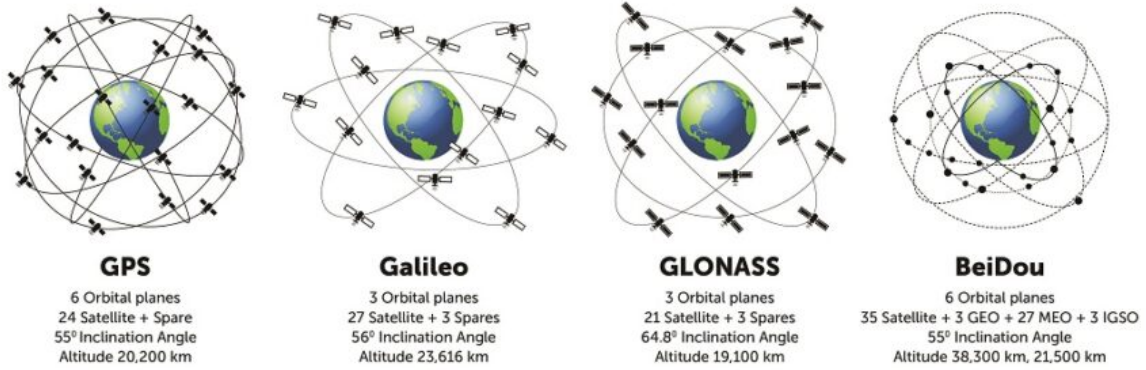


Figure 2.3: GNSS's orbital design.

2.1.1 GPS

The GPS NAVSTAR (i.e. *Global Positioning System NAVigation Satellite Time and Ranging*) was developed originally for the U.S. military in 1973 to offer accurate estimations of position, velocity and time, but an incident with the Korean Air Lines Flight 007 (that went off course into Soviet airspace and shot down by air defence, apparently due to inaccurate instrumentation) led the US Government to decide to make GPS use free for civilian purposes very early in its experimental phase. GPS is maintained by the United States government and it is freely accessible by anyone with a common GPS receiver. However, part of the very precise information, data and the full capability of the system are for military use only and for authorized users, that is the so-called *Precise Positioning Service* or PPS.

The *Standard Positioning Service* or SPS is for civil use. This double service feature is known as *Selective Availability SA*. For SPS service the accuracy achieved is around 4 m, while better GPS receivers (that use the L5 band) can have an accuracy of 30 cm, while high-end users (typically engineering and land surveying applications) are able to have accuracy within 2 cm, and even sub-millimeter accuracy for long-term measurements.

Concerning satellite communications, GPS signals are modulated on *three carriers* in L-band from a fundamental frequency $f_0 = 10.23$ MHz provided by the onboard atomic oscillator, they are:

- L1 = $f_0 \cdot 154 = 1575.42$ MHz ($\lambda = 19.05$ cm)
- L2 = $f_0 \cdot 120 = 1227.60$ MHz ($\lambda = 24.45$ cm)

- $L3 = f_0 \cdot 115 = 1176.45 \text{ MHz}$ ($\lambda = 25.50 \text{ cm}$)

a more exhaustive description, GPS signal plan is presented in Section 3.1.

[3]

Space Segment

The GPS Space Segment is defined as a constellation with satellites enough to ensure that the users will have, at least, 4 simultaneous SV-units in view from any point at the Earth surface at any time. To guarantee the availability of at least 24 satellites in operation, the Air Force has been flying around 30 GPS satellites for the past few years. The SVs in the nominal constellation are arranged into six equally-spaced orbital planes with an inclination of 55° ; each plane contains four “slots” occupied by baseline satellites.

Orbits are nearly circular (eccentricity $e < 0.02$) and the semi-major axis is $26'560 \text{ km}$, (i.e. an altitude of $20'200 \text{ km}$). The satellites have a speed of 3.9 km/s and a nominal period of $11\text{h } 58\text{min } 2\text{s}$, repeating the ground track each sidereal day.

The design of GPS satellites has evolved with time: each generation of satellites with similar characteristics is called a **Block**. A brief description of the different GPS blocks is in the Fig. 2.4. [3]

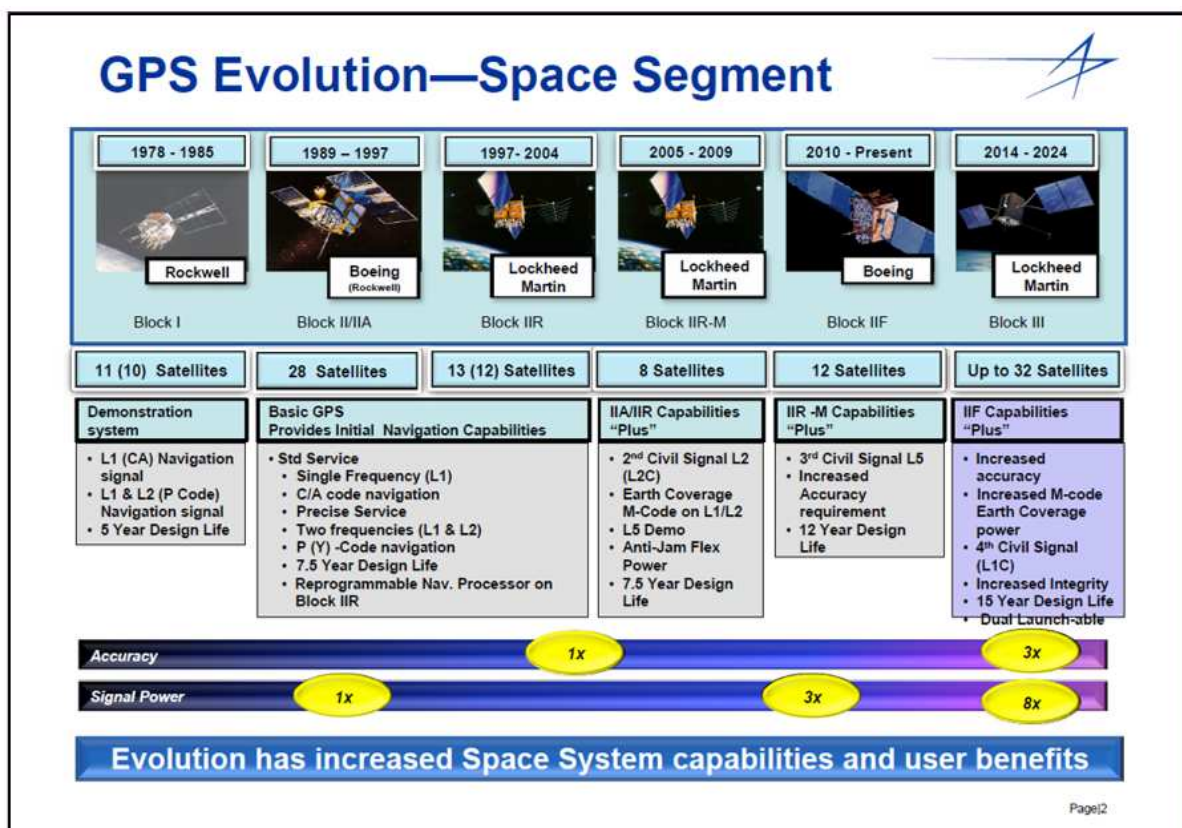


Figure 2.4: GPS evolution.

Control segment

The GPS Control Segment (shortly CS, also referred to as Ground Segment or Operational Control System) is responsible for the proper operation of the overall system. The main tasks performed by the CS are the following:

1. Monitoring and control of satellites' orbital parameters;
2. Monitoring health and status of the satellites' subsystems (solar arrays, battery power and the level of propellant used for maneuvers);
3. Activation of spare satellites;
4. Update of parameters in the navigation message (ephemeris, almanac and clock corrections);
5. Resolving satellites' anomalies;
6. Controlling Selective Availability (SA) and Anti-Spoofing (A/S)
7. Passive tracking of the satellites.

The GPS Ground Segment is composed of a network of five Monitor Stations (MS) which track the SVs, monitor their transmissions, perform analysis, and send data to the *Master Control Station* or MCS. The MCS processes and sends all the informations and commands to satellites. The CS is made up also of ground antennas which upload the clock and orbit errors, as well as the navigation data message to the GPS satellites. MSs controls all these parameters twice a day and every station can track 11 satellites at once.

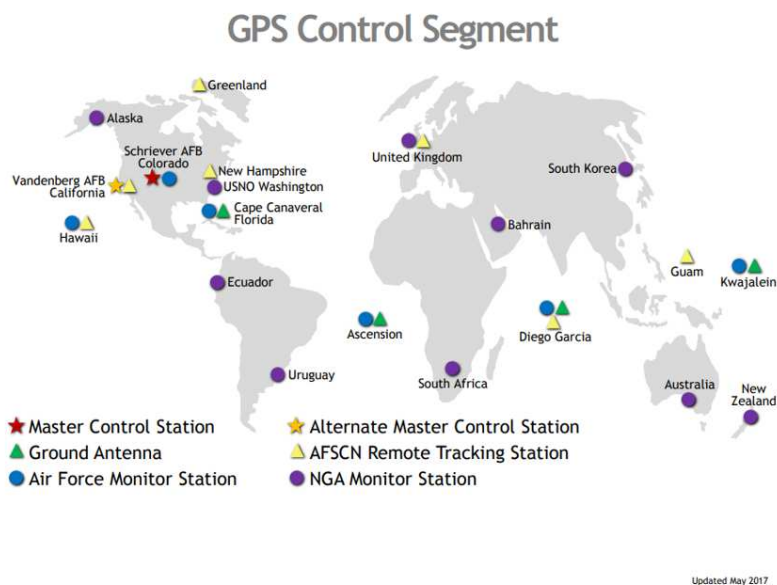


Figure 2.5: GPS Control Segment.

[4]

2.1.2 GLONASS

The *Global'naya Navigatsionnaya Sputnikova Sistema* (GLONASS) is a global navigation satellite system developed by the Russian Federation. The first spacecraft was launched

on 12 October 1982 in the Baikonur Cosmodrome in Kazakhstan (Fig. 2.6) where all the other satellites of the constellation were launched. GLONASS provides dual frequency L-band navigation signals and, as GPS, it delivers two types of services:

- An open service with unencrypted signals is available for all users without any limitations and it is transmitted on three frequency bands (L1, L2, and recently L3);
- A service for authorized users, using encrypted signals in presently two frequency bands (L1, L2).

Initiated in the 1980s, the system achieved its full capability in 1995 with 24 satellites in operation. However, because of internal economic crisis in Russia, part of the constellation was kept inoperative. The whole system was ultimately reestablished in 2011 with the support of Indian Space Agency and, since then, it has been in continuous service.

The standard-precision signal offers horizontal positioning accuracy within 5–10 m, vertical positioning within 15 m.

GLONASS has been the second global navigation satellite system to become operative, after GPS.



Figure 2.6: Soyuz launch in Baikonur Cosmodrome.

Space Segment

The GLONASS space segment consists of 24 operational satellites, evenly distributed over three orbital planes. To enhance the coverage, GLONASS adopts the so-called Walker 24/3/1 constellation geometry (this means there are 24 satellites in 3 orbital planes) with inclination $i = 64.8^\circ$. The longitude of the ascending node differs by 120° from plane to plane. There are eight satellites per plane, separated 45° in argument of latitude.

The satellites are located at 19'100 km altitude and they have a period of 11h 15min. GLONASS was designed also to ensure coverage at high latitudes (both north and south). The SVs' orbits have no resonance with Earth's rotation. The satellite's period was

selected so that satellites make 17 full orbits for eight equinoctial days (approximately eight constituent days), this means that for a stationary observer the same satellite is visible at the same point in the sky every eight sidereal days.

Control segment

The GLONASS Ground Segment is responsible for the proper operation of the GLONASS system. Like in GPS, the GLONASS Control Segment monitors the status of satellites, determines the ephemerides and satellite clock offsets and, twice a day, uploads the navigation data. The monitoring stations are in St. Petersburg, Schelkovo, Yenisseisk and Komsomolsk Na Amure.

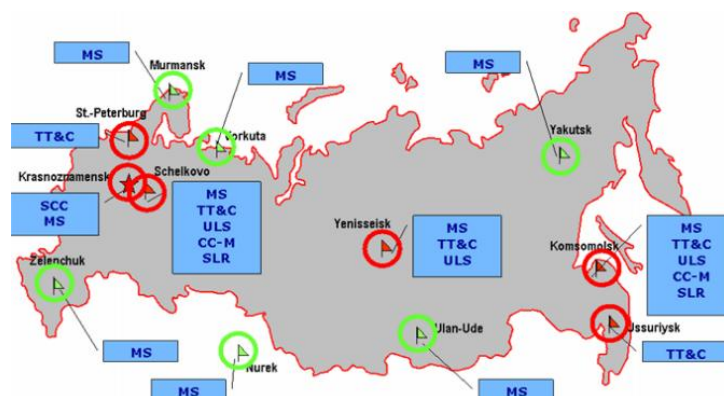


Figure 2.7: GLONASS ground segment.

[4]

2.1.3 Galileo

The European global navigation satellite system Galileo is designed as a self-standing satellite-based positioning system for worldwide service. It is completely independent from other systems, but compatible and interoperable with all of them. With the rise of Galileo, various technological innovations were introduced, such as passive maser clock technology in orbit and modernized signal concepts. Galileo provides navigation signals on three bands: E1, E6, and E5. The signals in E1 and E5 are coordinated with GPS L1 and L5, by using equivalent modulation principles. Unlike GPS and GLONASS, Galileo was designed to be entirely for civilian use, offering a greater level of service continuity. The services provided by Galileo are:

- Open Service (**OS**): with positioning accurate up to 1m, it is freely accessible;
- High Accuracy Service (**HAS**): a service complementing the OS by providing an additional navigation signal in a different frequency band. The HAS signal can be encrypted;
- Public Regulated Service (**PRS**): the Public Regulated Service is restricted to government-authorized users, for applications which require a high level of service continuity;

- Search and Rescue Service (**SAR**): Galileo’s worldwide search and rescue service will help a rescue coordination center by detecting emergency signals transmitted by beacons and relaying messages to them.

GIOVE-A (*Galileo In Orbit Validation Element*) was launched on 12 January 2006, the first operational satellite was launched on 21 October 2011.

Space segment

The Galileo constellation consists of 30 satellites, 24 operational and 6 spare, placed in MEO orbit and at 56° nominal inclination. In each of the three orbital planes, which are distributed evenly around the equator, there are 10 satellites (as GLONASS, it is a Walker 24/3/1 design). To reduce the impact of a potential failure upon the service continuity, the 6 spare satellites can replace any failed satellite within the same plane.

The orbit altitude of 23’222 km results in ground track that repeats after 10 days during which each satellite has completed 17 revolutions. The period of a Galileo satellite is 14 h 7 min. The altitude of the SVs has been selected to avoid gravitational resonances so that, after orbit kick off, during the lifetime station-keeping maneuvers will not be needed.

Control segment

The Galileo Control Segment (GCS) is responsible for a large range of functions to support the constellation control and management. These functions include control and monitoring of the satellites and payload, planning procedures that allow safe and correct operations and the support of payload related activities by Telemetry Tracking and Control (*TT&C*) stations links. The GCS provides the telemetry, telecommand and control function for the whole Galileo satellite constellation. Its elements are deployed within the Galileo Control Centres (GCC) and six globally distributed Telemetry Tracking and Control (*TT&C*) stations. The two Ground Control Centers (GCCs) are the core of the Ground Segment, they manage control functions supported by a Galileo Control Segment (GCS). There are two redundant stations located at Fucino (Italy) and Oberpfaffenhofen (Germany). The Galileo Mission Segment handles navigation system control and it consists of 20 Galileo Sensor Stations (GSS). Every ten minutes, each GSS processes data from which they compute precise orbits, clock offsets and an estimation of the prediction’s variability (i.e. *Signal In Space Accuracy, SISA*) for every satellite. Moreover the GSSs verify the integrity of the SVs and the reliability of transmitted signals.

[1] [4]

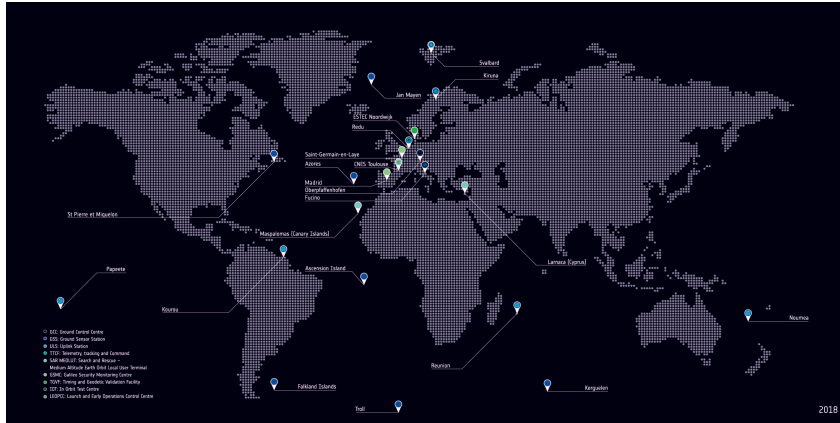


Figure 2.8: Galileo Ground Segment.

2.1.4 BeiDou

The BeiDou, also known as COMPASS, is China's second-generation satellite navigation system. It provides a continuous worldwide PVT service to users. The name Beidou comes from the Chinese word BěiDǒu (i.e. Big Dipper) that is the most important asterism historically used for orientation.

China started to develop it gradually with a three-step strategy:

- by 2000, the construction of BDS-1 was completed to provide PNT services to China;
- by 2012, the construction of BDS-2 was completed to provide PNT services to the Asia-Pacific region;
- the construction of BDS-3 was completed in 2020, with the launch of the last satellite on 23 June.

As a global system, BeiDou offers an Open Service similar to GPS and Galileo with an accuracy better than 10 m and an Authorized Service which ensures a higher reliability and precision. While as a regional service it offers wide area differential services which are foreseen to reach 1 m of position accuracy. A short message-exchange service, also called Positioning Report Service, is supported by BeiDou-1; it consists of 120 Chinese characters per message, which can be sent by the user to the station and vice versa. [5]

Space segment

The BeiDou Space Segment has a constellation of 35 satellites, which include 5 Geostationary orbit satellites, 27 in Medium Earth Orbit and 3 in Inclined Geosynchronous Orbit. The MEOs are deployed as a Walker constellation 24/3/1.

Control segment

The BeiDou Ground Segment consists of:

- Monitor Stations which collect BeiDou data from all the satellites in view from their locations;

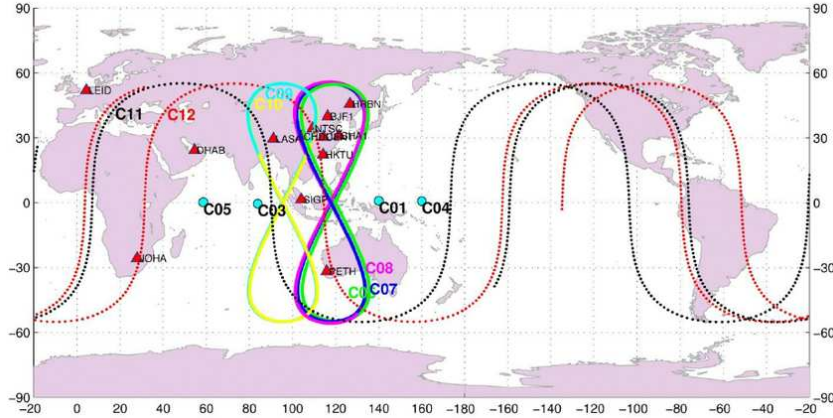


Figure 2.9: BeiDou’s satellites ground tracks.

- a Master Control Station which is responsible for satellite constellation control and processing the measurements received by the Monitor Stations to generate the navigation message;
- Upload Stations which are responsible for uploading the orbital corrections and the navigation message to all the BeiDou satellites.

Currently, the Ground Segment includes 1 Master Control Station, 2 Upload Stations and 30 Monitor Stations.

[4]

2.2 Regional Navigation Satellite System

The Regional Navigation Satellite Systems (RNSSs) aim to provide a regional service using a constellation with a lower number of satellites than other GNSSs’ space segments; this is accomplished using Geostationary Earth Orbits (GEO) and Inclined Geosynchronous Orbits (IGSO). Two regional systems implemented in Asia will be introduced in this Chapter: the Japanese QZSS and the Indian IRNSS.

2.2.1 QZSS

The Quasi-Zenith Satellite System (QZSS, also known as *Michibiki*, i.e. “Guide”) is a RNSS commissioned by the Japanese Government. It covers East Asia and Oceania region. QZSS can’t work independently: only by receiving and processing data from other GNSS satellites, it can provide PNT services. The first “Michibiki” satellite was launched on 11 September 2010, while the basic four-satellite system was announced as operational on 1 November 2018. The accuracy level depends on the type of service: the PNT service, which essentially supports GPS signals, has an accuracy <10 m; the SLAS (Sub-meter Level Augmentation), which is interoperable with other GPS-SBAS systems, reaches accuracy levels below the meter; the CLAS (Centimeter Level Augmentation), which works with Galileo E6, achieves <10 cm.

Space segment

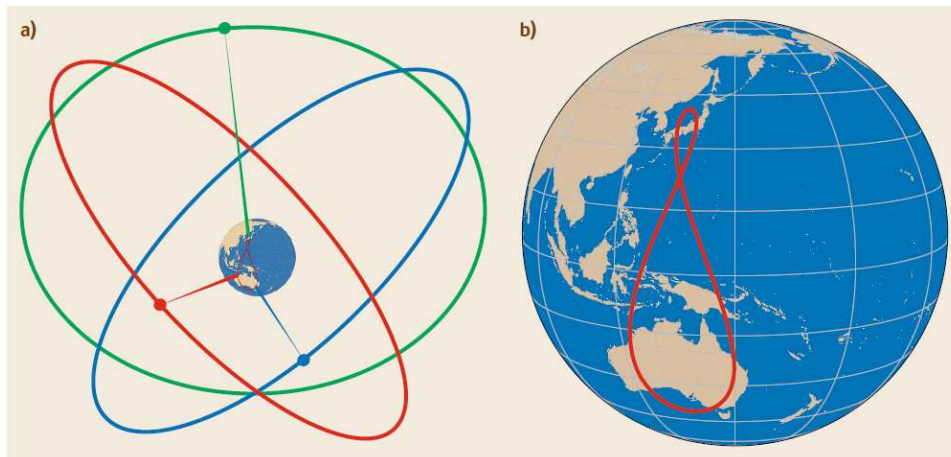


Figure 2.10: Orbit and ground track of QZSS HEO satellites.

The space segment consists of one GEO satellite and three Tundra-type satellites (i.e. a type of Highly Elliptical Orbit, HEO). The orbital planes of HEO satellites are tilted of 120° and they have an eight-shape analemma. QZSS is designed so that at least one out of three satellites is near zenith over Japan. This gave rise to the term “quasi-zenith” from which the system is named. In the Table 2.1 are summarized the most important keplerian parameters of the HE orbits.

Element	Value
Semimajor axis (a)	42164 km
Eccentricity (e)	0.075 ± 0.015
Orbital inclination (i)	$43^\circ \pm 3^\circ$
Argument of perigee (ω)	$270^\circ \pm 2^\circ$
RAAN spacing $\Delta\Omega$	120°

Table 2.1: QZSS orbital parameters of HEO satellites.

Control segment

The ground segment is composed of a master control station (MCS), tracking control stations (*TT&C*), laser ranging stations and monitoring stations. The network of monitoring stations covers East Asia and Oceania region.

[1] [4]

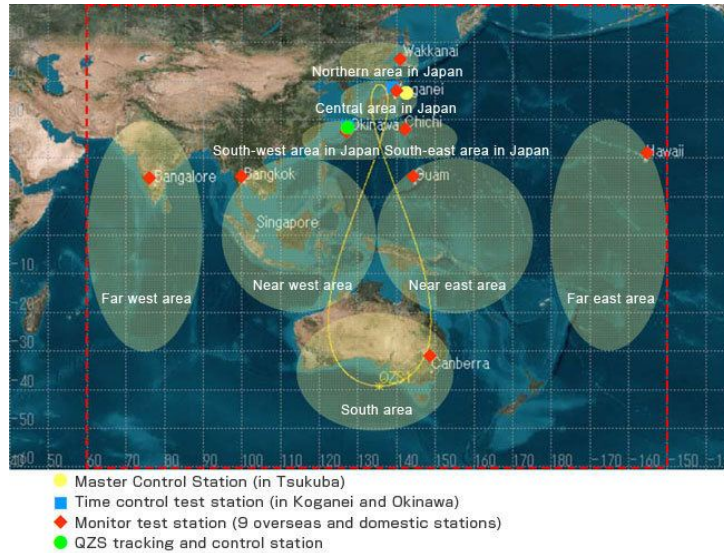


Figure 2.11: QZSS control segment.

2.2.2 IRNSS or NAVIC

The Indian Regional Navigational Satellite System (IRNSS, also known as NAVIC, i.e. Navigation Indian Constellation) is a RNSS owned by the Indian government. IRNSS can independently provide a positioning service with an accuracy of 1 m for the public service (Standard Positioning Service, SPS) and 10 cm for the encrypted one (Restricted Service, RS). Both services will be carried on L5 (1176.45 MHz) and S band (2492.028 MHz). [6]

Space segment

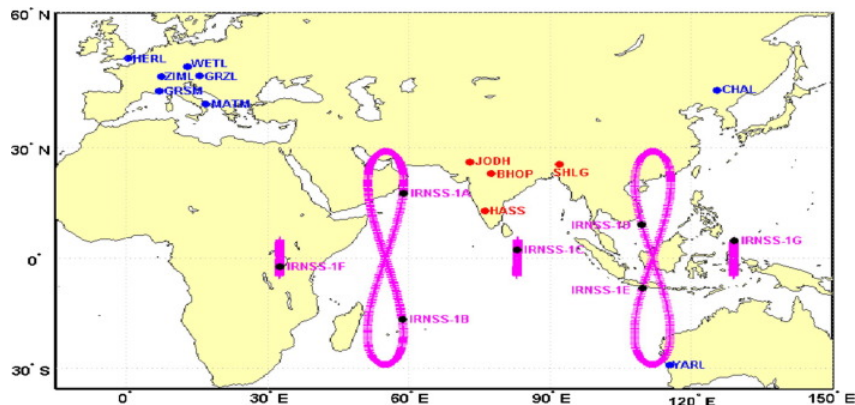


Figure 2.12: IRNSS satellites ground tracks.

ISRO (i.e. Indian Space Research Organization) has built nine satellites in the IRNSS series; of which eight are currently in orbit: 3 on GEO and 5 in GSO (i.e. *Geo Synchronous Orbit*). In Fig. 2.13 the IRNSS satellites are listed with their main specifications.

List of Navigation Satellites

	Launch Date	Launch Mass	Launch Vehicle	Orbit Type	Application	Remarks
IRNSS-1I	Apr 12, 2018	1425 kg	PSLV-C41/IRNSS-1I	GSO	Navigation	
IRNSS-1H	Aug 31, 2017		PSLV-C39/IRNSS-1H Mission		Navigation	Launch Unsuccessful
IRNSS-1G	Apr 28, 2016	1425 kg	PSLV-C33/IRNSS-1G	GEO	Navigation	
IRNSS-1F	Mar 10, 2016	1425 kg	PSLV-C32/IRNSS-1F	GEO	Navigation	
IRNSS-1E	Jan 20, 2016	1425 kg	PSLV-C31/IRNSS-1E	GSO	Navigation	
IRNSS-1D	Mar 28, 2015	1425 kg	PSLV-C27/IRNSS-1D	GSO	Navigation	
IRNSS-1C	Oct 16, 2014	1425 kg	PSLV-C26/IRNSS-1C	GEO	Navigation	
IRNSS-1B	Apr 04, 2014	1432 kg	PSLV-C24/IRNSS-1B	GSO	Navigation	
IRNSS-1A	Jul 01, 2013	1425 kg	PSLV-C22/IRNSS-1A	GSO	Navigation	

Figure 2.13: IRNSS satellites list.

Control segment

The Ground Segment is responsible for the maintenance and operation of the IRNSS constellation. The Ground segment includes:

- IRNSS Spacecraft Control Facility (IRSCF), which uplinks navigation data and is used for tracking, telemetry and command functions;
- ISRO Navigation Center (INC), which performs remote operations and data collection with all the ground stations;
- IRNSS Range and Integrity Monitoring Stations (IRIMS);
- IRNSS Network Timing Centre (IRNWT);
- IRNSS CDMA Ranging Stations (IRCDR);
- Laser Ranging Stations;
- IRNSS Data Communication Network (IRDCN).

[4]

2.3 Satellite Based Augmentation Systems

Satellite-Based Augmentation Systems (SBASs) are designed to enhance the performance of global and regional navigation satellite system (GNSS and RNSS) positioning. SBASs provide corrections for the major error sources such as clock drifts, ephemeris, or ionospheric delays. Several systems have been implemented around the world and several more are in development (Fig. 2.14). All of them have been developed using the same international standards, therefore each is interoperable with the others.

The SBAS space segment is composed of several geostationary satellites in charge of broadcasting, over the service area, the navigation message. While the main goal of

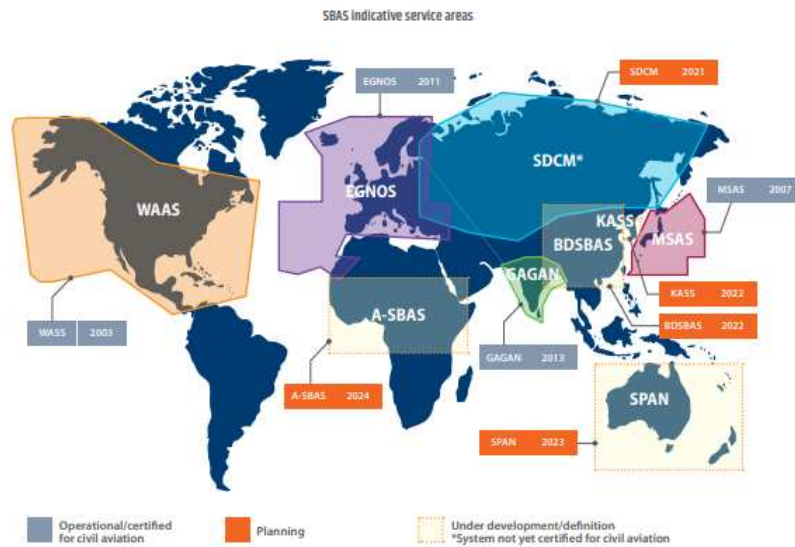


Figure 2.14: Coverage map of SBASs.

SBAS is to provide integrity assurance, it also increases the accuracy with position errors below 1 m (1σ).

In the following subsections are presented the most important SBAS and their basic characteristics.

WAAS

The *Wide Area Augmentation System* is the United States Satellite Based Augmentation System. It currently achieves coverage over North America, providing corrections to the GPS L1 signal. However, when the ionosphere is disturbed or when the constellation is weak, its availability may be reduced.

MSAS

The MTSAT (i.e. Multi-functional Transport Satellites) Satellite Augmentation System (i.e. MSAS) is the Japanese SBAS: a GPS Augmentation system which enhances its accuracy, integrity, and availability. The SBAS signal has been transmitted from the QZS-3 GEO satellite using the QZSS SBAS transmission service since April 2020.

EGNOS

European Geostationary Navigation Overlay Service (EGNOS) is the European satellite-based augmentation service. EGNOS provides the first European GNSS services to users and it, together with Galileo, is one of the major initiatives in Europe in terms of satellite navigation.

GAGAN

GPS Aided GEO Augmented Navigation is the SBAS implementation by the Indian government concurrently with IRNSS development. The space segment consists of three GEO satellites.

SDCM

System of Differential Corrections and Monitoring (SDCM) is the Russian Federation's SBAS and it is still in its development phase. SDCM further intends to augment both GPS and GLONASS. The SDCM Space Segment will be composed of 4 GEO satellites.

BDSBAS

The Republic of China is developing its own SBAS, called Satellite Navigation Augmentation System (SNAS). There is little public information available on this development. Now, the Chinese SBAS initiative refers to BeiDou Satellite-based Augmentation System (BDSBAS).

KASS

The Republic of Korea has also announced its intention to develop its own SBAS. This SBAS will consist of five or more reference stations, two central processing facilities, four GUSs (Ground Uplink Stations) and two GEOs. KASS is in the early development stage with a plan to have preliminary service by 2022.

[4] [1]

Chapter 3

GNSS Signals

In this Chapter the signal plans for each of the GNSS will be introduced and discussed.

The GNSS satellites continuously transmit navigation signals in two or more frequencies in L band. These signals contain ranging codes and navigation data to allow the users to compute the traveling time from satellite to receiver and the satellite coordinates at any epoch [4]. The timing for all components of all of the GPS navigation signals are coherently derived from an onboard frequency synthesizer driven by the active atomic clock as it will be seen on Section 5.2. The main signal components are:

- **Carrier**: Radio frequency sinusoidal signal at a given frequency.
- **Ranging code**: Binary sequences, which allow the receiver to determine the travel time of a radio signal from satellite to receiver. They are called Pseudo-Random Noise (PRN) sequences or PRN codes.
- **Navigation data**: A binary-coded message providing information on the satellite ephemeris (Keplerian elements or satellite position and velocity), satellite's clock bias parameters, almanac (with a reduced accuracy ephemeris data set), satellite health status, and other complementary information.

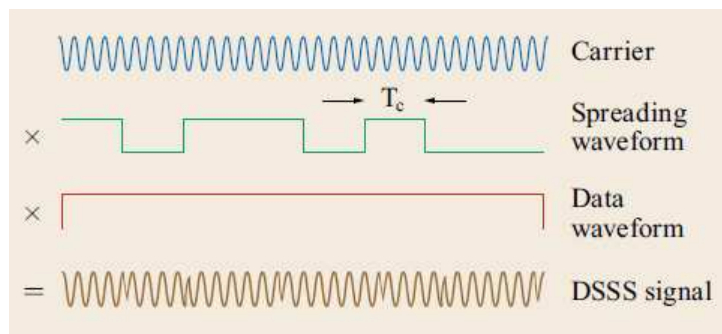


Figure 3.1: GPS signal modulation.

The code is combined with the binary navigation data using module-2 addition (i.e. if the code chip and the data bit are the same the result is 0, if the two are different the result is 1). The composite binary signal is then impressed upon the carrier (*modulation*); the two main modulations used in GNSS signals are binary phase shift keying (**BPSK**) or binary offset carrier (**BOC**). Each satellite transmits more than one code on the same band, each code can be used to accomplish a different service.

Taking as an example the GPS signals on L1 and L2, they can be modeled as:

$$\begin{aligned} s_{L1}^k &= \sqrt{2P_{C1}} \cdot x^k(t) \cdot D^k(t) \cdot \cos(2\pi f_{L1}t + \theta_{L1}) \\ &+ \sqrt{2P_{Y1}} \cdot y^k(t) \cdot D^k(t) \cdot \cos(2\pi f_{L1}t + \theta_{L1}) \\ s_{L2}^k &= \sqrt{2P_{Y2}} \cdot x^k(t) \cdot D^k(t) \cdot \cos(2\pi f_{L2}t + \theta_{L2}) \end{aligned}$$

where k is the satellite identifier, P_{C1} , P_{Y1} and P_{Y2} are the power for signals carrying the C/A-code and P(Y)-code on L1 and L2, x^k and y^k are sequences assigned at the satellite number k , D^k is the navigation data stream, f_{L1} and f_{L2} are the carrier frequencies corresponding to L1 and L2 and θ_{L1} and θ_{L2} are phase offsets.

[1] [3]

3.0.1 Modulation schemes

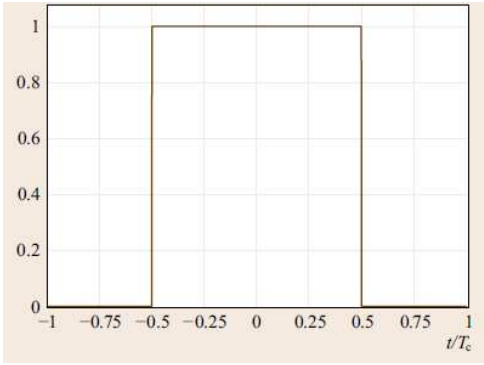


Figure 3.2: BPSK's chip shape

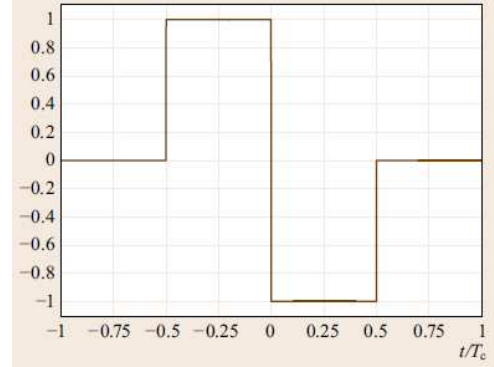


Figure 3.3: BOC(1,1)'s chip shape.

The GNSS signals, generally, use mainly two types of modulations: BPSK (Binary Phase Shift Keying) and BOC (Binary Offset Carrier Modulation). In Fig. 3.2 and 3.3 the different pulse shapes of these two types of modulations are shown..

Binary Phase Shift Keying

The Binary phase shift keying (**BPSK**) is the first modulation that had been used for Satellite Navigation. If the bit is 0 the carrier signal remains unchanged, while if it is 1 the carrier is multiplied by -1, which is equivalent to shift the phase of the sinusoidal signal by 180° , as shown in Fig. 3.4. The chip shape is rectangular as in Fig. 3.2.

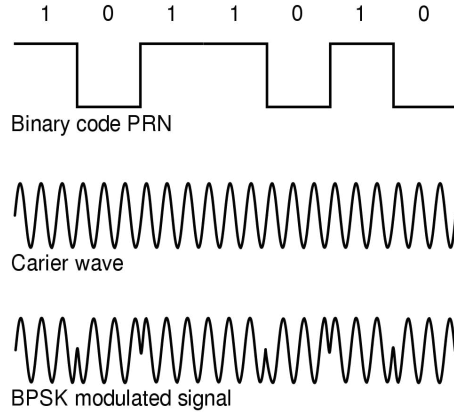


Figure 3.4: BPSK modulation.

Binary Offset Carrier Modulation

The Binary offset carrier modulation (or **BOC**) is a split-spectrum modulation scheme used by the Galileo navigation satellite system and also by GPS system and IRNSS system. BOC is a square subcarrier modulation: a signal is multiplied by a rectangular subcarrier with a frequency that is equal to or higher than the CDMA rate. Due to this subcarrier multiplication, the spectrum of the signal is divided into two parts. The purpose for using BOC modulation in Galileo is to reduce cross-interference with BPSK-modulated signals such as C/A GPS codes. BPSK signals have *sinc* function shaped spectra, with most of their spectral energy concentrated around the carrier frequency. In comparison, the BOC-modulated signals have low energy around the carrier frequency and two main spectral lobes further away from the carrier. As a result, the Galileo signals can easily coexist with GPS signals reducing the effect of interference, despite sharing the same 20MHz band centered at 1575.42MHz. [7] There are many variants of this type of modulation CBOC (composite BOC), MBOC (multiplexed BOC), TMBOC (time-multiplexed BOC) and AltBOC (Alternative BOC modulation).

3.0.2 Multiple Access Techniques employed in GNSS

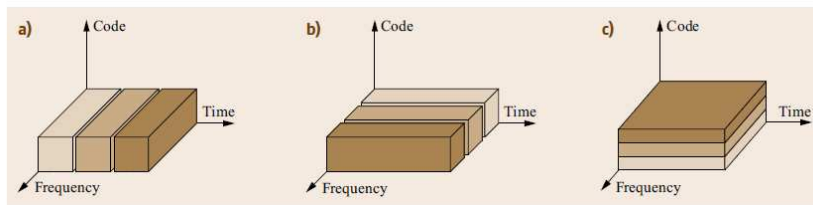


Figure 3.5: (a) Time division multiple access (TDMA), (b) frequency division multiple access (FDMA), and (c) code division multiple access (CDMA).

The satellites need to share the available bandwidth by using propagation channel access or multiple access (MA) techniques. There are three basic MA techniques:

- Code division multiple access (**CDMA**)
- Frequency division multiple access (**FDMA**)
- Time division multiple access (**TDMA**)

These three MA techniques separate signals in time, in frequency or by codes with the aim to ensure that the signals will be separated or even orthogonal. The principle of TDMA, FDMA, and CDMA is illustrated in Fig.3.5, where different shaded blocks resemble different channel users (satellites). In the case of TDMA (Fig.3.5a), channel users occupy the complete available bandwidth but at different time slots; thus, they transmit in turns in assigned time slots. In the case of FDMA (Fig.3.5b), channel users all transmit at the same time, but they occupy different sub-bands of the total available bandwidth. In the case of CDMA (Fig.3.5c), all channel users transmit at the same time and use the complete available bandwidth, but the channel users are separated by codes.

[1]

3.1 GPS signal plan

GNSS System	GPS	GPS	GPS	GPS
Service Name	C/A	L1C	P(Y) Code	M-Code
Centre Frequency	1575.42 MHz	1575.42 MHz	1575.42 MHz	1575.42 MHz
Frequency Band	L1	L1	L1	L1
Access Technique	CDMA	CDMA	CDMA	CDMA
Signal Component	Data	Data	Pilot	Data
Modulation	BPSK(1)	TMBOC(6,1,1/11)	BPSK(10)	BOC _{III} (10,5)
Sub-carrier frequency [MHz]	-	1.023 & 6.138	-	10.23
Code frequency	1.023 MHz	1.023 MHz	10.23 MHz	5.115 MHz
Primary PRN Code length	1023	10230	$6.19 \cdot 10^{12}$	N.A.
Code Family	Gold Codes	Weil Codes	Combination and short-cycling of M-sequences	N.A.
Secondary PRN Code length	-	-	1800	-
Data rate	50 bps / 50 sps	50 bps / 100 sps	-	50 bps / 50 sps
Minimum Received Power [dBW]	-158.5	-157	-161.5	N.A.
Elevation	5°	5°	5°	5°

Figure 3.6: Table of GPS signals in L1

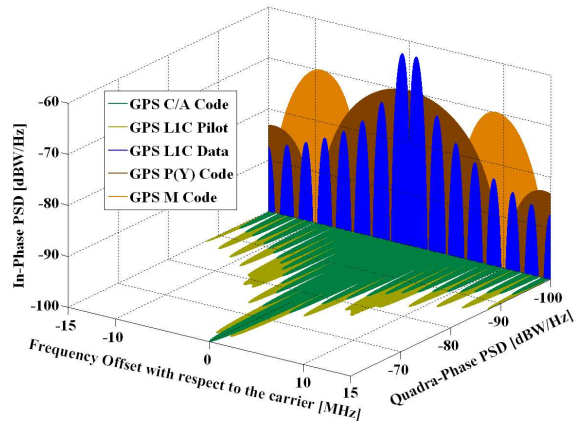


Figure 3.7: Spectra of GPS signals in L1

As it was described in the beginning of this Chapter, also GPS’s signal structure consists of a carrier, ranging code and navigation data, and it works with a CDMA strategy.

GPS’ satellites transmit signals in L1, L2 and L5, respectively on 1575.42 MHz, 1227.60 MHz and 1176.45 MHz. The legacy GPS signals includes:

- the coarse/acquisition (C/A) code signal on the L1;
- the precision (P) code signal on L1 and L2;
- the military (M) code on both L1 and the L2;
- the modernized L1C for civilian use;
- the modernized L2C (more precisely L2CM and L2CL)
- L5I and L5Q

, The C/A-code is open (unencrypted), while the P-code signal is only for authorized use and is normally encrypted. When the P-code is in this encrypted mode of operation, it is formally referred to as the Y-code. The Coarse/Acquisition (C/A) code signal was primarily thought for acquisition of the P (or Y) code, hence its name, and has become nowadays the most important signal for mass market applications.

Each C/A code is a **unique sequence of 1023 bits** repeated each millisecond, each of these bits is called *chip*. A chip duration is $1ms/1023 \approx 1\mu s$, hence chip width (in terms of distance traveled while on air) is $\lambda = c \cdot 1\mu s \approx 300m$ and the *chipping rate* is 1.023MHz. The P-code is a unique sequence of approximately 10^{14} chips that repeats after a week, the chipping rate is ten times bigger than the C/A-code (10.23 *Mcps*) and the chip width is 30m, this leads to a better precision (the smaller the λ the better is the accuracy of ranging measurement).

On L1 there are also:

- the modernized military signal (M-Code), which is designed exclusively for military use and is intended to eventually replace the P(Y) code, it provides better jamming resistance and allows much better performance than the P(Y) Code and more flexibility;
- the new L1 Civil signal (L1C) has been designed for interoperability with Galileo E1. It is compatible with current L1 signal but broadcast at a higher power level and includes advanced design for enhanced performance.

GNSS System	GPS	GPS	GPS	GPS
Service Name	L2 CM	L2 CL	P(Y) Code	M-Code
Centre Frequency	1227.60 MHz	1227.60 MHz	1227.60 MHz	1227.60 MHz
Frequency Band	L2	L2	L2	L2
Access Technique	CDMA	CDMA	CDMA	CDMA
Spreading modulation	BPSK(1) result of multiplexing 2 streams at 511.5 kHz		BPSK(10)	BOCsin(10,5)
Sub-carrier frequency	-	-	-	10.23 MHz
Code frequency	511.5 kHz	511.5 kHz	10.23 MHz	5.115 MHz
Signal Component	Data	Pilot	Data	N.A.
Primary PRN Code length	10,230 (20 ms)	767,250 (1.5 seconds)	6.19 x 1012	N.A.
Code Family	M-sequence from a maximal polynomial of degree 27		Combination and short-cycling of M-sequences	N.A.
Secondary PRN Code length	-	-	-	N.A.
Data rate	IIF 50 bps / 50 sps IIR-M Also 25 bps 50 sps with FEC	-	50 bps / 50 sps	N.A.
Minimum Received Power [dBW]	II/IIA/IIR -164.5 dBW IIR-M -161.5 dBW IIF -161.5 dBW	-	II/IIA/IIR -164.5 dBW IIR-M -161.4 dBW IIF -160.0 dBW	N.A.
Elevation	5°		5°	5°

Figure 3.8: Table of GPS signals in L2

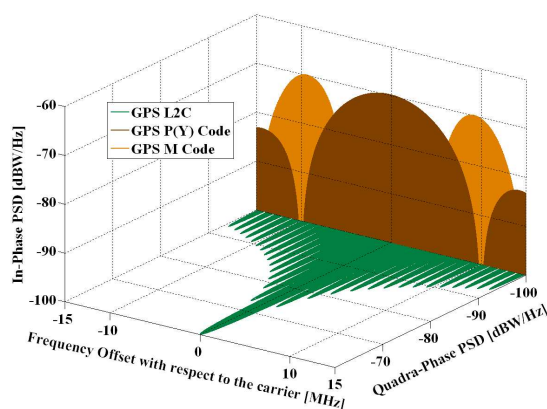


Figure 3.9: Spectra of GPS signals in L2

In the L2 band other signals are transmitted, in particular:

- L2C which is dedicated to commercial use and **enables the dual frequency solution**;

- P(Y) which has the same characteristics of the one described for L1;
- M-code which has the same characteristics of the one described for L1.

For the latest Block of GPS's satellites (Block IIR-M and IIF) there are other two new signals: L2 Civil Moderate code and L2 Civil Long code, which are time multiplexed (with a TCDMA strategy) to implement the pilot component. Two unique PRN codes per satellite are generated at $511.5kHz$ (exactly a half of $1.023MHz$ C/A-code chipping rate). The chips from the two PRN codes are alternated, that is, the first transmitted chip is from the first PRN, the second chip from the second PRN and so forth. The chips generated from the first PRN code are modulated by navigation data, and the chips generated from the second PRN code are not. The resultant signal has the same power spectrum as the C/A-code, but only half the chips in the spreading waveform are modulated by navigation data.

The L5 signal is one of the new signals belonging to the GPS modernization plan. The signal is designed to be used in combination with L1 C/A to improve accuracy (via ionospheric correction) and robustness (via signal redundancy). It is transmitted at a higher power level than current civil GPS signals, has a wider bandwidth and has lower frequency which enhances reception for indoor users.

The L5 signal consists of two carrier components that are in phase quadrature with each other (i.e. L5I and L5Q). Each carrier component is BPSK modulated by a separate bit train. One bit train is module-2 sum of the I5-code, NAV data, and synchronization sequence, while the other is the Q5-code with no NAV data (pilot), but with another synchronization sequence.

GNSS System	GPS	GPS
Service Name	L5 I	L5 Q
Centre Frequency	1176.45 MHz	1176.45 MHz
Frequency Band	L5	L5
Access Technique	CDMA	CDMA
Spreading modulation	BPSK(10)	BPSK(10)
Sub-carrier frequency	-	-
Code frequency	10.23 MHz	10.23 MHz
Signal Component	Data	Pilot
Primary PRN Code length	10230	10230
Code Family	Combination and short-cycling of M-sequences	
Secondary PRN Code length	10	20
Data rate	50 bps / 100 sps	-
Minimum Received Power [dBW]	-157.9 dBW	-157.9 dBW
Elevation	5°	5°

Figure 3.10: Table of GPS signals in L5

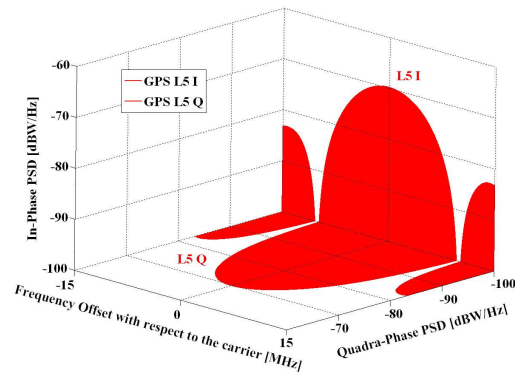


Figure 3.11: Spectra of GPS signals in L5

3.2 GLONASS signal plan

Traditionally, GLONASS makes use of frequency division multiple access (FDMA) modulation. Here, signals transmitted by individual satellites employ the same ranging code, but slightly different frequencies to allow concurrent processing in the receiver. With the first GLONASS-K1 satellite launched in 2011, GLONASS started to transmit additional

code division multiple access modulation (CDMA) signals on the new L3 signal. As part of the ongoing GLONASS modernization, CDMA signals will also be transmitted in the L1 and L2 bands to improve interoperability with other GNSSs, specifically GPS. Originally, the system transmitted the signals within two bands: L1, 1602.0–1615.5 MHz, and L2, 1246.0–1256.5 MHz, at frequencies spaced by 0.5625MHz at L1 and by 0.4375 MHz at L2. This arrangement provided 25 channels, so that each satellite in the full 24-satellite constellation could be assigned a unique frequency. The system now uses only 14 primary frequency channels with k values ranging from -7 to $+6$, including two channels for testing purposes (currently -5 and -6). To avoid interference, the same channel is used by antipodal satellites.

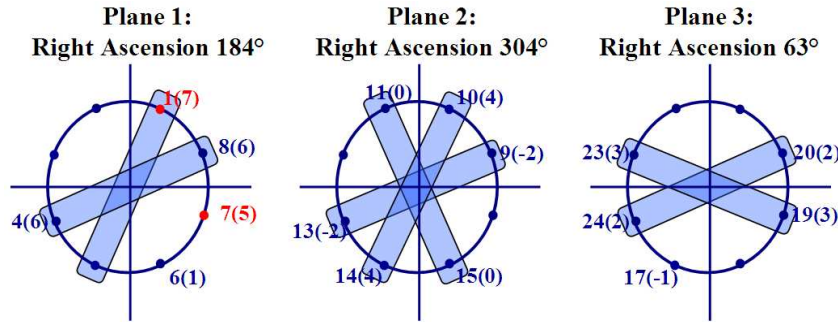


Figure 3.12: Antipodal Assignment of GLONASS Satellites. The parameter $i(k)$ indicates that the satellite in almanac slot i transmits on frequency number k (red in maintenance, blue operational satellite).

Therefore for each i satellite:

$$\begin{aligned}
 f_{i,L1} &= f_{0,L1} + k\Delta f_{L1} \\
 f_{i,L2} &= f_{0,L2} + k\Delta f_{L2} \\
 f_{i,L3} &= f_{0,L3} + k\Delta f_{L3}
 \end{aligned}
 \tag{3.1}$$

where, k is the frequency channel, $f_{0,L1} = 1602MHz$, $\Delta f_{L1} = 562.5kHz$, $f_{0,L2} = 1246MHz$, $\Delta f_{L2} = 437.5kHz$, $f_{0,L3} = 1201MHz$ and $\Delta f_{L3} = 437.5kHz$,

GLONASS signals include two pseudorandom noise (PRN) ranging codes associated with the type of service: ST (for *Standartnaya Tochnost* or Standard Precision) and VT (for *Visokaya Tochnost* or High Precision) similar to the GPS C/A- and P-codes, respectively (but at half the chipping rates), modulated onto the L1 and L2 carriers. The GLONASS ST code is 511 chips long with a rate of 511 kilochips per second, giving a repetition interval of 1 millisecond. The VT-code is 33554432 chips long with a rate of 5.11 megachips per second. The code sequence is truncated to give a repetition interval of 1 second. Unlike GPS satellites, all GLONASS satellites transmit the same codes. On L1 CDMA Open Service Navigation Signal, called L1OC, are also transmitted (on the carrier frequency $f_{L1} = 1565 \cdot f_b = 313 \cdot 5.115MHz = 1600.995MHz$, where $f_b = 1.023$) and consists of two components of the same power: L1OCd (data component) and L1OCp (pilot component). Signals transmitted on L2 have exactly the same structure of the ones transmitted on L1, the only difference is the frequency of the carrier which is in interval 1242.939375-1248.625 MHz. For a given channel number k , the ratio of the L1 and L2

GNSS System	GLONASS	GLONASS
Service Name	C/A Code	P Code
Centre Frequency	(1598.0625-1605.375) MHz \pm 0.511 MHz	
Frequency Band	L1	L1
Access Technique	FDMA	FDMA
Spreading modulation	BPSK(0.511)	BPSK(5.11)
Sub-carrier frequency	-	-
Code frequency	0.511 MHz	5.11 MHz
Signal Component	Data	Data
Primary PRN Code length	511	N/A
Code Family	M-sequences	N/A
Meander sequence	100 Hz	N/A
Data rate	50 bps	N/A
Minimum Received Power [dBW]	-161 dBW	N/A
Elevation	5°	N/A

Figure 3.13: Table of GLONASS signals in L1

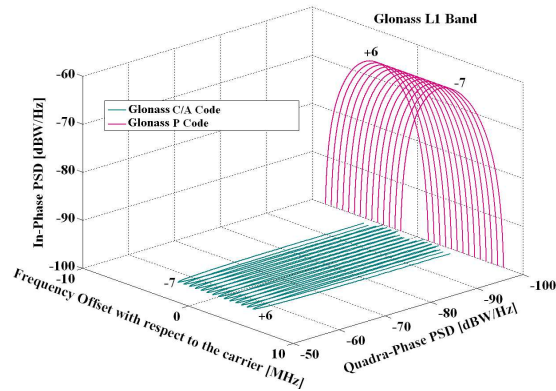


Figure 3.14: Spectra of GLONASS signals in L1

frequencies attains a fixed value of:

$$\frac{f_{L1}(k)}{f_{L2}(k)} = \frac{9}{7} \quad (3.2)$$

CDMA Open Service Navigation Signal in L2 frequency band is called L2OCp. It is transmitted on carrier frequency (nominal value) $f_{L2} = 1220 \cdot f_b = 244 \cdot 5.115 MHz = 1248.06 MHz$.

GNSS System	GLONASS	GLONASS
Service Name	C/A Code	P Code
Centre Frequency	(1242.9375...1248.625) MHz \pm 0.511 MHz	
Frequency Band	L2	L2
Access Technique	FDMA	FDMA
Spreading modulation	BPSK(0.511)	BPSK(5.11)
Sub-carrier frequency	-	-
Code frequency	0.511 MHz	5.11 MHz
Signal Component	Data	Data
Primary PRN Code length	511	N/A
Code Family	M-sequences	N/A
Meander sequence	100 Hz	N/A
Data rate	50 bps	N/A
Minimum Received Power [dBW]	-167 dBW	N/A
Elevation	5°	N/A

Figure 3.15: Table of GLONASS signals in L2

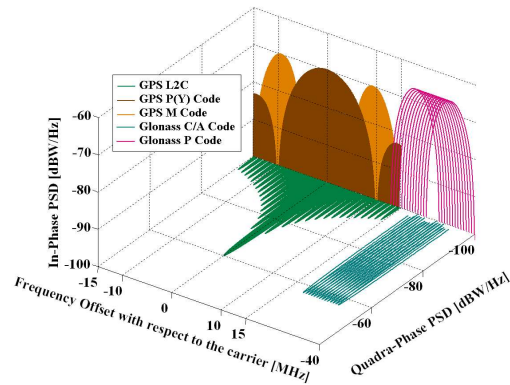


Figure 3.16: Spectra of GPS and GLONASS Signals in L2.

On L3 are transmitted only CDMA Open Service Navigation Signal, called L3OC. It is transmitted on carrier frequency (nominal value) $f_{L3} = 1175 \cdot f_b = 235 \cdot 5.115 MHz = 1202.025 MHz$ and consists of two BPSK components of the same power: L3OCd (data component) and L3OCp (pilot component). These components are in phase quadrature with each other and L3OCd is delayed 90°.

3.3 Galileo signal plan

Galileo satellites transmit permanently on 3 frequency bands: E1 at 1575.420 MHz, E5 at 1191.795 MHz and E6 at 1278.750 MHz. The E5 signal is further subdivided into signals denoted E5a (1176.450 MHz) and E5b (1207.140 MHz). Each signal contains several components, comprising always at least one pair of pilot and data components. The signals and components are assigned to three types of positioning services:

1. The Open Service (**OS**) comprising the data-pilot pairs E1-B/C, E5a-I/Q and E5b-I/Q, representing the publicly accessible positioning service
2. The Public Regulated Service (**PRS**) on E1-A and E6-A, a restricted access positioning service for government-authorized users
3. The Commercial Service (**CS**) through the datapilot pair E6-B/C, a navigation signal on a third frequency, optionally encrypted, for the provision of future added value services.

Galileo uses CBOC (Composite Binary Offset Carrier) modulation in E1, AltBOC (alternative binary offset carrier) modulation in E5 and standard BPSK modulation for E6 public service. Three different types of public navigation messages are provided through the Galileo navigation signals: the high data rate and short page length I/NAV (historically derived from Integrity NAVigation message), the low data rate F/NAV (Free NAVigation message) and the fast C/NAV Commercial channel NAVigation message.

GNSS System	Galileo	Galileo	Galileo
Service Name	E1 OS		PRS
Centre Frequency	1575.42 MHz		
Frequency Band	E1		
Access Technique	CDMA		
Spreading modulation	CBOC(6,1,1/11)		$\text{BOC}_{\cos}(15,2.5)$
Sub-carrier frequency	1.023 MHz and 6.138 (Two sub-carriers)		15.345 MHz
Code frequency	1.023 MHz		2.5575 MHz
Signal Component	Data	Pilot	Data
Primary PRN Code length	4092		N/A
Code Family	Random Codes		N/A
Secondary PRN Code length	-	25	N/A
Data rate	250 sps	-	N/A
Minimum Received Power [dBW]	-157		N/A
Elevation	10°		N/A

Figure 3.17: Table of Galileo signals in E1.

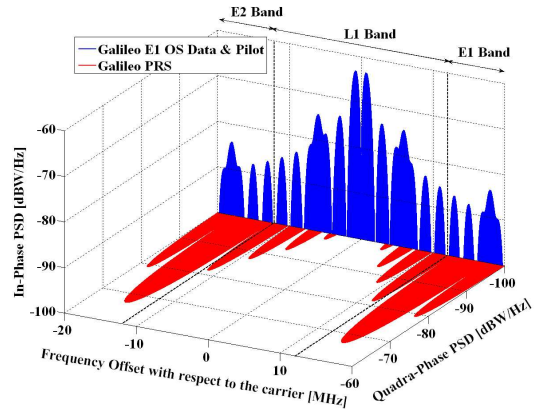


Figure 3.18: Spectra of Galileo E1.

Signals for the OS service transmitted on E1 are:

- e_{E1-B} from the I/NAV navigation data stream D_{E1-B} and ranging code C_{E1-b}
- e_{E1-C} (pilot component) from the ranging code C_{E1-C} including its secondary code

both modulated with a CBOC (Composite Binary Offset Carrier, a particular implementation of MBOC). On E1 is also transmitted E1-A for the public regulated service modulated with a $\text{BOC}_c(15,2.5)$. All the specifications are illustrated on Fig. 3.17

E6 band is on 1260-1300 MHz and two signals of commercial service are transmitted:

GNSS System	Galileo	Galileo	Galileo
Service Name	E6 CS data	E6 CS pilot	E6 PRS
Centre Frequency	1278.75 MHz		
Frequency Band	E6		
Access Technique	CDMA		
Spreading modulation	BPSK(5)	BPSK(5)	BOC _{cos} (10,5)
Sub-carrier frequency	-	-	10.23 MHz
Code frequency	5.115 MHz		
Signal Component	Data	Pilot	Data
Primary PRN Code length	5115	5115	N/A
Code Family	Memory codes		
Secondary PRN Code length	-	100	N/A
Data rate	1000 sps	-	N/A
Minimum Received Power [dBW]	-155		N/A
Elevation	10°		N/A

Figure 3.19: Table of Galileo signals in E6.

- a data component, **E6-B** modulated by C/NAV navigation data stream D_{E6-B} modulated with the encrypted ranging code C_{E6-B}
- a pilot component, **E6-C** modulated by the ranging code C_{E6-C}

E6 signals are modulated with a binary phase shift keying BPSK at a carrier frequency of 1278.75 MHz.

GNSS System	Galileo	Galileo	Galileo
Service Name	E1 OS		PRS
Centre Frequency	1575.42 MHz		
Frequency Band	E1		
Access Technique	CDMA		
Spreading modulation	CBOC(6,1,1/11)		BOC _{cos} (15,2.5)
Sub-carrier frequency	1.023 MHz and 6.138 (Two sub-carriers)		15.345 MHz
Code frequency	1.023 MHz		2.5575 MHz
Signal Component	Data	Pilot	Data
Primary PRN Code length	4092		N/A
Code Family	Random Codes		
Secondary PRN Code length	-	25	N/A
Data rate	250 sps	-	N/A
Minimum Received Power [dBW]	-157		N/A
Elevation	10°		N/A

Figure 3.21: Table of Galileo signals in E5.

The different Galileo E5 signal components are:

- eE5a-I from the F/NAV navigation data stream $DE5a-I$ modulated with the unencrypted ranging code $CE5a-I$
- eE5a-Q (pilot component) from the unencrypted ranging code $CE5a-Q$
- eE5b-I from the I/NAV navigation data stream $DE5b-I$ modulated with the unencrypted ranging code $CE5b-I$
- eE5b-Q (pilot component) from the unencrypted ranging code $CE5b-Q$

The E5 modulation is AltBOC.

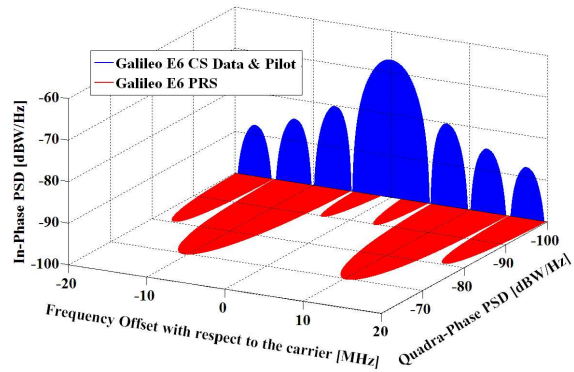


Figure 3.20: Spectra of Galileo E6.

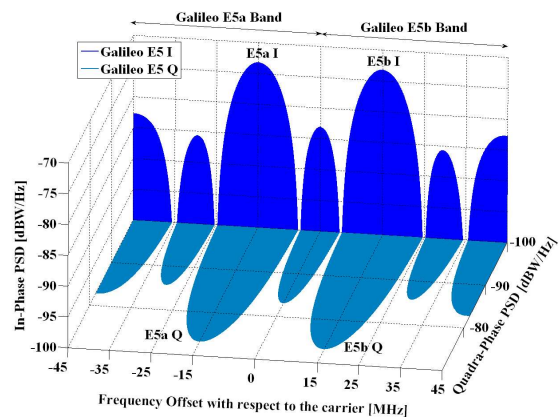


Figure 3.22: Spectra of Galileo E5.

3.4 BeiDou signal plan

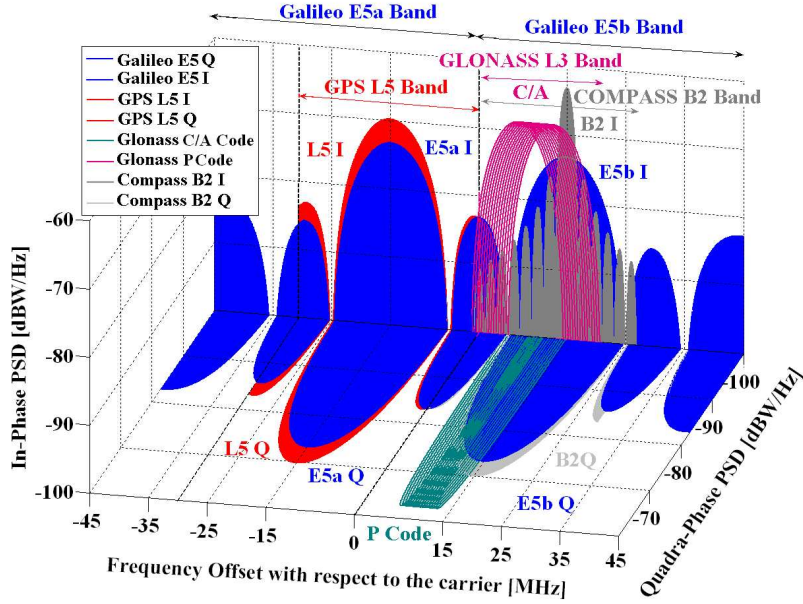


Figure 3.23: Compass (i.e. BeiDou) signal plan and compared with GPS, GLONASS and Galileo signal bands.

As seen in Section 2.1.4, operational BDS satellites are 35: 5 GEO satellites, 7 IGSO satellites and 21 MEO satellites, which can be further divided as 15 BDS-2 satellites and 18 BDS-3 satellites. The BDS-2 satellites transmit a total of six signals in three distinct frequency bands: B1 at a center frequency of 1561.098MHz, B2 at a center frequency of 1207.14MHz, and B3 at a center frequency of 1268.52MHz. The B1 and B3 frequencies are offset by about 14MHz and 10MHz, respectively, from the E1/L1 and E6 bands of Galileo/GPS, while the B2 center frequency matches that of the Galileo E5b as shown in Fig. 3.23. Each carrier frequency is modulated with two signals in phase quadrature using ranging codes of 2.046MHz or 10.23MHz chipping rate. The in-phase components of the B1 and B2 signals are assigned to open service while the remaining four signals are reserved for the authorized service. The open service is specified to offer signal-in-space range errors (SISREs) of better than 2.5m and a horizontal and vertical positioning accuracy of better than 10m at a 95% confidence level within the BDS-2 service area. BDS-3 provides an open service and an authorized service in four frequency bands, including B1, B2 and B3 with center frequencies (different from the ones transmitted by BDS-2 legacy) of 1575.42MHz, 1191.795MHz, and 1268.52MHz. On B1 there are four signals transmitted (on 2 different carriers and from different generations of satellites):

- B1I is an open service transmitted on 1561.098 MHz, with a BPSK modulation.
- B1Q is an authorized service transmitted on 1561.098 MHz, with a BPSK modulation.
- B1C is an open service and it utilizes a MBOC(6,1,1/11) multiplexed binary offset carrier modulation. It consists of two components, namely the B1-CD data channel

and the B1-CP pilot channel, which are transmitted in phase quadrature. It is transmitted by BDS-3 satellites (in particular MEO satellites and the IGSO) on carrier frequency 1575.42 MHz.

- B1A is an authorized signal and employs a BOC(14,2) binary offset carrier modulation and as B1C, is transmitted by BDS-3 satellite on 1575.42 MHz.

On B2 there are:

- B2I transmitted by all BDS-2 satellites on 1207.14 MHz, it is an open service and modulated with a BPSK strategy, it is similar to B1I.
- B2Q as B2I is transmitted on 1207.14 MHz, it is an authorized service.
- B2a is another open signal modulated with an AltBOC(15,10) strategy and it has a center frequency of 1176.45 MHz. B2a consists of a data channel (B2a-D) and a pilot channel (B2a-P) in phase quadrature.
- B2b is transmitted on 1207.14 MHz with an AltBOC(15,10) modulation, it is an open service.

In the B3-band, two authorized signals (B3 and B3- A) with a total of four individual components are transmitted at a common center frequency of 1268.52MHz. The B3I and B3Q signals are modulated in quadrature phase shift keying (QPSK) with a 10.23Mchips/s PRN code and a 500 bps binary navigation data stream. The B3-A signal is modulated in BOC(15,2.5) and consists of two components, B3-AD and B3-AP, in phase quadrature.

[4]

Chapter 4

Receiver Architecture

To obtain the PVT of the user, Signals In Space (SIS) must be processed with a GNSS receiver. This is a device necessary to extract the information from the satellites' broadcasted signals and to demodulate the data message from them. A receiver requires a specific design to fulfill this task. First, an antenna is needed to capture the GNSS signal; then a front-end down-converts, filters, amplifies and digitizes the incoming signals; a local oscillator, and a signal processing phase (or baseband processing) that firstly searches for the presence of these radio signals (acquisition) and, then synchronize with them, and finally decodes the navigation message (tracking).

The **antenna** must be able to receive GNSS signals (that are typically Right-Hand Circularly Polarized, RHCP) in L-band. Antenna design takes into account some basic requirements, for example: gain in relation to azimuth and elevation; multipath and interference rejection and size, shape with respect to environmental constraints. Generally they don't need any electrical power to operate, thus they are referred to as passive antennas.

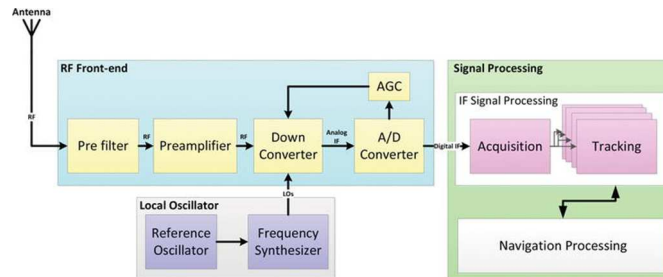


Figure 4.1: GNSS Receiver architecture scheme.

The **preamplifier** is the first active component that comes after the antenna. It is often housed in the same enclosure as the antenna element. Because the antenna can receive multiple frequency bands, typically, there is one preamplifier per band; nonetheless, a single preamplifier may cover multiple bands. The preamplifier amplifies the signal at the antenna's output and generally has three distinct components:

- a **preselector filter** that removes out-of-band interference and limits the noise bandwidth,
- **burnout protection** that prevents possible high-power interference with the electronic components of the receiver,

- a **low-noise amplifier (LNA)**.

GNSS signals are typically around -160 dBW or 10^{-6} W; thus, a LNA is needed to amplify the signals to make them suitable for processing. Usually a LNA increases signals by 20 to 35 dB.

At this point the received signal must be sampled and cleaned before the signal processing phase. The **RF front end** has this task: it amplifies, down-converts, and digitizes the signal.

Filtering is crucial for several reasons: it rejects out-of-band signals, reduces noise in the received signal, and lessens the impact of aliasing. Wide bandwidth signals can provide high-resolution measurements in the time domain, but demand higher sampling rates, causing the receiver to consume much more power. A filter can mitigate this by allowing narrower band signals.

Down-conversion is the process performed by the front end to lower the RF signal frequency to either an intermediate frequency or directly to baseband. This is necessary to facilitate the sampling and filtering processes. The down conversion is often done using a mixer which multiplies the received signal by a locally generated replica and, then filters the output signal to remove double-frequency terms. The filtering and down conversion of the signal frequencies are typically achieved in multiple, consecutive, stages due to the difficulty in implementing a stable bandpass filter with a high central frequency.

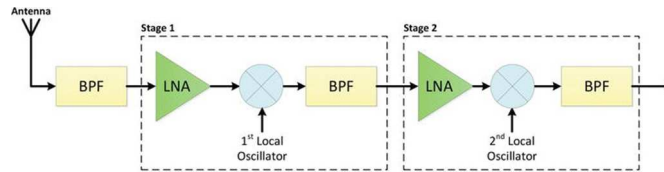


Figure 4.2: Down conversion scheme.

The last stage in the processing of the signal inside the RF front end is the conversion of the analogue signal to a digital signal. The bandpass sampling completes both discretization and down conversion of the signal. Receivers make their measurements using the estimates of the signal Time Of Arrival (TOA) and received carrier phase and frequency. A single local reference oscillator (see Figure 4.2) forms all frequency references in the receiver. Because the oscillator is critical to receiver performance, particular attention needs to be given to its size, power consumption, stability (both short and long terms), and its temperature and vibration sensitivity. In some cases, receivers have multiple frequency references for down conversion. In these instances, each mixer requires a precise reference frequency. The process of producing reference frequencies in the receiver from the local oscillator is called frequency synthesis, which uses a combination of integer and fractional frequency multiplications. At this point, the conditioned signal is ready to be processed; the baseband processing block is responsible for providing the observables (code pseudo-ranges and carrier phase measurements, as well as navigation data) using several channels that process a given signal.

Now the acquisition process starts, its goal is to provide an estimate of code delay and Doppler frequency. It is based on several correlations between the incoming signal and multiple replicas of the possible “expected” signals, generated for different code delays and Doppler frequencies. In fact, because the signal is originated by moving satellites,

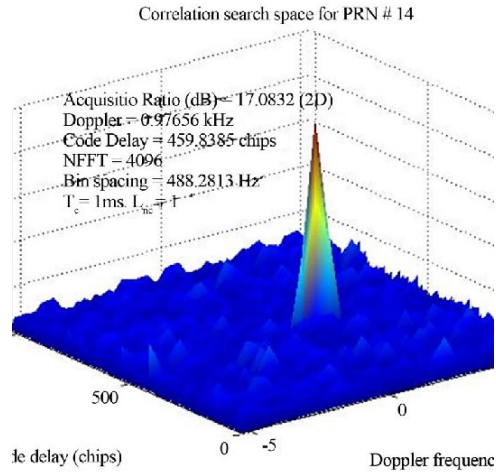


Figure 4.3: Acquisition; this image shows the Doppler / code delay search space and correlation peak.

there is a Doppler and code delay effect observed in the received signals. To search for the signals, different local replicas (corresponding to different code delay / Doppler frequency pairs) are generated and correlated with the input signals. When the local replica and the incoming signal are aligned, their correlation generates a peak (see Fig. 4.3), and the code delay / Doppler frequency pair corresponding to this peak is assumed to be a good estimate to initialize the tracking process.

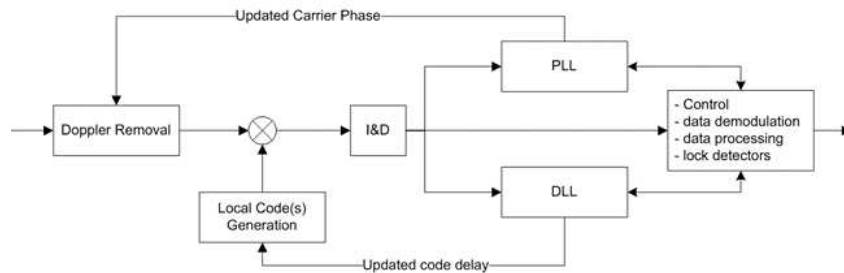


Figure 4.4: Generic diagram of a single channel in the Baseband Processing block.

During the tracking, the incoming signal is first stripped of its Doppler frequency (according to the current estimation), and then correlated with one (or more) PRN code replicas generated locally (according to the current estimation of code delay). Then new estimations of the Doppler frequency and code delay are computed based on the assessment of the correlation outputs. This process is implemented in an iterative way, usually using PLL (phase lock loop) and DLL (delay lock loop) tracking loops to track the incoming signal's phase and code delay, respectively. In parallel, the receiver extracts the navigation data of the incoming signal, and ensures monitoring and control.

The basic principle of GNSS baseband processing relies on the correlation process. The underlying idea is that GNSS signals convey ranging codes that are built in a way that:

- when the code is correlated with an aligned replica of itself, the correlation output is maximum: high auto-correlation properties,

- when the code is correlated with a non-aligned replica of itself, the correlation output is low,
- when the code is correlated with another code of the same family, the correlation output is low: low cross-correlation properties.

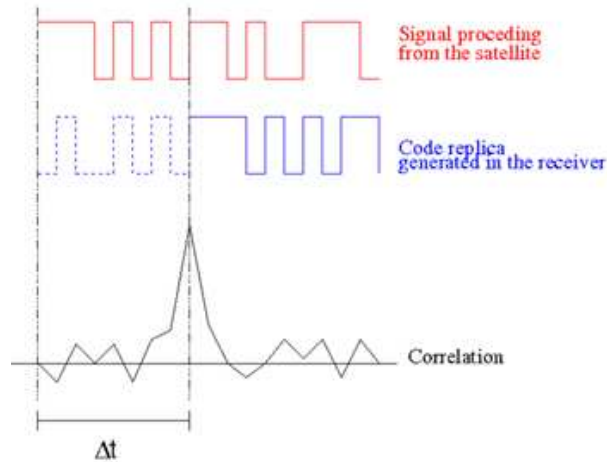


Figure 4.5: The correlation process: the receiver shifts the code replica (by changing Δt) until it finds a peak in the correlation output.

The receiver first assigns each channel with a PRN code: for GNSS based on CDMA (such as GPS and Galileo), each satellite transmits a dedicated PRN code on the same carrier, whereas for GNSS based on FDMA (such as GLONASS), the PRN code is the same for all satellites, but modulated on different carriers. At channel level, the incoming signal is correlated with the local replica of this PRN code over time. This local replica is generated in such a way that its code delay and phase characteristics vary, representing a two-dimensional search over code and (Doppler) frequency. Whenever the local replica parameters (code and frequency) match those of the incoming signal, the correlation output will reach a maximum, and the receiver will consider this pair (code and frequency) as the current estimates for these parameters. [8]

4.1 RINEX Files

The Receiver Independent Exchange Format (RINEX) is a data interchange format for raw satellite navigation system data [9]. It contains information and data of a series of measurements from one or more satellite constellations, called observables, which are usually: pseudoranges, Doppler shifts, carrier-phases and the observation time. At the present time three major format versions have been developed:

- RINEX Version 1 presented at and accepted in 1989,
- RINEX Version 2 presented at and accepted in 1990, mainly adding the possibility to include tracking data from different satellite systems (GLONASS, SBAS),
- RINEX Version 3, currently the most used.

From RINEX version 2.11 it is possible to store pseudorange, carrier-phase and Doppler measurements from GPS, GLONASS and augmentation systems like EGNOS

and WAAS in the same file. With the development of new global navigation satellite systems like Galileo and BEIDOU, it became clear that a new standard, which will fully integrate all the satellite systems, is needed. With this purpose RINEX Version 3 has been developed. The most recent version is RINEX 4.00 from December 2021. The RINEX format covers three different ASCII files:

- Observation files,
- Navigation files,
- Meteorological file.

Each file contains a header session and a data session. The header is placed at the beginning of the file and contains information about the station that collects the data and global information applicable to the entire file. Each observation file and meteorological file contains data from one site and one session, while the navigation RINEX file contains the navigation message broadcasted by the satellites. As such, receivers monitoring the same satellite will receive the same navigation messages.

Since RINEX formats are based on ASCII files that can get quite large (for instance a mixed RINEX observation file, with records every second, can reach sizes in the order of 300MB), a dedicated compress/decompress algorithm was developed by Yuki Hatanaka. The Hatanaka compression scheme is commonly used to reduce the size of RINEX files, resulting in an ASCII-based CompactRINEX or CRINEX format.

```

3.04 OBSERVATION DATA M (MIXED) RINEX VERSION / TYPE
Assistant 1.0 StaticToRinex 20211007 152244 LCL PGM / RUN BY / DATE
G = GPS R = GLONASS C = BDS COMMENT
S = SBAS J = QZSS E = GALILEO COMMENT
I = IRNSS COMMENT
0000 MARKER NAME
1360879072 MARKER NUMBER
MARKER TYPE
OBSERVER / AGENCY
5580662100058 GEOELECTRONIC 1.0.2021-04-13- REC # / TYPE / VERS
0 ANT # / TYPE
3006904.3530 639252.0229 5569759.7827 APPROX POSITION XYZ
0.0000 0.0000 0.0000 ANTENNA: DELTA H/E/N
G 12 CLC L1C D1C S1C C2M L2M D2M S2M C2L L2L D2L S2L SYS / # / OBS TYPES
R 8 CLC L1C D1C S1C C2C L2C D2C S2C SYS / # / OBS TYPES
C 8 C2I L2I D2I S2I C7I L7I D7I S7I SYS / # / OBS TYPES
E 8 CLC L1C D1C S1C C7Q L7Q D7Q S7Q SYS / # / OBS TYPES
DBHZ SIGNAL STRENGTH UNIT
1.000 INTERVAL
2021 10 07 12 24 32.0970000 GPS TIME OF FIRST OBS
2021 10 07 13 20 14.0940000 GPS TIME OF LAST OBS
0 RCV CLOCK OFFS APPL
G LIC 0.00000 SYS / PHASE SHIFT
G L2M 0.00000 SYS / PHASE SHIFT
C L2L -0.25000 SYS / PHASE SHIFT
R LIC 0.00000 SYS / PHASE SHIFT
R L2C 0.00000 SYS / PHASE SHIFT
C L2I 0.00000 SYS / PHASE SHIFT
C L7I 0.00000 SYS / PHASE SHIFT
E LIC 0.50000 SYS / PHASE SHIFT
E L7Q -0.25000 SYS / PHASE SHIFT
18 GLONASS COD/PHS/BIS LEAP SECONDS
*** Above antenna height is from mark to PHASE CENTER. COMMENT
0 0 0.0000 ANT MEASURE TYPE/HEIGHT COMMENT
0.0000 0.0000 0.0000 0.0000 0.0000 COMMENT
ROVER STATION COMMENT
2 0 END OF HEADER
> 2021 10 07 12 24 32.0970000 0 10 0.0000000000000
G02 23187226.856 121849699.270 5 1665.900 35.000
G03 21670628.109 113878918.673 5 -3615.645 34.000
G06 20081781.339 105530473.111 6 -301.276 40.000
G09 19454309.056 102233083.950 7 -179.740 43.000
G11 22014576.722 115687380.369 5 1849.945 34.000

```

Figure 4.6: Screenshot of a RINEX Obs 3.04.

[9] [10]

Chapter 5

The positioning

The idea of the positioning technique used by GNSSs systems consists in **pseudo-range multilateration**.

Let's start with the simplest case of trilateration (or more precisely true-range trilateration, i.e. defined with correct distances from known references): it is a geometrical problem that consists in determining an unknown position on a 2D plane using the distances from two or more known reference points. In two-dimensional geometry, if a point lies on the intersection of three circles, then the circles's centers and the three radii provide sufficient information to compute the position (Fig. 11.1). While in three-dimensional space, the radii and coordinates' centers of three intersecting spheres are needed to place the unknown point (the intersections are two points, but one can be easily dismissed, because it lies far out in space); however, unless the centers lie on a straight line, a fourth sphere's radius and its center's coordinates are required to estimate also the the time synchronization of the onboard clock, as shown in Fig. 11.2.

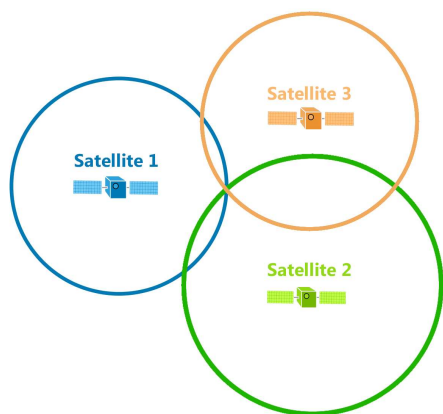


Figure 5.1: Bidimensional positioning.

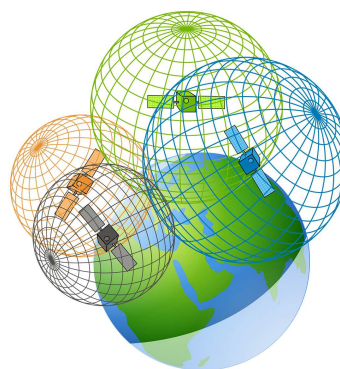


Figure 5.2: Tridimensional positioning.

In the satellite navigation case, each distance measurement from a SV places the receiver on a spherical shell. By taking several of such measurements and then looking where they meet, a fix is generated. These measurements are known as pseudo-ranges, and they are “pseudo” because the raw distance's estimations contain some errors and delays (as it will be described in Section 5.3).

The fix is calculated from the ranges using iterative algorithms of *Weighted Least*

Squares or *Kalman filtering* as it will be seen in Chapter 6.

5.1 Ranging Measurements

There are three types of measurements done by the receiver during the signal acquisition: **the arrival time** τ , **the Doppler shift** f_d and, if the ultimate precision is desired, **the carrier phase offset** $\delta\theta$. In the PNT the key measurement that leads to the estimation of the position is τ : as long as GNSS signals are electromagnetic waves traveling at the speed of light, knowing the time of arrival and the time of transmission, the distance between the receiver and the satellite (i.e. **pseudorange**) can be obtained. These signals have frequencies in L-band, more precisely between 1.2 and 1.6 GHz, an interval that allows measurements with affordable and compact instrumentations and they are not affected severely by degradation due to the atmospheric environment. Usually, GNSSs transmit in more than one frequency, as it will be explained on Section 5.3.1, to compensate the effect of ionospheric delay, (concept inherited by Transit design).

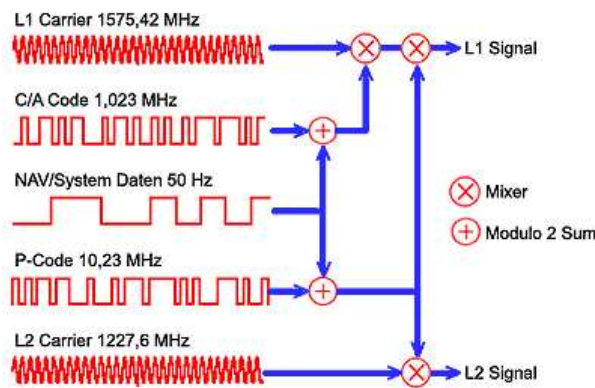


Figure 5.3: GPS signal modulation with two frequencies.

The informations carried by the signals are extracted from the receiver thanks to the tracking loop (i.e. **DLL** or Delay Lock Loop, see Chapter 4), which compares and aligns the local copy of the PRN sequence (*pseudo-random noise*, that is used by the receiver to identify a SV from its signal) to the one received. The receiver continuously measures the instantaneous code phase, the transmission time and the signal propagation time, and, upon multiplication by the speed of light c , the distance between the user and the satellite.

To reach a good fix of the position, the time offset of the satellite's clock must be also estimated: satellites are equipped with highly stable onboard clocks (rubidium or cesium atomic frequency standards or also hydrogen masers, as in Fig. 5.5), whose time offsets can be accurately predicted. All the parameters and the model (usually polynomial) to compute the satellite's clock bias are provided in the navigation message. [1]

5.2 Time reference frames and clocks

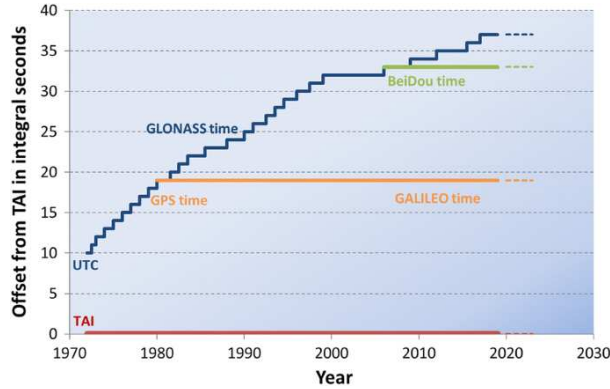


Figure 5.4: Different times references.

As long as the Global Navigation Satellites Systems must provide an optimal accuracy and precision, the time reference frames have become more and more uniform and well-defined. In the past, the Earth rotation was used as a time reference, generating the well known Universal Time (UT) and Greenwich Sidereal Time (GST). However, the motion of Earth is irregular, it is drifting periodically and secularly due to the distribution of its mass, thus, the Atomic Time (AT) was introduced to provide a more stable and accurate time reference. UT diverges from AT along the time, for this reason UTC was defined. UTC is an atomic time that keeps itself within 0.9 s from UT, thanks to the introduction of the **leap seconds**.

GNSS System Time

As long as the measurements of distance are derived from a measurement of time, the time reference must be well defined to ensure a good position fix. Thus, all satellite navigation systems rely on very accurate clocks and time standards. To suit the needs of internal time synchronization, each GNSS maintains a specific system time. The time systems of the four global navigation satellite systems, GPS, GLONASS, Galileo, and BeiDou are realized by using different clock technologies and have different t_0 and offsets with respect to Atomic Time.

GPS time (GPST) is determined from atomic clocks within the GPS Control Segment as well as the atomic frequency oscillators onboard the GPS satellites. GPS time deviates from UTC by at most 1s. However, GPS time is not adjusted by leap seconds and, thus, it is permanently late by a constant amount from AT: $t(GPS) = AT - 19s$.

GLONASS Time (GLST) is always 3h ahead of UTC because of the time zone difference between Greenwich and Moscow. Thus, $t(GLONASS) = UTC + 3h$; GLST is obtained from hydrogen-masers in the GLONASS ground segment and synchronized to UTC using two-way time transfer with a specified tolerance of 1s.

Both the Galileo and BeiDou System Times show a constant offset from the Atomic Time. The origin for Galileo time is defined to be identical to that of GPS Time, but the origin for the BeiDou time system has been chosen as January 1.0, 2006 UTC. Thus, $t(Galileo) = AT - 19s$ and $t(BeiDou) = AT - 33s$. Similar to Galileo, continuous

time scales with a fixed $-19s$ offset from AT are also adopted by the Japanese Quasi-Zenith Satellite System (QZSS) and the Indian Regional Satellite Navigation System (IRNSS/NAVIC).

Clocks

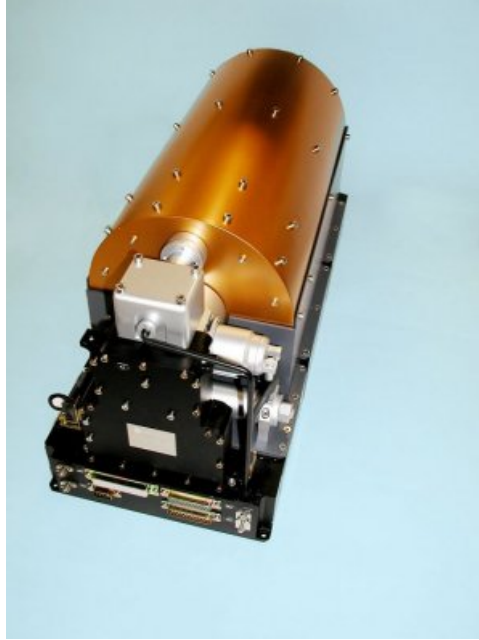


Figure 5.5: Passive Hydrogen Maser Clock; navigation satellites have extremely precise atomic clocks on board. Atomic clocks use the oscillations of a particular atom as their “metronome”, while receiver’s clocks are small quartz oscillators.

GNSS receivers usually use Quartz Crystal Oscillators as clocks, which are based on properties of piezoelectric materials which can produce electrical signals by mechanical deformation; thus, if it is linked to an electronic circuit, it is possible to create an electrical signal with a precise frequency by using the mechanical resonance. While an atomic clock, that is used onboard of navigation satellites, is based on the interaction of electromagnetic radiation with the excited states of certain atoms (i.e. cesium and rubidium). As onboard clocks, hydrogen masers, in Fig. 5.5, are also used, they are the most stable frequency standards commercially available for use in laboratory and ground station environments. A maser (Microwave Amplification by Stimulated Emission of Radiation) produces coherent electromagnetic waves through amplification by stimulated emission.

Both receiver’s clock and onboard clock are not perfect, hence a model to estimate the time’s offset is needed to have a correct estimation of the *time of flight* of the signal.

The onboard clock offset can be calculated thanks to a polynomial model, whose coefficients are broadcasted by the satellite in the navigation message; the model is quadratic:

$$\Delta t = a_0 + a_1(t - Toc) + a_2(t - Toc)^2 - 2\frac{\mathbf{r} \cdot \mathbf{v}}{c^2} \quad (5.1)$$

where Toc is the *Time of Clock* and it is the reference time (written in the navigation message), a_0 (called *clock offset*), a_1 (called *clock drift*) and a_2 (called *clock jerk*) are

the polynomial's coefficient and $\frac{r \cdot v}{c^2}$ is the relativistic correction (it is explained better in Section 5.3.2). These coefficients (Toc , a_0 , a_1 and a_2) are updated every 1-2 hours (depending on the system's ephemeris's update).

The receiver's clock bias affects the computation of the position significantly, but unfortunately it is unknown. Thus, this offset is estimated with the position thanks to the least squares algorithm: using this method (described in Section 6.1.1), it is possible to approximate iteratively the three coordinates that determine the position and the receiver's clock bias; if the number of measurements (provided by satellites in sight) is $n \geq 4$; the more are the measurements the more are the unknown that can be estimated. [1] [4]

5.3 Source of errors and error mitigation

In this Section are illustrated the most significant sources of error in ranging positioning; the first type of delays is due to the atmosphere in particular ionosphere and troposphere, while the in the second group are listed all the others (which can lead back to noises, instrumentations or second-tier phenomena as relativity). In the Table 5.1 are listed all the sources of errors and their potential error size.

Error type	Potential error size	Residual error after mitigation
ECEF rotation	20-30 m	0
Ionospheric delay	2-10 m in zenith direction	Single frequency 50-70% of iono delay* Dual frequency 0 m**
Tropospheric delay	2.3-2.5m in zenith direction	0.1-1 m
Multipath	0.5-1m	Depending on antenna's design and enviroment
Relativity	overall ≈ 1 m	≈ 0 m
Instrumental delays	<1 m	<1 cm
Receiver noise	0.25-0.5 m	Mitigation through receiver's design

Table 5.1: Table of GNSS errors and delays and their potential size (* depending on ionospheric correction model used, ** iono-free combination reduces up to 99.9% of iono delay). [3] [1]

5.3.1 Signal propagation in refractive and dispersive media

GNSS signals are affected by the medium through which they propagate: they travel with a speed equal to $c = 299792458$ m/s for almost all their journey, then in the last 1000 km (which corresponds to the final 5% of distance traveled) they encounter the atmosphere. In particular the **ionosphere** is a layer of the atmosphere in which solar radiations ionize gasses, hence the signals have to travel through a electrically charged environment; then

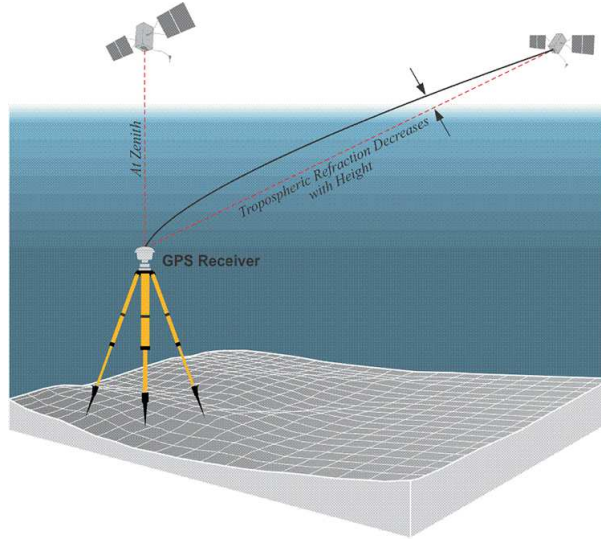


Figure 5.6: Difference of path due to atmosphere for GPS signal

at 40 km the signals encounter **troposphere** which is neutral, but contain a variable rate of vapor and humidity, which can change the index of refraction of the medium.

As shown in Fig. 5.6, the refraction changes the path of the signal and the speed of propagation, hence this alterations lead to a different time of travel and an apparently bigger range; the refractive index of the atmosphere is not uniform, thus the signal travels on a curved path (**Snell's law**) making the path longer than the geometrical straight line. If the refractive index of a medium depends on the frequency of the signal it is called *dispersive*. Because of this ionosphere's property, GNSS signals are affected by the *code-carrier divergence*, to explain it, the concepts of *phase velocity* and *group velocity* must be introduced.

$s(x, t)$ is a monochromatic sinusoidal wave, moving in the x-direction:

$$s(x, t) = s_0 \cos(\omega t - kx + \phi_0) \quad (5.2)$$

where s_0 is the amplitude of the wave, ω is the circular frequency which is $\omega = 2\pi/T$, k is the wave number which is $k = 2\pi/\lambda$. The phase of the wave is constant if $(\omega t - kx)$ is constant, for example:

$$x = \frac{\omega}{k}t = \nu_p t \quad (5.3)$$

where $\nu_p = \lambda \cdot f = \frac{\lambda}{T} = \frac{\omega}{k}$ is the *phase velocity* of the wave. Hence, it is possible to rewrite the 5.2 as:

$$s(x, t) = s_0 \cos[\omega(t - x/\nu_p) + \phi_0] \quad (5.4)$$

The all sinusoidal pattern moves along the x-direction with speed ν_p . The wave is modulated in time, hence, as an example, with the expression of a simple AM modulation is:

$$s(t) = \cos(\omega_m t) \cos(\omega_c t) \quad (5.5)$$

where ω_c is the carrier circular frequency and ω_m is the modulation circular frequency, thus $\omega_m \ll \omega_c$. In the case of GPS $\omega_c \approx 1.5GHz$ and $\omega_m \approx 1MHz$. Thanks to trigonometric

identity, the modulated signal can be rewritten as:

$$s(t) = \frac{1}{2} [\cos(\omega_c + \omega_m)t + \cos(\omega_c - \omega_m)t]. \quad (5.6)$$

Hence, if $s(t)$ travels through a dispersive medium, each of the sinusoidal signals travels at a slightly different speed.

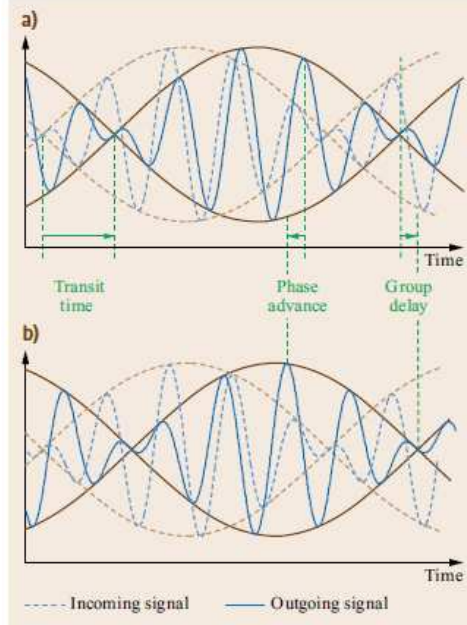


Figure 5.7: Propagation of a modulated signal in a) free space b) in a dispersive medium.

After the signal traveled a distance x in the dispersive medium:

$$s(x, t) = \frac{1}{2} [\cos((\omega_c + \omega_m)t - (k + \Delta k)x) + \cos((\omega_c - \omega_m)t - (k - \Delta k)x)] \quad (5.7)$$

And using the same trigonometric identity:

$$\begin{aligned} s(x, t) &= \cos(\omega_m t - \Delta k x) \cdot \cos(\omega_c t - k x) \\ &= \cos \omega_m \left(t - \left(\frac{\Delta k}{\omega_m} \right) x \right) \cos \omega_c \left(t - \frac{k}{\omega_c} x \right) \end{aligned} \quad (5.8)$$

As ω_m gets smaller, $\Delta k / \omega_m \rightarrow dk / d\omega$, hence:

$$s(x, t) = \cos \omega_m \left(t - \frac{dk}{d\omega} x \right) \cos \omega_c \left(t - \frac{k}{\omega_c} x \right). \quad (5.9)$$

The modulation function $\cos(\omega_m t)$ travels with a *group velocity* $\nu_g = \frac{d\omega}{dk}$. In free space $\nu_g = \nu_p$, thus the net result it's an envelope riding on top of the carrier waves, both propagating at the same speed. While in a dispersive medium, as the wave travels along, the envelope riding on them travels slower, i.e. $\nu_g < \nu_p$. This leads to a too long measurement of the code phase and a too short measurement of the carrier phase. It follows that position error occurs. [3]

Ionospheric delay

The ionosphere extends from 50 km to about 1000 km over the Earth's surface and it is composed of different layers (D, E, F1 and F2) with varying content of ions (F2 at 250-400 km has the highest electron density). However, the electron density can change substantially between day and night and also from day to day depending on solar activity.

We can define *TEC*, *Total Electron Content*, as the electron columnar number density (the number of electrons in a tube of 1 m^2 cross section extending from the receiver to the satellite), i.e.:

$$TEC = \int_{sat}^{rec} n_e(l) dl \quad (5.10)$$

where $n_e(l)$ is the electron density along the signal's path and the integral is done along the signal path from the satellite and the receiver. Since the signal's path is shorter if the satellite is on the zenith, the nearer is the satellite's elevation to 90° , the lower is the *TEC*.

The refractive index for a radio wave of frequency f is:

$$n_p \approx 1 - \frac{40.3n_e}{f^2} \quad (5.11)$$

where n_p is the phase refractive index and n_e is the electron density. From 5.11, the excess phase delay (in seconds) $\Delta\tau_p$ can be computed:

$$\begin{aligned} \Delta\tau_p &= \frac{1}{c} \int_S^R (n_p(l) - 1) dl \\ &= -\frac{1}{c} \int \frac{40.3n_e(l)}{f^2} dl \\ &= -\frac{40.3 \cdot TEC}{cf^2} \end{aligned} \quad (5.12)$$

$\Delta\tau_p < 0$, thus the phase is in advance and it is proportional to the number of the electrons in the path of the signal. It is possible to write the excess phase delay in meters:

$$I_\phi = c\Delta\tau_p = -\frac{40.3 \cdot TEC}{f^2}. \quad (5.13)$$

From the definitions of phase velocity and group velocity: $n_g = n_p + f \frac{dn_p}{df}$, hence:

$$\begin{aligned} n_g &= 1 + \frac{40.3 \cdot TEC}{f^2} \\ I_\rho &= \frac{40.3 \cdot TEC}{f^2}. \end{aligned} \quad (5.14)$$

The signal path length through the ionosphere varies with the satellite position in the sky: the lower the satellite, the longer the path length and the higher *TEC*; to characterize *TEC* along the signal path the *obliquity factor OF* is introduced:

$$I(\zeta) = I_z \cdot OF(\zeta) \quad (5.15)$$

where ζ is the zenith angle, I_z the zenith delay, $I(\zeta)$ the ionospheric delay and OF the obliquity factor. The OF can be calculated relating vertical TEC to TEC on the line of sight:

$$TEC(\zeta) = \frac{1}{\cos \zeta'} \cdot TEC_V \quad (5.16)$$

where the OF is the $1/\cos \zeta'$, see Fig. 5.9; to rewrite the obliquity factor as function of known parameters using the law of sines:

$$\frac{\sin \zeta}{R_E + h} = \frac{\sin \zeta'}{R_E} \quad (5.17)$$

hence, it becomes:

$$OF = \left[1 - \left(\frac{R_E \sin \zeta}{R_E + h} \right)^2 \right]^{-1/2} \quad (5.18)$$

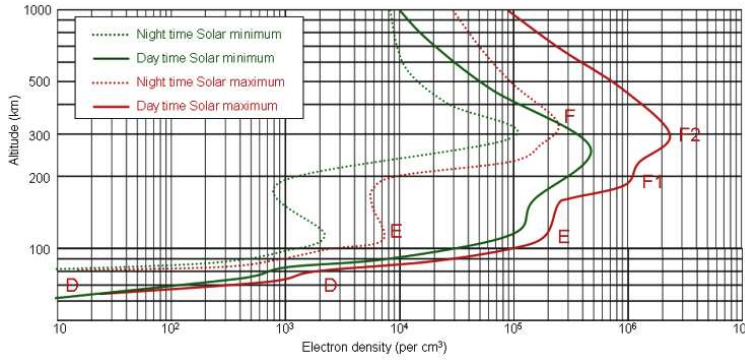


Figure 5.8: Ionospheric layers.

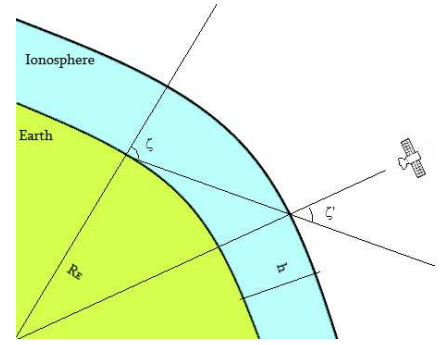


Figure 5.9: The propagation path length through ionosphere.

There are 2 different ways to face the problem of the ionospheric delay: the first one consists in applying corrections provided by an **empirical model** whose parameters are broadcasted by the satellites and it is usually employed from receivers limited to only one frequency; the second one is used if the receiver can get 2 or more frequencies and it relies on the so called **iono-free combination**.

The most used empirical models to correct the ionospheric delays are NeQuick-G (used by the Galileo system) and Klobuchar. NeQuick-G is a three-dimensional and time dependent ionospheric electron density model based on an empirical climatological representation of the ionosphere, which predicts monthly mean electron density from analytical profiles, depending on solar-activity-related input values [11]. Klobuchar is named after his contriver John A. Klobuchar, and it represents the zenith delay $I_{z,L1}$ as a constant value at nighttime and a half-cosine function in daytime:

$$\frac{I_{z,L1}}{c} = \begin{cases} A_1 + A_2 \cos \frac{2\pi(t-A_3)}{A_4} \\ A_1 \end{cases} \quad (5.19)$$

where $A_{2,4}$ are parameters listed on the navigation message, while $A_{1,3}$ are fixed.

A user equipped with a dual frequency receiver can estimate the ionospheric group delay and the phase advance and essentially delete the ionosphere as a source of error. As it will be seen in Section 5.4, the pseudorange model can be written as:

$$p_{L1}^s = \rho^s + c(dt_r - dt^s + \delta t^{rel}) + I_{L1}^s + T_{L1}^s + e_{L1}^s \quad (5.20)$$

where ρ^s is the geometric distance between the receiver and the satellite, dt_r and dt^s are the time of arrival and the time of transmission of the signal, δt^{rel} is the relativity correction, I_{L1}^s is the ionospheric correction, T_{L1}^s is the tropospheric correction and e_{L1}^s is a term containing all receiver's noises and multipath errors (see Section 5.3.2 and 5.4). It is possible to write 5.20 as a contribution of the *ionosphere-free pseudorange* p_{IF} and ionospheric delay (expression 5.14):

$$p_{L1} = p_{IF} + \frac{A}{f_{L1}^2} \quad (5.21)$$

where $A = 40.3 \cdot TEC$. Both A and p_{IF} can be estimated from dual frequency measurements, hence the ionospheric group delay becomes:

$$I_{L1} = \frac{A}{f_{L1}^2} = \frac{f_{L2}^2}{f_{L1}^2 - f_{L2}^2}(\rho_{L2} - \rho_{L1}) \quad (5.22)$$

Hence, the iono-free pseudorange is:

$$\begin{aligned} p_{IF} &= \frac{f_{L1}^2}{f_{L1}^2 - f_{L2}^2} p_{L1} - \frac{f_{L2}^2}{f_{L1}^2 - f_{L2}^2} p_{L2} \\ &= 2.546 \cdot p_{L1} - 1.546 \cdot p_{L2}. \end{aligned} \quad (5.23)$$

Thanks to this strategy the ionospheric error can be deleted, but other sources of errors (as troposphere) are not; moreover, the combination of two measurements leads to an **higher level of noise**.

[3] [12]

Tropospheric delay

The troposphere is the lowest layer of the Earth's atmosphere, it extends from the surface to more or less 18 km. In this part of the atmosphere weather phenomena take place, therefore most of the water vapor and aerosols are concentrated here, more precisely the most of water vapor is below 4 km and all of it is below about 12 km. At higher regions of the troposphere, dry gasses can be found in gradually thinning quantities. Unlike the ionosphere, the troposphere is **neutral and non-dispersive** for GNSS frequencies (hence it is not possible to cancel its effect with dual frequency measurements), but the speed of the signals crossing this medium is lower (because the refractive index is larger than 1, at the sea level $n \approx 1.0003$), hence the apparent range is longer (generally by 2.5-25 m depending upon the elevation of the satellite). This delay depends on the temperature, pressure, humidity as well as the transmitter and receiver antennas location [4]; more precisely the refractive index of a medium depends upon its density, which can be calculated as the sum of the densities of dry gasses and water vapor and these densities are function of partial pressures of the components and temperature. Dry and

wet components influence the propagation of a signal in a different way, hence they are modeled independently taking into account also the slightly different composition of the atmosphere changing with respect to time, latitude, longitude and altitude and season. [3]

A brief description on the atmosphere dry and wet component effects on the GNSS signals is given as follows:

- **Hydrostatic component delay:** it is caused by the dry gasses present at the troposphere (78% N₂, 21% O₂, 0.9% Ar ect...). Its effect varies with local temperature and atmospheric pressure in quite a predictable manner, besides its variation is less than the 1% in a few hours. The error caused by this component is about 2.3 meters in the zenith direction and 10 meters for lower elevations.
- **Wet component delay:** it is caused by the water vapour and condensed water in form of clouds and, thence, it depends on weather conditions. The excess delay is small in this case, only some tens of centimeters, but this component varies faster than the hydrostatic component and quite randomly, being very difficult to model.

The dry atmosphere can be modeled from surface pressure and temperature using the laws of the ideal gasses. The wet component is more unpredictable and difficult to model, thence for high precision navigation, this delay is estimated together with the coordinates.

The tropospheric delay depends on the signal path through the neutral atmosphere, and thence, can be modeled as a **function of the satellite elevation angle**. Due to the differences between the atmospheric profiles of the dry gasses and water vapour it is better to use different mappings for the dry and wet components.

Several nominal tropospheric models are available in the literature, which differ on the assumptions made on the vertical profiles and mappings. Basically, they can be classified in two main groups: Geodetic-oriented or Navigation-oriented. The first group Sastamoinen, Hopfield, among others are more accurate but generally more complex, and need surface meteorological data, being their accuracy affected by the quality of these data. The second group is less accurate, but meteorological data is not needed.

[13]

5.3.2 Other types of delays and corrections

In this Section other types of delays and errors are listed and explained: the relativistic effect, the multipath and the instrumental delays.

Relativistic effect

GNSS may be considered as one of the first practical applications where relativistic effects are taken into account, not just from the theoretical point of view, but as a regular engineering constraint on the overall design requirements [14]. Relativity, both general and special, show up in GNSS in two different ways:

- deviations of the satellite clock frequency (δt_{clk}^{rel}): according to the Special Theory of Relativity, a clock aboard a satellite traveling at constant speed would appear to lose time relative to a clock on the ground, while, according to the General Theory

of Relativity, a clock in a satellite would run faster than one on the ground due to the difference in gravitational potential, thus the net effect for a MEO satellite is a gain of $38.4 \mu s$ per day.

- delays affecting the signal path due to the Earth's gravitational potential (δt_{stc}^{rel}) known also as the Shapiro effect: assuming a user on the surface of the Earth, the maximum Shapiro effect is approximately $60 ps$ or $2 cm$ for medium Earth orbit (MEO) satellites for satellites on inclined geosynchronous orbits (IGSO), it is on the order of $70 ps$.

These effects caused by special and general relativity lead to a frequency offset of the onboard clock with respect to a ground-based clock. To mitigate this effect, the satellite's clock frequencies are actually offset from their nominal values. However, noncircular satellite orbits cause deviations from the mean frequency offset. The correction can be formulated using the satellite's position and velocity vector:

$$\delta t_{clk}^{rel} = -\frac{2}{c^2}(\mathbf{r}^s \cdot \mathbf{v}^s) \quad (5.24)$$

[14]

Multipath and noise

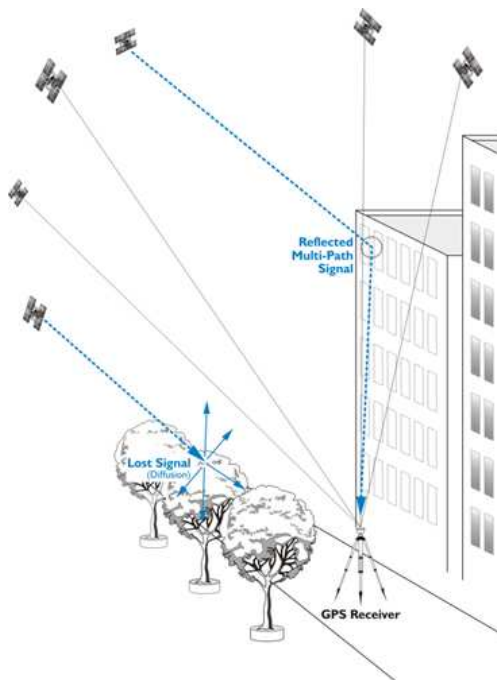


Figure 5.10: Multipath in a city.

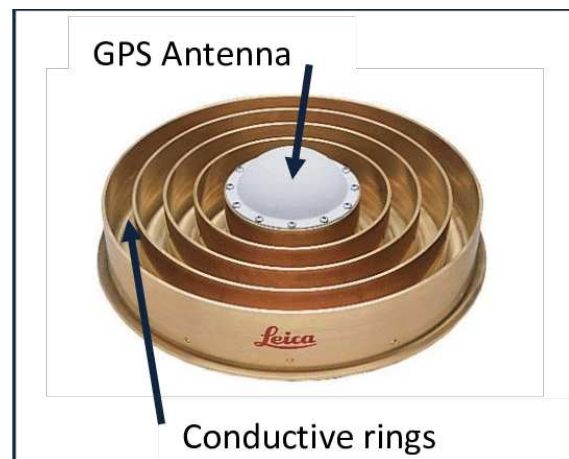


Figure 5.11: Choke ring antenna to reject multipath.

When signals reach an antenna via two or more paths the **multipath** phenomenon occurs; it is caused generally by the multiple reflection of the signal from the ground or from structures in the nearby. The reflected signal is usually weaker and delayed with respect to the direct one. A simple, but not always possible solution is to place the antenna far from every obstacle to reduce the reflection, then there are some antenna's

design that can reduce it, as the choke ring antenna (i.e. a particular form of omnidirectional antenna which consists of a number of conductive concentric cylinders around a central antenna, see Fig. 5.11).

[1]

Instrumental delays

The capability of commercial receivers to track multiple GNSSs poses the problem of mutual alignments of reference frames and time scales [15]: GNSS receivers are affected by systematic offsets related to delays in the analogue or digital part of the overall signal generation, transmission and processing chain. These instrumental delays affect both, code and carrier measurements. The receiver instrumental delay is lumped in the receiver clock. The total bias can be splitted into a receiver-dependent $d_{r,j}$ and a satellite-dependent term d_j^s (where r stands for receiver, s for satellite and j for the signal), since the receiver-dependent part is equal for all the signals received and tracked by the same receiver, while the satellite-dependent term is assumed to be equal for every receiver tracking the corresponding signal. The j identifies the frequency and signal, because the processing chains of the signals differ, thus their instrumental delays may differ. The absolute delay of a single signal is unobservable, only Differential Code Biases (**DCBs**) become observable by selecting one signal (or a combination of signals) and referencing the other signals to it. A differential code bias d_{BA}^s is defined as the difference between the absolute biases of the signals A and B $d_{BA}^s = d_A^s - d_B^s$. For each navigation system, the system time refers to a specific signal or to a signal combination, and the satellite clock correction terms refer to the deviation of the satellite clock from the system time. The absolute biases of the reference signal or combination are unobservable and lumped into the satellite clock correction terms. In the case of GPS, the ionosphere-free combination of the legacy P(Y) signals on L1 and L2 is used as a reference to compute the clock solution. If a user processes single frequency observations or a different combination of observations, the corresponding biases must be corrected for. For this purpose, each GPS satellite transmits a correction parameter, the so-called Time Group Delay **TGD**, which allows the correction of the bias between the ionosphere-free linear combination of L1/L2-P(Y) signals and the single-frequency P(Y) signals. The TGD is expressed in terms of the L1/L2 P(Y) DCB as:

$$T_{GD} = -\frac{f_{L2}^2}{f_{L1}^2 - f_{L2}^2} (d_{GC1W}^s - d_{GC2W}^s) \quad (5.25)$$

In this notation, the frequency index j has been replaced by a four-letter signal label, which consists of the three-letter receiver independent exchange (RINEX) v3 observation code preceded by a satellite system indicator, in this case G for GPS. With the help of the time group delay correction, the P(Y) single frequency observations can be aligned with the ionosphere-free clock reference. The newer generation of GPS satellites will also transmit so-called Inter-Signal Corrections (**ISCs**), which contain the necessary DCBs for single-frequency positioning with C/A, L2C, and L5 code. In addition to the TGD or ISC values provided by the navigation system itself, precise estimates of these values are also available from IGS analysis centers. The situation becomes even more complicated if observations of different navigation systems are being used. In addition to the previously

mentioned DCB corrections, which users may have to apply depending on the signal selection for processing, two different navigation systems are likely to exhibit offsets between their system timescales as well. [1]

Within the MGEX ((Multi-GNSS Experiment, i.e. broadcast ephemeris from all the constellations per day)) files, several GNSS stations make their multi-GNSS data freely available in the standard RINEX 3 format, which has been specifically designed to accommodate data from multiple GNSS constellations. An important input to the reference frame and satellite time scale issues is coming from the **IGS (International GNSS Service)** which publishes on a regular basis in the standard SP3 format the tabular ECEF (earth-centered, earth-fixed) coordinates in the IGS08/IGb08 reference frame and clock offsets of the satellites relative to a common time scale (e.g., GPS) of several, though unfortunately not all, GNSS systems. [15]

5.4 Pseudorange model

In this Section the pseudorange model is introduced, using all the concepts explained in the previous Chapters. The measured time of travel of the GNSS signal is affected by all the phenomena listed in Section 5.3. Hence let's name the time of arrival t_A and the time of transmission t_E and the signal travel time τ (that is about 70-90 *ms* depending on the position of the satellite with respect to the receiver), and it is possible to write t_A as:

$$t_A = t_E + \tau + \delta t_{stc}^{rel} + \frac{1}{c}T + \frac{1}{c}I \quad (5.26)$$

where δt_{stc}^{rel} is the relativistic correction due to the space-time curvature, T is the tropospheric correction and I is the ionospheric correction. While τ is equal to:

$$\tau = \frac{\rho_r^s + \xi_r^s}{c} \quad (5.27)$$

where ρ_r^s is the geometric range computed between the satellite center of mass of the satellite and the receiving antenna's reference point and ξ_r^s is the phase center offset of the transmitting and receiving antenna. Since the local oscillator of the receiver is not synchronized with the GNSS time, the measured arrival time \tilde{t}_A (as measured by the receiver) deviates from the true arrival time due to the receiver clock offset dt_r , instrumental delays d_r , and other errors like receiver noise and multipath e_r^s , hence:

$$\tilde{t}_A = t_A + dt_r + d_r + \frac{1}{c}e_r^s \quad (5.28)$$

The signal emitted by the satellite is affected by the clock offset of the onboard clock dt^s , the instrumental delays d^s , and the relativistic effect δt_{clk}^{rel} . Summarizing these terms leads to the following expression for the apparent emission time \tilde{t}_E :

$$\tilde{t}_E = t_E + (dt^s + \delta t_{clk}^{rel}) + d^s \quad (5.29)$$

Hence the *pseudorange* measurement is given by:

$$p_r^s = c(\tilde{t}_A - \tilde{t}_E) \quad (5.30)$$

. Substituting 5.26-5.28 into 5.30 and introducing the signal identifier j:

$$p_{r,j}^s = \rho_r^s + \xi_{r,j}^s + c(d_{r,j} - d_j^s) + c(dt_r - dt^s + \delta t^{rel}) + I_{r,j}^s + T_{r,j}^s + e_{r,j}^s \quad (5.31)$$

The ρ_r^s term must be further corrected because of the rotation of the Earth-Centered Earth-Fixed reference frame during signal propagation (the Sagnac effect): during the time of flight, the reference system rotate by a not negligible angle that is $\tau \cdot \omega_E$, where ω_E is the Earth rotation rate, thus:

$$\rho_r^s = \sqrt{[x^s(t_E) + \omega_{E\tau} \cdot y^s - x_r]^2 + [y^s(t_E) - \omega_{E\tau} \cdot x^s - y_r]^2 + [z^s(t_E) - z_r]^2} \quad (5.32)$$

that comes from the multiplication of the $\tilde{\mathbf{x}}^s$, which is the position of the satellite at the time $t_E = t_a - \tau$ in the ECEF reference frame at t_E , and the rotation matrix to transform the ECEF reference to t_E to t_A :

$$\mathbf{x}^s = \begin{bmatrix} \cos \omega_{E\tau} & \sin \omega_{E\tau} & 0 \\ -\sin \omega_{E\tau} & \cos \omega_{E\tau} & 0 \\ 0 & 0 & 1 \end{bmatrix} \tilde{\mathbf{x}}^s \approx \begin{bmatrix} x^s + \omega_E \cdot y^s \\ -\omega_E \cdot x^s + y^s \\ z^s \end{bmatrix} \quad (5.33)$$

In 70-90 ms of signal transit time, the earth rotation amounts about $7 \cdot 10^{-6}$ radians, hence it is justified the simplification: $\cos \omega_{E\tau} \approx 1$ and $\sin \omega_{E\tau} \approx \omega_{E\tau}$; this rotation may seems small, but it can introduce an error of 10-20 m. [1] [3] [16]

Chapter 6

Position and Velocity Estimation

The theory and the methods for the complete PVT fix are explained in this following Chapter.

In the first Section 6.1, the main techniques to solve the pseudoranges multilateration problem are presented. Generally two types of algorithms are used: the *Weighted Least Squares* and the *Kalman Filter*.

In the second Section 6.2 of this Chapter, the Doppler's model and the speed estimation are illustrated and in the third 6.3 a complete algorithm for the computation of both position and speed is described using a **multiGNSS strategy**, hence with data coming from all the constellation visible.

6.1 Pseudoranges positioning

In this Section the two most used algorithms to solve the multilateration problem are explained, they are:

- *Weighted Least Squares*: method for estimating the unknown parameters in a linear regression model, minimizing the measurement residuals (i.e. the difference between an observed value, and the fitted value provided by a model);
- *Kalman Filter*: in case of dynamic parameters, the Kalman filter estimates them recursively with a strategy of prediction-update.

The least squares method (in particular the Weighted Least Squares algorithm) has been used in the software's code, while Kalman filtering is presented for completeness.

6.1.1 The Least squares algorithm

The least squares method was developed and published in 1805 by Adrien-Marie Legendre, but it was attributed also to Carl Friedrich Gauss who may have previously used it in his work.

The geometrical problem consists in finding the position of a point knowing its distances from other known points in a 2D or 3D space.

In other words, the least squares algorithm estimates the solution of **overdetermined systems** by minimizing the sum of the squares of the residuals. Least squares method

can be classified in two categories depending on whether or not the residuals are linear in all the unknowns (linear or ordinary least squares and nonlinear least squares). The **linear least squares** can be analytically solved while the nonlinear problem is usually solved by iterative ways; at each iteration the system is approximated by a linear one, and thus the core calculation is similar in both cases.

LS model

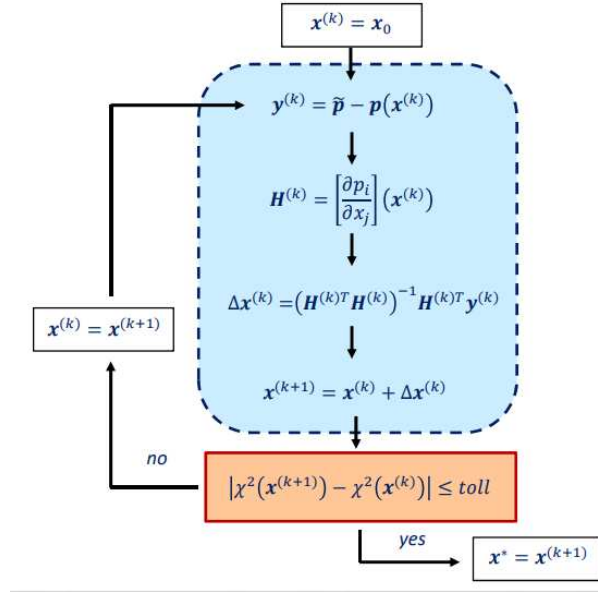


Figure 6.1: Least squares method scheme. [17]

For simplicity, the problem solved is bidimensional. First of all, the geometrical distance p_i in 2D is computed:

$$p_i = \sqrt{(x_i - x_0)^2 + (y_i - y_0)^2} + \epsilon_i \quad (6.1)$$

where x_i and y_i are the coordinates of the known points (with $i = 1 \dots n$), (x_0, y_0) are the a priori coordinates of the unknown point and ϵ_i is measurement error. The distances p_i are known from measurement campaigns, so there are n equations, one for each known point. Therefore, the solution is found by solving an algebraic, non linear and inhomogeneous, system. To solve the system, $J^2(x_0, y_0)$ has to be defined: it is a functional that consists in the sum of the squares of all the differences between the measured distances (p_i) and the calculated ones $\sqrt{(x_i - x_0)^2 + (y_i - y_0)^2}$:

$$J^2(x_0, y_0) = \sum_{i=1}^n (p_i - \sqrt{(x_i - x_0)^2 + (y_i - y_0)^2})^2 \quad (6.2)$$

Geometrically $J^2(x_0, y_0)$ is a tridimensional surface, more precisely a paraboloid. The solution of the overdetermined system coincides with the minimum of this tridimensional surface; it can be derived with respect to the couple (x_0, y_0) . If the minimum is sought in the neighbourhood of the solution couple $(\underline{x}_0, \underline{y}_0)$, the expression could be linearized;

if the distances computed with respect to (x_0, y_0) , are called ρ_i , the difference between the distances is: $\tilde{y}_i = p_i - \rho_i$. Consequently, the Taylor expansion of \tilde{y}_i is:

$$\begin{aligned} \tilde{y}_i = & \left. \frac{\partial \sqrt{(x_i - x_0)^2 + (y_i - y_0)^2}}{\partial x_0} \right|_{x_0=x_0, y_0=y_0} (x_0 - \underline{x_0}) \\ & + \left. \frac{\partial \sqrt{(x_i - x_0)^2 + (y_i - y_0)^2}}{\partial y_0} \right|_{x_0=x_0, y_0=y_0} (y_0 - \underline{y_0}) + \dots \end{aligned} \quad (6.3)$$

and then, computing the derivatives:

$$\begin{aligned} \left. \frac{\partial \sqrt{(x_i - x_0)^2 + (y_i - y_0)^2}}{\partial x_0} \right|_{x_0=x_0, y_0=y_0} &= - \frac{x_i - \underline{x_0}}{\sqrt{(x_i - \underline{x_0})^2 + (y_i - \underline{y_0})^2}} \\ \left. \frac{\partial \sqrt{(x_i - x_0)^2 + (y_i - y_0)^2}}{\partial y_0} \right|_{x_0=x_0, y_0=y_0} &= - \frac{y_i - \underline{y_0}}{\sqrt{(x_i - \underline{x_0})^2 + (y_i - \underline{y_0})^2}}. \end{aligned} \quad (6.4)$$

These terms are the **versors** defining the directions of each distance between the known points and the (x_0, y_0) , hence it is possible to factor out this terms in a matrix (**H matrix of partial derivatives**) and write:

$$\tilde{y} = H \Delta x + \epsilon \quad (6.5)$$

where H is:

$$H = \begin{bmatrix} -\frac{x_{P1}-x_0}{\rho_{P1}} & -\frac{y_{P1}-y_0}{\rho_{P1}} \\ -\frac{x_{P2}-x_0}{\rho_{P2}} & -\frac{y_{P2}-y_0}{\rho_{P2}} \\ -\frac{x_{P3}-x_0}{\rho_{P3}} & -\frac{y_{P3}-y_0}{\rho_{P3}} \\ \dots & \dots \\ -\frac{x_{Pn}-x_0}{\rho_{Pn}} & -\frac{y_{Pn}-y_0}{\rho_{Pn}} \end{bmatrix}, \quad (6.6)$$

where (x_{P_i}, y_{P_i}) are the known points' coordinates.

The functional $J^2(\Delta x)$:

$$\begin{aligned} J^2(\Delta x) &= [\tilde{y} - H \Delta x]^T [\tilde{y} - H \Delta x] = \\ & \tilde{y}^T \tilde{y} - \tilde{y}^T H \Delta x - \Delta x^T H^T \tilde{y} + \Delta x^T H^T H \Delta x. \end{aligned} \quad (6.7)$$

It is important to notice that J^2 is a scalar. The Δx that minimizes J^2 is found putting the derivative of J^2 with respect to Δx equal to zero:

$$H^T H \Delta x = H^T \tilde{y} \quad (6.8)$$

Assuming that $H^T H$ is invertible:

$$\Delta x = [H^T H]^{-1} H^T \tilde{y} \quad (6.9)$$

$H^T H$ is invertible if the observations are linearly independent, that means the known points must be spreaded around the unknown point evenly and not distributed in a line.

The Δx found is the vector that has to be summed to the a-priori coordinates (x_0, y_0) to update them in the position of iteration 1 (x_1, y_1) . The next iteration, the coordinates computed (x_1, y_1) become the new a-priori coordinate to be updated (x_0, y_0) . The algorithm could take time to converge, but generally in 3, 4 iterations a good precision is achieved; anyway it is possible also to stop the algorithm checking the norm of the residuals: if the norm of the residuals is below a certain threshold, a possible solution has been reached.

By definition, the covariance matrix is:

$$\Delta x \Delta x^T = [H^T H]^{-1} \tilde{y}^T \tilde{y}, \quad (6.10)$$

from this matrix, it is possible to get some important information.

$\tilde{y} \tilde{y}^T$ is the covariance matrix of post-fit residuals:

$$\tilde{y} \tilde{y}^T = I \sigma_y^2 \quad (6.11)$$

it is diagonal and contains measurements' variances (thus is $n \times n$).

$H^T H$ is representative of the distributions of the known points in the plane (i.e. of the satellites' distribution in the sky), the more they are spread evenly around the unknown point, the more the determinant of $H^T H$ is far from zero.

[16]

Weighted Least Squares application

In GNSS a position in a tridimensional space must be found, hence all the formulas in the previous paragraph have to be re-written adding a dimension, for example the 6.1 become:

$$p_i = \sqrt{(x_i - x_0)^2 + (y_i - y_0)^2 + (z_i - z_0)^2} + \epsilon_i \quad (6.12)$$

Moreover, in the pseudorange problem, the receiver's clock bias is unknown too, thus an additional unknown must be estimated in the algorithm; for this reason the matrix H is $n \times 4$, where n is the number of measurements (in view satellites) and 4 equals to 3 spatial coordinates plus one temporal (if the data are from 1 constellation only):

$$H = \begin{bmatrix} -\frac{x_{S1}-x_0}{\rho_{S1}} & -\frac{y_{S1}-y_0}{\rho_{S1}} & -\frac{z_{S1}-z_0}{\rho_{S1}} & 1 \\ -\frac{x_{S2}-x_0}{\rho_{S2}} & -\frac{y_{S2}-y_0}{\rho_{S2}} & -\frac{z_{S2}-z_0}{\rho_{S2}} & 1 \\ -\frac{x_{S3}-x_0}{\rho_{S3}} & -\frac{y_{S3}-y_0}{\rho_{S3}} & -\frac{z_{S3}-z_0}{\rho_{S3}} & 1 \\ \dots & \dots & \dots & \dots \\ -\frac{x_{Sn}-x_0}{\rho_{Sn}} & -\frac{y_{Sn}-y_0}{\rho_{Sn}} & -\frac{z_{Sn}-z_0}{\rho_{Sn}} & 1 \end{bmatrix} \quad (6.13)$$

thus $H^T H$ is 4×4 , (if there is data from for example GPS+Galileo, the columns of H become 5, see Chapter 7).

Often, some measurements are not as good as the others, some can have a greater error (due to multipath and noise), hence the measurements quality can be incorporated in the fitting criteria by introducing a **weighting matrix W**. [18]

This matrix W is diagonal and w_{ii} can be one or zero, where the w_{ii} are the weighting parameters; they can be selected with different criteria: using a threshold on the elevation and putting the weight equal to zero if the satellite is below it, checking the pre-fit or post-fit residuals, checking the signal-to-noise ratio on the RINEX file etc...

Introducing this matrix, the functional J^2 become:

$$J^2(\Delta x) = [\tilde{y} - H\Delta x]^T W [\tilde{y} - H\Delta x] = \tilde{y}^T W \tilde{y} - \tilde{y}^T W H \Delta x - \Delta x^T H^T W \tilde{y} + \Delta x^T W H^T H \Delta x. \quad (6.14)$$

and minimizing it, putting its first derivative with respect to Δx equal to zero:

$$H^T W H \Delta x = H^T W \tilde{y} \rightarrow \Delta x = [H^T W H]^{-1} H^T W y \quad (6.15)$$

This strategy helps in obtaining a better fix, with higher precision, because bad measurements that may lead to wrong positioning are deleted by the zero weights.

It is possible to compute some parameters from the matrix $H^T H$ that can be useful to determine how satellites are spreaded in the sky and consequently and if $H^T H$ is invertible; the first one is the PDOP (Position Dilution Of Precision):

$$PDOP_{3D} = \sqrt{[(H^T H)_{xx}^{-1} + (H^T H)_{yy}^{-1} + (H^T H)_{zz}^{-1}]} \quad (6.16)$$

if $PDOP < 3$ data are acceptable. [16] Hence also GDOP (Geometric Dilution Of Precision) and TDOP (Time Dilution Of Precision) can be introduced:

$$GDOP = \sqrt{[(H^T H)_{xx}^{-1} + (H^T H)_{yy}^{-1} + (H^T H)_{zz}^{-1} + (H^T H)_{tt}^{-1}]} \quad (6.17)$$

$$TDOP = \sqrt{[(H^T H)_{tt}^{-1}]} \quad (6.17)$$

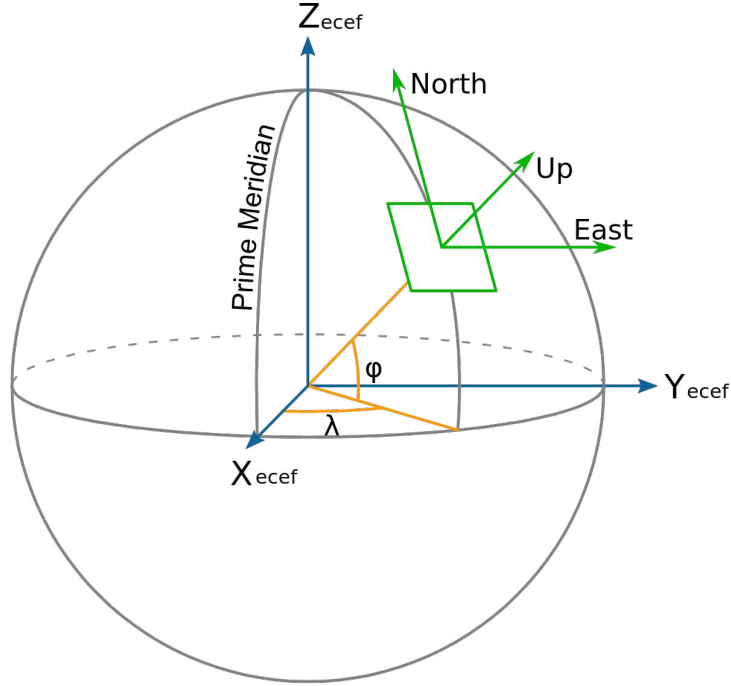


Figure 6.2: ECEF system of reference and NEU.

Other DOPs can be obtained by rotating the $H^T H$ matrix from the ECEF reference system to NEU (i.e North-East-Up, that is a local reference, centered on the receiver, see Fig. 6.2):

$$\begin{bmatrix} dn \\ de \\ du \end{bmatrix} = \begin{bmatrix} -\sin \varphi \cos \lambda & -\sin \lambda & \cos \varphi \cos \lambda \\ -\sin \varphi \sin \lambda & \cos \lambda & \cos \varphi \sin \lambda \\ \cos \varphi & 0 & \sin \varphi \end{bmatrix}^{-1} \begin{bmatrix} dx \\ dy \\ dz \end{bmatrix} \quad (6.18)$$

Hence, HDOP and VDOP (Horizontal and Vertical Dilution Of Precision) can be introduced:

$$\begin{aligned} HDOP &= \sqrt{[(H_{NEU}^T H_{NEU})_{ee}^{-1} + (H_{NEU}^T H_{NEU})_{nn}^{-1}]} \\ VDOP &= \sqrt{[(H_{NEU}^T H_{NEU})_{uu}^{-1}]} \end{aligned} \quad (6.19)$$

As a rule of thumb, acceptable values are $HDOP < 2$ and $VDOP < 3$. [16] [18]

6.1.2 Kalman filter

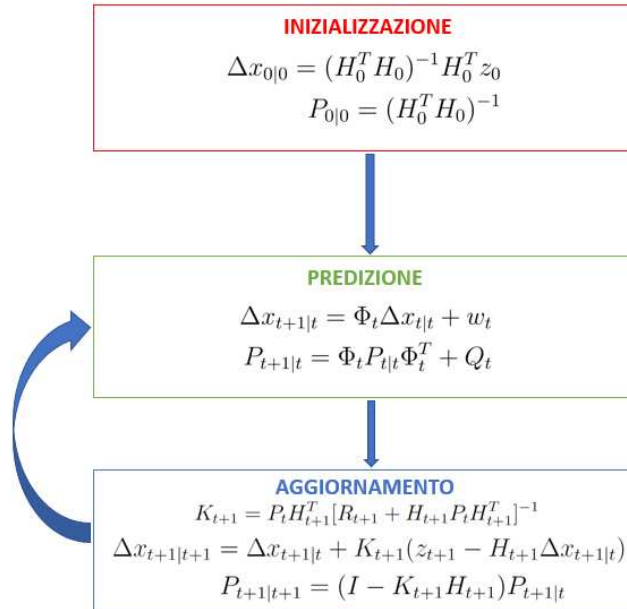


Figure 6.3: Kalman filter procedure.

The Kalman filter is named after Rudolf E. Kálmán, who was one of the primary developers of its theory. This method consists in a *stochastic algorithm* that, from measurements, data and the statistical model, permits the fix of a user who changes its positions over time.

The principle of Kalman filtering can be roughly summarized as the weighted least squares solution of the linearised observation system augmented with a prediction of the estimate as additional equations. More precisely, it is a recursive method to estimate the random states of a dynamic system in a way that minimizes the mean squared prediction error. After its initialization, the Kalman filter follows a recursive two-step procedure. It consists of the following phases (see Fig. 6.3):

- **Initialization:** it is the first phase, in which the algorithm computes the position at the time t_0 with the least squares method, then, at $t + 1$ the position is computed in two different phases:

1. **Prediction:** a prediction of the *state* (i.e. the position of the user) and of the covariance matrix at the time $t + 1$ is computed from the state and the covariance matrix of the previous epoch t and from the *transition matrix* Φ ;
2. **Update:** the predicted state and covariance matrix is corrected, from the observations, measurements and data collected at the epoch $t + 1$.

In the following paragraphs, the different phases are illustrated.

Initialization

At t_0 a certain number n of observations is given, hence from the least squares theory:

$$z = H\Delta x + \epsilon$$

where z is the vector of pre-fit residuals equal to $z_i = z_{observed} - z_{computed}$, both referred to t_0 . From the minimization of the functional J^2 , the best estimation of the state vector and of the covariance matrix at the time t_0 :

$$\begin{aligned}\Delta x_{0|0} &= (H_0^T H_0)^{-1} H_0^T z_0 \\ P_{0|0} &= (H_0^T H_0)^{-1}\end{aligned}$$

In a certain number of iterations, the initial position is obtained. The initialization is necessary because at this point the position of the user is unknown, hence the use of the least squares method substantially reduces the convergence time of the filter, otherwise considerable.

Prediction

To get the prediction of the position at the following instant, the transition matrix Φ must be introduced; Φ propagates the state vector and the covariance matrix:

$$\begin{aligned}\Delta x_{t+1|t} &= \Phi_t \Delta x_{t|t} + w_t \\ P_{t+1|t} &= \Phi_t P_{t|t} \Phi_t^T + Q_t\end{aligned}$$

The transition matrix is derived from a model of the dynamics; if the only position estimation is desired (and not speed and acceleration), it is $\Phi = I$, hence the prediction at time t_{t+1} coincides with the state vector at time t_t . If a better description of the user's cinematics is desired, it is possible to add components to the state vector, 2 for the speed (and 2 for the accelerations) in the bidimensional plane, thus the state vector and Φ become:

$$\begin{aligned}\Delta \mathbf{x}_{t+1|t} &= (\Delta x, \Delta v_x, \Delta y, \Delta v_y) \\ \Phi_t &= \begin{pmatrix} 1 & \Delta t & 0 & 0 \\ 0 & 1 & 0 & 0 \\ 0 & 0 & 1 & \Delta t \\ 0 & 0 & 0 & 1 \end{pmatrix} \end{aligned} \tag{6.20}$$

The matrix $Q_t = w_t w_t^T$ contains in the diagonal the a priori covariance of state vector's elements for each axis (in the bidimensional case σ_x^2 and σ_y^2) and it depends on the user dynamic.

Update

In this phase, measurements obtained in the epoch $t + 1$ are used to compute z_{t+1} and to correct the state vector $\Delta x_{t+1|t}$. Hence:

$$\begin{aligned}\Delta x_{t+1|t+1} &= \Delta x_{t+1|t} + K_{t+1}(z_{t+1} - H_{t+1}\Delta x_{t+1|t}) \\ P_{t+1|t+1} &= (I - K_{t+1}H_{t+1})P_{t+1|t}(I - K_{t+1}H_{t+1})^T + K_{t+1}R_{t+1}K_{t+1}^T\end{aligned}$$

where $R_t = \epsilon_t \epsilon_t^T$ is the covariance of the errors' measurements. K , the matrix of the **Kalman gain** is defined as:

$$K_{t+1} = P_t H_{t+1}^T [R_{t+1} + H_{t+1} P_t H_{t+1}^T]^{-1} \quad (6.21)$$

Therefore the updated covariance matrix become:

$$P_{t+1|t+1} = (I - K_{t+1}H_{t+1})P_{t+1|t} \quad (6.22)$$

[19]

6.2 Velocity estimation

In this Section the model for the speed estimation with Doppler measurements is presented. In the RINEX files the Doppler data are stored in a column named D1C (if the carrier is L1 and the code C/A, for L2 C/A it is D2D etc... see [10]) and its unit of measure is cycles of the carrier per second.

By definition, the Doppler shift is the projection of the relative speed vector, on the line-of-sight vector multiplied by $-f/c$, where f is the carrier frequency of the signal and c is the speed of light: $D = -\frac{\Delta \mathbf{v} \cdot \mathbf{I}_{\text{los}}}{c} \cdot f$. In the following model the Doppler shift is expressed in m/s, hence without the multiplication by f/c .

The relative motion between the satellite and the user results in changes in the observed frequency of the satellite signal; given the satellite speed, the Doppler shift can be used to compute the user velocity. It can be shown that the *pseudorange rates* (i.e. the time derivative of the pseudoranges) are:

$$\begin{aligned}\dot{p}^s &= \dot{\rho}^s + (\dot{d}t_r - \dot{d}t^s) + \dot{I}^s + \dot{T}^s \\ &= (\mathbf{v}^s - \mathbf{v}_r) \cdot \mathbf{I}_{\text{los}} + \dot{d}t_r + \dot{\epsilon}\end{aligned} \quad (6.23)$$

where \mathbf{v}^s and \mathbf{v}_k are the satellite speed vector, obtained from the RINEX navigation data, and the user speed vector to be estimated, $\dot{d}t^s$, $\dot{d}t_r$ are the rates of change of the satellite and receiver clocks (expressed in m/s), \dot{I} and \dot{T} are the time derivative of iono and tropo delays, I_{los} is the user-to-satellite line of sight and $\dot{\epsilon}$ is a combined error. The \dot{p}^s is called

pseudodoppler measure. The error due to multipath, ionosphere and troposphere is usually negligible, hence the main sources of error are the receiver clock drift (the satellite clock drift is known from the broadcast message and can be corrected) and the prediction of satellite position and speed \mathbf{v}^s .

The equation 11.2 can be rewritten as:

$$\dot{p}^s - \mathbf{v}^s \cdot \mathbf{I}_{\text{los}} = -\mathbf{v}_r \cdot \mathbf{I}_{\text{los}} + \dot{dt}_r + \dot{\epsilon} \quad (6.24)$$

denoting $(\dot{p}^s - \mathbf{v}^s \cdot \mathbf{I}_{\text{los}}) = \dot{p}^k$ and writing the 6.24 in matrix notation:

$$\dot{\mathbf{p}} = -\mathbf{H} \begin{bmatrix} \mathbf{v}_r \\ \dot{dt}_r \end{bmatrix} + \dot{\epsilon} \quad (6.25)$$

where H is the matrix of partial derivatives seen in the previous section. Expanding the 6.25:

$$\begin{Bmatrix} \dot{p}^1 \\ \dot{p}^2 \\ \dot{p}^3 \\ \vdots \\ \dot{p}^n \end{Bmatrix} = \begin{bmatrix} \frac{x_{S1}-x_0}{\rho_{S1}} & \frac{y_{S1}-y_0}{\rho_{S1}} & \frac{z_{S1}-z_0}{\rho_{S1}} & 1 \\ \frac{x_{S2}-x_0}{\rho_{S2}} & \frac{y_{S2}-y_0}{\rho_{S2}} & \frac{z_{S2}-z_0}{\rho_{S2}} & 1 \\ \frac{x_{S3}-x_0}{\rho_{S3}} & \frac{y_{S3}-y_0}{\rho_{S3}} & \frac{z_{S3}-z_0}{\rho_{S3}} & 1 \\ \dots & \dots & \dots & \dots \\ \frac{x_{Sn}-x_0}{\rho_{Sn}} & \frac{y_{Sn}-y_0}{\rho_{Sn}} & \frac{z_{Sn}-z_0}{\rho_{Sn}} & 1 \end{bmatrix} \begin{Bmatrix} v_x \\ v_y \\ v_z \\ \dot{dt}_r \end{Bmatrix} + \begin{Bmatrix} \dot{\epsilon}_1 \\ \dot{\epsilon}_2 \\ \dot{\epsilon}_3 \\ \vdots \\ \dot{\epsilon}_n \end{Bmatrix} \quad (6.26)$$

where (x_{Si}, y_{Si}, z_{Si}) are the satellites coordinates and (x_0, y_0, z_0) are receiver's coordinates.

It is important to notice the **sign** of the elements of matrix H, that is opposite of the one chose for the positioning problem; this is because of the minus sign of $\mathbf{v}_r \cdot \mathbf{I}_{\text{los}}$ in equation 6.24. [3]

6.3 PVTZ multiGNSS algorithm

The crucial challenge of modern satellite navigation is to estimate position, time synchronization and speed of a receiver, using *simultaneously all the constellations visible* in that precise moment. It is quite a remarkable number of satellites (some tens), seen from different directions and different elevations, thus with *different tropospheric delay*. For this reason, it is convenient to also value the *zenithal delay* which absorbs residual errors such as ionosphere, troposphere and multipath, doing therefore a **PVTZ**.

The variables to estimate are 3 coordinates for the receiver's position (x_r, y_r, z_r) and 3 components for speed (v_x, v_y, v_z) , zenithal delay, a certain number of synchronization errors equal to the number of visible constellations and their drift. In fact, the receiver must line up its time scale with all GNSSs, estimating the receiver clock bias and the receiver clock drift with respect to each time scale. In the PVT generally pseudorange and pseudodoppler measurements are used: first data for the position's computation and they are affected by clock biases, while seconds are used for the speed and are affected by clock drift.

In this work, data are collected from 4 constellation (GPS, GLONASS, Galileo and BeiDou) hence the *state vector* (i.e. the vector of the unknown) is 15×1 :

$$\{x \ y \ z \ dt_G \ dt_R \ dt_E \ dt_C \ ZTD \ v_x \ v_y \ v_z \ \dot{dt}_G \ \dot{dt}_R \ \dot{dt}_E \ \dot{dt}_C\} \quad (6.27)$$

where dt is the receiver clock bias plus the system time correction of the different constellations (i.e. G=GPS, R=GLONASS, E=Galileo and C=BeiDou) and \dot{dt} is the receiver clock drift and ZTD is the zenithal tropospheric delay.

If the PNT multiGNSS problem is considered (hence with the computation of **the position only**, not the speed), the matrix of partial derivatives is:

$$H = \begin{bmatrix} -\frac{x_{G1}-x_0}{\rho_{G1}} & -\frac{y_{G1}-y_0}{\rho_{G1}} & -\frac{z_{G1}-z_0}{\rho_{G1}} & 1 & 0 & 0 & 0 \\ -\frac{x_{G2}-x_0}{\rho_{G2}} & -\frac{y_{G2}-y_0}{\rho_{G2}} & -\frac{z_{G2}-z_0}{\rho_{G2}} & 1 & 0 & 0 & 0 \\ \dots & \dots & \dots & \dots & \dots & \dots & \dots \\ -\frac{x_{R1}-x_0}{\rho_{R1}} & -\frac{y_{R1}-y_0}{\rho_{R1}} & -\frac{z_{R1}-z_0}{\rho_{R1}} & 0 & 1 & 0 & 0 \\ \dots & \dots & \dots & \dots & \dots & \dots & \dots \\ -\frac{x_{Rn}-x_0}{\rho_{Rn}} & -\frac{y_{Rn}-y_0}{\rho_{Rn}} & -\frac{z_{Rn}-z_0}{\rho_{Rn}} & 0 & 1 & 0 & 0 \\ -\frac{x_{E1}-x_0}{\rho_{E1}} & -\frac{y_{E1}-y_0}{\rho_{E1}} & -\frac{z_{E1}-z_0}{\rho_{E1}} & 0 & 0 & 1 & 0 \\ \dots & \dots & \dots & \dots & \dots & \dots & \dots \\ -\frac{x_{En}-x_0}{\rho_{En}} & -\frac{y_{En}-y_0}{\rho_{En}} & -\frac{z_{En}-z_0}{\rho_{En}} & 0 & 0 & 1 & 0 \\ -\frac{x_{C1}-x_0}{\rho_{C1}} & -\frac{y_{C1}-y_0}{\rho_{C1}} & -\frac{z_{C1}-z_0}{\rho_{C1}} & 0 & 0 & 0 & 1 \\ \dots & \dots & \dots & \dots & \dots & \dots & \dots \\ -\frac{x_{Cn}-x_0}{\rho_{Cn}} & -\frac{y_{Cn}-y_0}{\rho_{Cn}} & -\frac{z_{Cn}-z_0}{\rho_{Cn}} & 0 & 0 & 0 & 1 \end{bmatrix} \quad (6.28)$$

it is important to notice that in this case the matrix H is $n \times 7$ where n is the number of visible satellites. The vector of the unknown is:

$$\Delta x = \left\{ \begin{array}{c} x - x_0 \\ y - y_0 \\ z - z_0 \\ \tilde{dt} + TSC_G \\ \tilde{dt} + TSC_R \\ \tilde{dt} + TSC_E \\ \tilde{dt} + TSC_C \end{array} \right\} \quad (6.29)$$

where dt is written splitting the effective receiver clock bias \tilde{dt} and the time system correction TSC_i of each constellation i .

If the Doppler model (presented in Section 6.2) is considered to get also the user speed and the zenith delay, the pseudodoppler data and the ZTD must be added and the matrix 6.28 has to be expanded in the following way:

$$H = \begin{bmatrix} (6.28) & 1/\sin(el) & 0 \\ 0 & 0 & -(6.28) \end{bmatrix} \quad (6.30)$$

where el is the elevation of each satellite.

The minus sign of 6.28 on the lower right is due to the adopted model of Doppler, see equation 6.24.

It is important to notice that theoretically the pseudodoppler depends on the receiver's coordinates, hence the submatrix on the lower left isn't zero, but these derivatives are really small with respect to the pseudorange derivatives, hence neglecting them is an acceptable approximation.

The unknown vector become:

$$\Delta x = \begin{Bmatrix} 6.29 \\ ZTD \\ 6.29 \end{Bmatrix} \quad (6.31)$$

that matches with the vector 6.27.

Vector y of prefit residuals will have $2n$ rows, where n is the total number of acquired satellites, assuming that pseudorange and pseudodoppler data are available for each of them. First n elements' dimensions are meters, second n elements are meters per second and not necessarily on the same frequencies. If a weighted least squares is applied, the data of pseudorange and pseudodoppler are weighted in the same way. [16]

Chapter 7

Software architecture

In this Chapter the software architecture is presented. The *multiGNSS_v3 suite* is a software that permits the PNT of some static receivers (**stations**) all around the Earth.

Beside the multiGNSS programs presented in Section 7.1, some specific modified versions have been created for this work to permit different types of analysis (i.e. with different inputs and outputs), together with the multiGNSSvelocity code (see Section 7.2) which is the brand new program part, designed to compute the user's velocity with multiple constellation strategy as the main aim of the thesis initially stated.

The original code is composed by several parts, each with a certain task, grouped in different directories:

- *bin*: in this directory the third party tools are stored, which are used for example to decompress RINEX files from the Hatanaka compression;
- *AutoMGNSS*: in it there are some auxiliary scripts for multiGNSS;
- *config*: here all the configuration files (.cfg) are saved; they contain all the settings (the most important are AutoMultiGNSS.cfg and multiGNSS.cfg)
- *input*: this directory is divided in other 4 subdirectories:
 1. *brdm*: it contains all the broadcast ephemeris saved or downloaded named with their DOY and year and (after the decompression) with the constellation's name;
 2. *obs*: this subdirectory is divided into 50 other subdirectories, each of them contains observation data from a different station;
 3. *dcb*: in it DCB (differential code biases) files are saved, when downloaded from the internet;
 4. *sp3*: in this subdirectory Sp3 orbit files (known as "Precise Ephemeris", they contain data records for the orbit and clock states) are saved;
- *logs*: in it there are some log files in which informations on fatal errors occurred in the installation or analysis are listed;
- *mgnssPre*: in this directory there are all the scripts used in the pre-processing phase, these scripts are written in PERL and they permit the download, the decomposition, the conversion and the smoothing of the data;
- *program*: in this directory the essential functions and the scripts of the software are stored, they are described in Section 7.1;
- *mgnssUtil*: in this directory there are other functions, which are called from the main, they are designed for example to convert the date or to process the broadcast

orbit files;

- *results*: here all the results and log files are collected, divided in the same 50 stations subdirectories of the input directory;
- *mgnsPost*: here all the post-processing scripts and functions are stored together with the results of the post-processing.

[20]

7.1 multiGNSS_v3 Suite programs

In this Section the structure and the functions of the software *multiGNSS_v3 suite* are presented; it is a software which puts into practice the theory of multiGNSS positioning explained in Section 6.3 (N.B. only positioning, not speed computation).

multiGNSS_v3 suite was designed to operate a **static positioning** of a list of on Earth stations, downloading the RINEX data of the observation by the respective websites and the RINEX MGEX (Multi-GNSS Experiment, i.e. broadcast ephemeris from all the constellations per day) from the IGS website (<https://igs.bkg.bund.de/>); it computes also the precision of this fix for each epoch.

This is done thanks to two groups of codes written in MATLAB and in PERL:

- the PERL scripts and functions provide the necessary files (downloading them from a list of websites) and convert them in a suitable way to ease their reading in the pre-processing phase (multignssPre directory), see Fig. 7.1 and 7.2;
- the MATLAB part reads the observation files and the ephemeris files, samples them and computes the position thanks to the software core, the function multiGNSS_v3, described in detail in Section 7.1.1.

Figure 7.1: The observation file before the decomposition.

Figure 7.2: The observation file after the decomposition.

Figure 7.3: The decomposition process is done to permit an easier transcription of the data in MATLAB matrices or vectors. It creates from the obs file some other files, one for each constellation, with ordered data, such as the one in the Fig. 7.2. This process is done also for broadcast ephemeris and Sp3 files if present.

This function multiGNSS_v3 is called from the script AutoMultiGNSS_v3 which has some important and essential tasks such as: it reads the configuration files (AutoMulti-

GNSS.cfg and multiGNSS.cfg, they contain some important specifications like the elevation cutoff, the sampling rate, the stations' list and the visible constellations from their locations, the initial a priori position and much more...), executes the PERL scripts for the downloading of the broadcast ephemeris files (downloadNav.pl) or the Sp3 files, the decomposition of the obs and nav files (decompObs.pl, decompNav.pl and decompSp3.pl) and also, if it is desired, it converts the broadcast ephemeris to the precise format Sp3. Then, from this script, some important flags or settings can be specified such as the fIF , which sets the computation on the iono-free dual frequency combination mode or the single frequency mode; the type of ephemeris file to be used; the DOY (Day Of the Year) and the year of the data.

It is important to underline that this script executes the function multiGNSS_v3 for each station, which are 50.

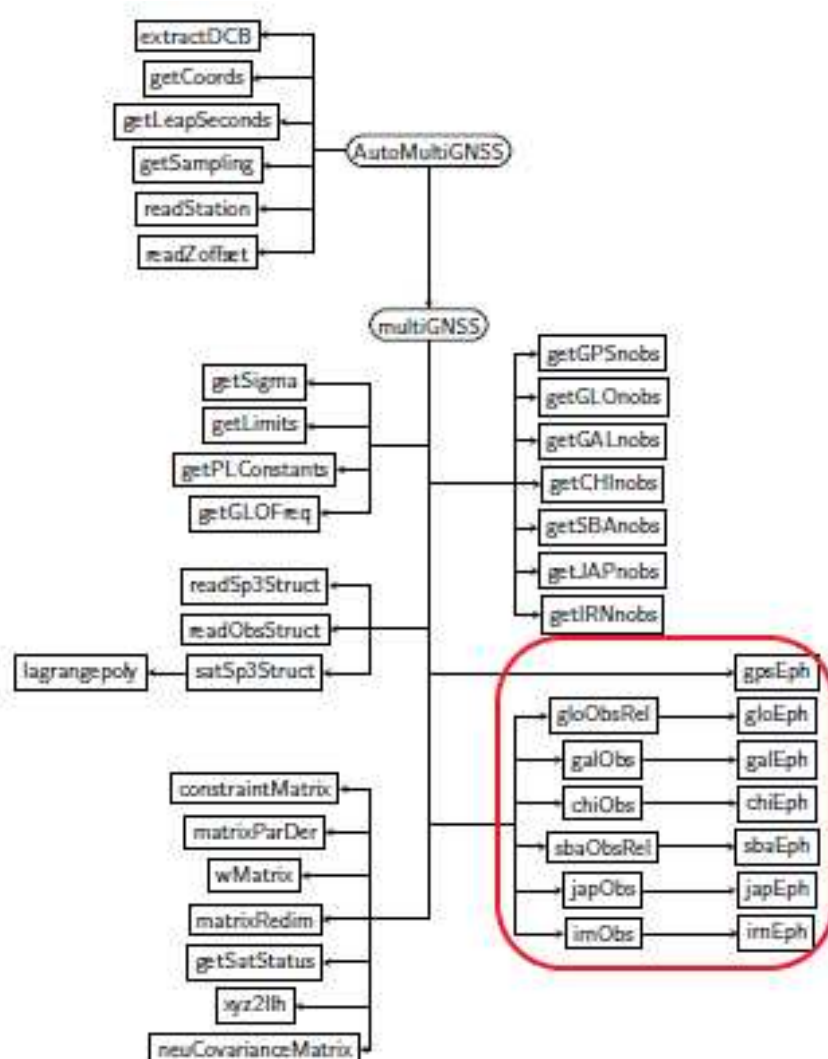


Figure 7.4: multiGNSS_v3 structure

As Fig. 7.4 shows, the AutoMultiGNSS_v3 and multiGNSS_v3 function need a certain number of other functions to work properly; these functions are located in the directory *program* of the suite, each of them has a different task, in particular the functions

highlighted from the red square are designed for the elaboration and the reading of the observation and navigation files providing the satellites coordinates, the pseudorange observations, the weight to be assigned, the relativity correction and the satellites clock offsets. [20]

7.1.1 multiGNSS_v3 function

This function is the most important part of all the software, it executes the weighted least squares algorithm using the multiGNSS data. For each epoch sampled, it requires in input:

- the name and the a-priori position of the station computed (x_0, y_0, z_0) ;
- the year and the DOY;
- the constellations to be considered.

In output it produces some files saved in the *results* directory (in the specific subdirectory of the computed station) such as:

- *partialsDOY0.csv*: in this file for each epoch, the matrix of the partial derivatives is stored (where the *DOY* is replaced by the actual DOY);
- *multiGNSSDOY0.log*: in this file there are **all** the informations about the analysis, from the reading procedure to the post processing, it is very useful for the debugging;
- *CorrDOY0.csv*: one for each constellation, it is a file for the validation of the relativistic and tropospheric correction;
- *PostFitDOY.csv*: one for each constellation, it contains the the postfit residuals;
- *posDOY0.csv*: it contains for each epoch analyzed the vector Δx , the initial position (x_0, y_0, z_0) , HDOP, VDOP and some other parameters;
- *timeOffsetDOY0.csv*: it contains time corrections for each constellation.

After the reading part, the code assign the weight to each measurement following some criteria: the satellite's elevation angle must be over the elevation cutoff, observations on two frequencies must be present, ephemeris must be present and a check on prefit residual is done, verifying that is under a certain residual threshold; if all this requisites are confirmed the measure is weighted 1, else 0.

After all the partial derivatives are computed, the matrix H is assembled thanks to a function (*matrixParDer.m*) and then resized, deleting unused columns and rows.

At this point the WLS is initialized: the default number of iteration is 2, the vector oc (the \tilde{y} in Chapter 6) is computed as:

$$oc = code - range - cBiasG + dT \cdot c + dTrel \cdot c - tropo + dcb; \quad (7.1)$$

where *code* is the iono-free combination, *range* is the computed geometric range, *cBias* is the estimated receiver clock bias plus the system time correction, $dT \cdot c$ the satellite clock offset, *tropo* is the tropospheric correction and *dcb* is the differential code bias correction. Then, the oc vector is multiplied by H^T and with the formulas explained in Section 6.1.1 the Δv vector is computed and added to the a-priori position.

After the two iterations, the post processing phase starts, computing the post-fit residuals, the RMS error, the standard deviations and the DOPs. [20]

7.1.2 Modified versions of the multiGNSS_v3 function

In this Section a brief description of the changes made on the AutoMultiGNSS_v3.m and multiGNSS_v3.m to operate the different types of analysis.

The original flow of the software is the one shown in Fig. 7.5: the position fix in this case is done only for the stations listed in the multiGNSS.cfg file, using downloaded data, hence to give in input different data to the software main function multiGNSS_v3.m, the AutoMultiGNSS_1stat was created.

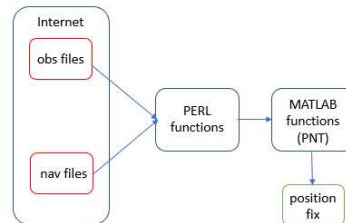


Figure 7.5: multiGNSS_v3 scheme

This script doesn't call the download functions of the multignssPre, but takes the data from a "fictitious" station directory (called "giul") in which stonex RINEX files are stored. The initial idea was to use the RINEX navigation files provided by the stonex receiver, but they weren't correct (probably because of some error in the transcription phase or conversion phase from the binary file), hence broadcast navigation message were downloaded manually and saved into the `/input/brdm` subdirectory.

Some other changes were made to permit the *dynamic positioning* and easy the computation of user's velocity: the check on the prefit residuals has been relaxed (i.e. the reference threshold has been raised), the sampling rate has been increased and other output files has been created: `velDOY.log` which contains the satellites' speed at the analyzed epochs (computed from the satellites positions using difference quotient) and the `coordDOY.log` file in which the position of the user (in terms of latitude, longitude and height) at each epoch is saved. The `velDOY.log` is used to compute the a-priori Doppler in multiGNSSvelocity.m (see Section 7.2), while the `coordDOY.log` is used to compute the rotation matrix from ECEF to NEU system of reference.

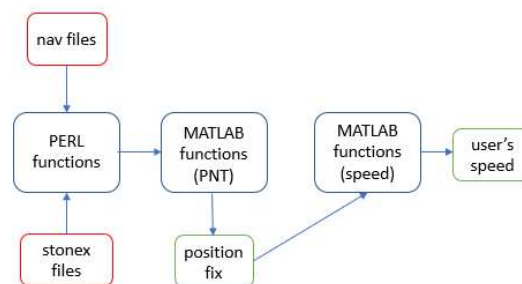


Figure 7.6: Modified version, for analysis of Stonex data

The last modification was made to permit the PNT of the Sentinel 3A, a LEO satellite of Copernicus constellation (see Chapter 9). In this case not only the AutoMulti-

GNSS_v3.m was edited, but also the multiGNSS_v3.m, creating AutoMultiGNSS_LEO.m and multiGNSS_v3LEO.m.

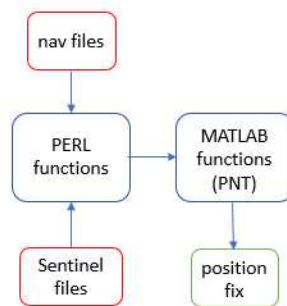


Figure 7.7: Modified version, for analysis of Sentinel data

The main difference between the previous analysis is the much more higher speed of the receiver, hence the a-priori position given in input to multiGNSS_v3.m function, can't be always the same for every epoch, as done for the static positioning, but the one computed in the previous epoch. Therefore the algorithm was modified to do this and, also, all the atmospheric correction were deleted, because at 800 km from Earth surface these effect are negligible: tropospheric delay is absolutely assent, but a residual part of the ionosphere is still present, thus in principle the iono-free dual combination should be used, however the single frequency solution was selected for simplicity.

7.2 multiGNSSvelocity code

The multiGNSSvelocity code is the part of the software expressly developed for this work.

The integration of this new part with the original code's suite was necessary to permit the determination of the receiver's dynamics, to complete the description of its motion and to enhance its precision.

The Doppler measures are very accurate and clean, because they are not affected by atmospheric delays, hence very precise information could be extracted from them. Therefore instead of computing the speed as the time derivative of the position (running into pseudorange error amplification and propagation), a new model and a new code have been created, taking advantage of this other set of measures.

This code has been written in MATLAB and it puts into practice the theory of Section 6.2. The script multiGNSSvelocity.m must be executed after the AutoMultiGNSS_v3 analysis; this because many inputs for the speed computation are taken from the outputs files of the PNT fix (while others are the same of the previous analysis), such as:

- partial derivatives file, to rebuilt the H matrix;
- the velocity file, which contains the satellite's speed to compute the a-priori Doppler;
- the coordinates position file, with latitude, longitude and height of the receiver;
- the observation file, to get the pseudodoppler observations;
- the broadcast ephemeris, to get satellites' positions and satellites' clock drifts.

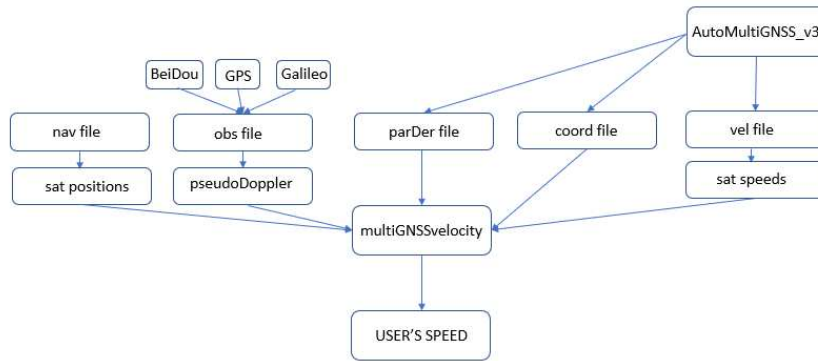


Figure 7.8: multiGNSSvelocity input scheme

First of all, the epochs are read from the observation file, then using 5 functions (one for each of the input files written in the previous list) the necessary data are provided. Each of these functions has been created to gather and to process information from **GPS**, **Galileo** and **BeiDou** constellations. After the reading part, the matrix and the vector of pseudodopplers from each constellation are concatenated, then the prefit residuals (oc , i.e. observed minus calculated) are computed as:

$$oc = D - d + clockdrift \cdot c; \quad (7.2)$$

where D is the pseudodoppler measure, d is the computed Doppler and $clockdrift$ is satellite clock drift expressed in s/s .

The matrix W is inherited from the previous analysis and it is read by the partial derivatives file; although W is given, in some cases the measure's weight can be modified to avoid mistakes due to bad or not present measures, for example if the Doppler measure is not present or it is present, but it is weighted to zero, or the satellite's speed is not present and many other possibilities.

When all the data are ready to be processed, they are used for the computation of Δv and the updating of the speed vector.

The algorithm's strategy is different from the one shown in Section 6.3, it follows the principle of the weighted least squares, but instead of doing a single analysis for both speed and position, it computes them separately in a consecutive way: first the position and then the speed. In this way some calculations are easier, because some things are known from the previous analysis, such as the matrix H and also the weight matrix W . Therefore only one iteration is needed to get the speed components and the receiver's clock drift.

In output a log file (`multiGNSSvelocityDOY0.log`, see Fig. 7.9) is created; it contains all the information of the analysis from the reading procedure to the computation of RMS and postfit residuals. All the results are presented in the following Chapter 8.

```

*****READING GPS DATA*****
*** STEP 1.1: READING PARTIAL DERIVATIVE FILE ***

SAT YEAR MO DY HR MN SS      PARX      PARY      PARZ W
G 2 2021 8 21 0 0 0.000      -0.385      -0.824      0.415 1
G 6 2021 8 21 0 0 0.000      -0.058      -0.998      -0.001 1
G10 2021 8 21 0 0 0.000      -0.200      0.947      -0.251 1
G12 2021 8 21 0 0 0.000      -0.782      0.331      -0.528 1
G15 2021 8 21 0 0 0.000      -0.937      -0.129      0.325 1
G17 2021 8 21 0 0 0.000      0.385      -0.551      -0.741 1
G19 2021 8 21 0 0 0.000      -0.047      -0.684      -0.728 1
G24 2021 8 21 0 0 0.000      -0.662      -0.233      -0.712 1
G25 2021 8 21 0 0 0.000      -0.677      0.727      -0.117 1
G32 2021 8 21 0 0 0.000      0.162      0.680      -0.715 1

*** STEP 2.1: READING DOPPLER RINEX FILE ***

SAT YEAR MO DY HR MN SS      Doppler [s/s] W
G 2 2021 8 21 0 0 0.000      2747.562      1
G 6 2021 8 21 0 0 0.000      2554.070      1
G10 2021 8 21 0 0 0.000      -1765.414      1
G12 2021 8 21 0 0 0.000      1647.773      1
G15 2021 8 21 0 0 0.000      -3630.113      1
G17 2021 8 21 0 0 0.000      -2815.801      1
G19 2021 8 21 0 0 0.000      -1429.363      1
G24 2021 8 21 0 0 0.000      -445.957      1
G25 2021 8 21 0 0 0.000      3060.113      1
G32 2021 8 21 0 0 0.000      2992.797      1

*** STEP 3.1: READING BROADCAST EPHEMERIS FILE ***

SAT YEAR MO DY HR MN SS      ClockDrift [s/s]
G 2 2021 8 21 2 0 0.000      -2.3874e-12
G 6 2021 8 21 2 0 0.000      6.5938e-12
G10 2021 8 21 2 0 0.000      -7.7307e-12
G12 2021 8 21 2 0 0.000      -5.3433e-12
G15 2021 8 21 2 0 0.000      2.7285e-12
G17 2021 8 21 2 0 0.000      5.6843e-12

```

Figure 7.9: The output multiGNSSvelocityDOY0.log contains for each constellation the reading obs and nav part, the concatenation part, the computation of prefit residuals and $H^T H$ matrix, the results, the computation of postfit residuals, the DOPs and RMS errors.

Chapter 8

Experimental tests and results

In this Chapter the results of the experimental campaigns are presented.

The first analysis describes the elaboration of the data acquired by the receiver of CISAS (station PADO); this was done to assess whether the installation was made correctly and everything worked properly.

Thereafter, data from an external source has been used: the STONEX S580 receiver carried out some experimental tests, in particular two static and two dynamic detections (one static and two dynamic are presented in this work). Places for the experimental campaigns were selected as clear as possible and with no high obstacles which could hamper signals from the sky.

The static detections were implemented to test the modified version of the suite multiGNSS_v3 and to make sure it took the correct inputs.

The original code (multiGNSS_v3 suite) is completely automatic, the input (in terms of DOY and year) is given from the command prompt and it downloads all the files needed for the PVT of the fifty stations memorized inside the configuration file. Therefore, to execute the PVT from a new receiver, a new “fictitious” station folder has been created, containing all the data from the STONEX S580 receiver.

To fulfill the purpose of this thesis, Doppler measurements from satellites were needed (as well as pseudorange) to determine the speed of the user, thus dynamic detections were done to test the computation of the velocity and verify the precision and the accuracy.

8.1 Static positioning

The first static positioning has been done using Padua station observation data. This passage was necessary to initialize and to test multiGNSSvelocity with a static fix, using a known position and **accurate pseudorange data** from a reliable receiver.

Then another static positioning has been done using STONEX S580 data to be sure that the receiver worked properly, to evaluate its performances and to test multiGNSSvelocity code.

DOY 233, Padua station data

Padua station (more precisely the CISAS “Giuseppe Colombo”) has a **STONEX SC2200** (see Fig. 8.1), a very advanced receiver, used for professional applications when high pre-



Figure 8.1: STONEX SC2200 receiver.



Figure 8.2: CISAS DOY 233, Google Earth rendering.

cision and maximum reliability are needed. Therefore, from this analysis the results expected are, for the positioning, coordinates with an error of ≈ 1 m and an almost null speed (because it is a static receiver).

The settings used for this analysis are listed in Table 8.1.

Analysis	used const	elev cutoff [°]	residual threshold [m]	sampling rate [s]	duration	iterations
Positioning	G R E C	5	150	900	24 h	2
Speed	G E C	5	- *	900	24 h	1

Table 8.1: Table of analysis of DOY 233, Padua station. * No check on prefit residuals has been done on the pseudodoppler.

This parameters were selected specifically for this analysis: the residual threshold (i.e. the threshold applied on prefit residuals to verify their quality) is low because the expected variation of the coordinate with respect to the a-priori (x_0, y_0, z_0) is small and, for the same reason, the number of the iteration is 2 (while for the other analysis the iteration number is 3). The sampling rate was set to a sample every 15 min: the receiver is static, thus a low sampling rate is sufficient to determine its position and the precision of the fix. The cutoff angle is 5° , it permits the rejection of too low satellites on the horizon, which could be much more affected by multipath and atmospheric effects and damage the final result's accuracy and precision.

The coordinates obtained are:

$$\begin{aligned}
 \lambda &= 45.411156 = 45^\circ 24' 40.16'' N \\
 \phi &= 11.896061 = 11^\circ 53' 45.82'' E \\
 h &= 64.4m
 \end{aligned}
 \tag{8.1}$$

where the height is computed with respect to the mean spheroid defined by WGS84 and the coordinates' accuracy is ≈ 1 m. The Google Earth rendering is in Fig. 8.2.

Looking at Fig. 8.3, it is possible to see that the biggest errors (over the meter) are observed when the DOPs are high, hence when the position of the satellites is not appropriate. However, when the DOPs have lower values, the precision is really good.

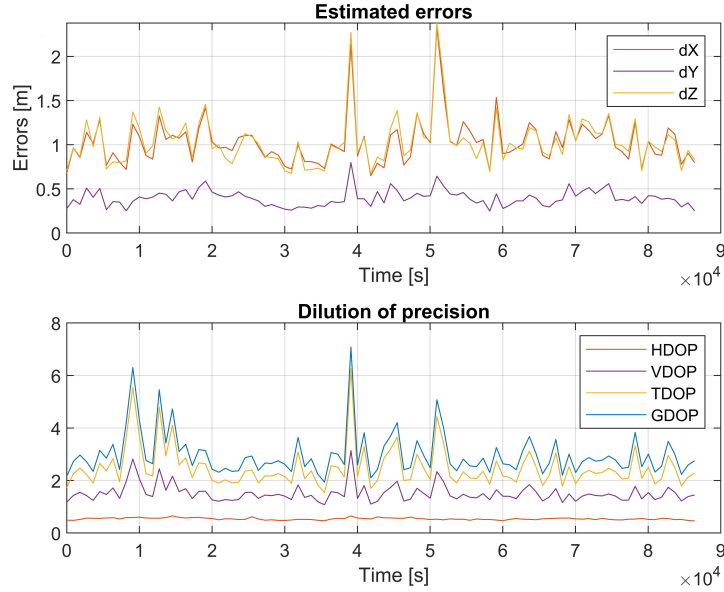


Figure 8.3: Estimated uncertainties on the position and Dilutions of precisions, DOY 233. N.B. The uncertainty is computed as: $RMS \cdot \sigma_i$, where $i = x, y, z$ and $\sigma = \sqrt{(H^T H)_{ii}^{-1}}$.

Another check has been done on the tropospheric correction: it is expected to be quite constant (mean value $\approx 2.2m$), because no vertical displacement was done by the receiver; in Fig. 8.5, the tropospheric correction has some fluctuation, due to different atmospheric and humidity conditions in time (in 15 min, weather changes slightly).

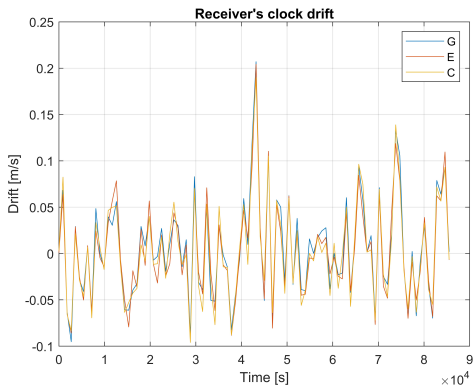


Figure 8.4: Receiver's clock drifts DOY 233.

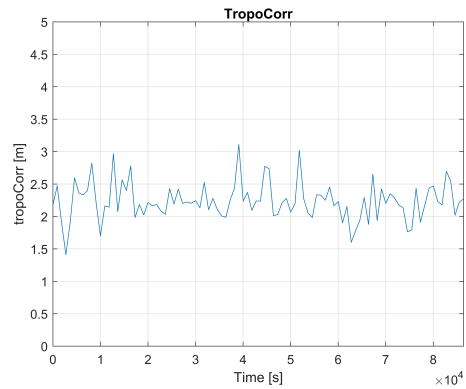


Figure 8.5: Tropospheric correction, DOY 233.

Thereafter, the speed determination has been done, executing the multiGNSSvelocity code; a first check has been made on the receiver's clock drift to assess whether the computation was correct: \dot{dt} must be the same with respect to each different time system reference, and in the order of $\approx ns$, because:

$$\dot{dt} = \frac{\partial(dt + TimeSysCorr)}{\partial t} \quad (8.2)$$

since the $TimeSysCorr$ is nearly constant, its derivative is zero and the \dot{dt} must be the same for each constellation. Therefore, from Fig. 8.4, it is ascertained that they have almost the same value and the same variations.

The clock bias and the clock drift has been computed respectively in the multiGNSS_v3 and multiGNSSvelocity codes, and the results are; **STONEX SC2200**:

1. $dt_{PADO} = 16 \text{ ns}$
2. $\dot{dt}_{PADO} = 0.01 \text{ ns/s}$.

These values show that this receiver's clock is really stable and reliable.

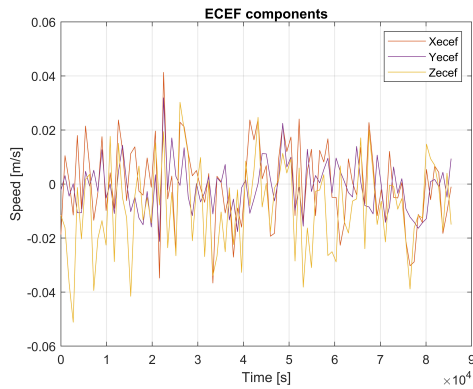


Figure 8.6: Speed componente in ECEF, DOY 233.

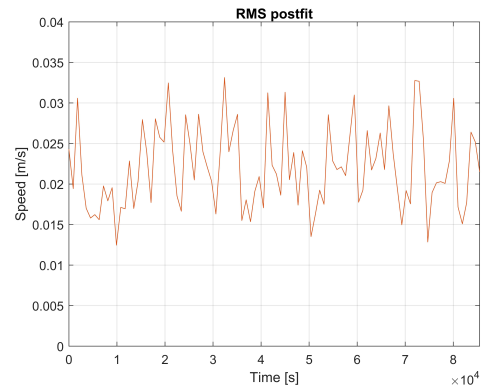


Figure 8.7: RMS postfit residuals of the speed.

The receiver was static, thus the real speed is zero; from Fig. 8.6, it is possible to see that for each ECEF component of the speed the mean value is zero and the fluctuations are in the order of cm/s; more precisely the average of postfit residuals is $\approx 0.18 \text{ mm/s}$, the mean RMS is $\approx 2.1 \text{ cm/s}$, see Fig. 8.7. Thus the precision of the speed computation is very good.

DOY 328, STONEX S580 data



Figure 8.8: STONEX S580.



Figure 8.9: Pianiga (VE), DOY 328.

In this paragraph, the results of a static analysis done with data from the STONEX S580 receiver are presented.

This data were collected in Pianiga (near Venice), the antenna has been placed in a free space, without hurdles on the horizon, at a height of 210 cm.

The obtained coordinates are:

$$\begin{aligned} \lambda &= 45.460689 = 45^{\circ}27'38.48''N \\ \phi &= 12.042286 = 12^{\circ}02'32.23''E \\ h &= 60.3m \end{aligned} \tag{8.3}$$

if they are compared with the coordinates given by the receiver's GUI (see Fig. 8.11), a quite good precision can be verified (except for the altitude, probably computed with respect to a different system of reference).

The Google Earth rendering is in Fig. 8.9.

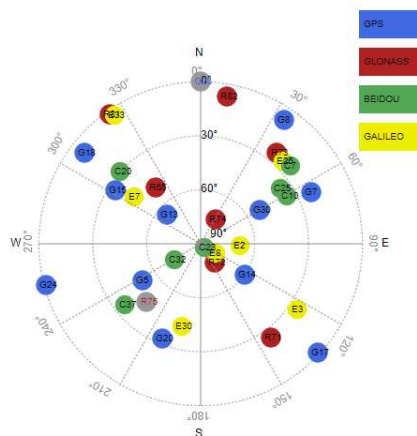


Figure 8.10: Skyplot DOY 328, Pianiga.

Satellites	32/38	Solution	Single
Longitude	12°12'32.5154"	Latitude	45°27'38.5921"
Altitude	50.651	HRMS	0.184
VRMS	0.23	PDOP	0.75
HDOP	0.48	VDOP	0.58
Date	2021-11-24	Time	13:58:08
Differential Delay	0(s)		
Reference Lon	0°0'0.0000"	Reference Lat	0°0'0.0000"
Reference Alt	0.000	Reference Distance	0.0000(km)

Figure 8.11: Position given by the receiver, DOY 328.

In Fig. 8.10, the skyplot of one epoch is illustrated, showing the number and the types of satellites present in that moment; this image is the visual representation of the DOPs, in particular HDOP, which give a quantified information of the position of the satellites, in this case, for this epoch it is acceptable.

In Table 8.2 are listed the settings for this analysis. It is important to notice that the number of iteration is bigger: this because after two iterations the algorithm converges

Analysis	used const	elev cutoff [°]	residual threshold [m]	sampling rate [s]	duration	iterations
Positioning	G R E C	5	150	60	56 min	3
Speed	G E C	5	-	60	56 min	1

Table 8.2: Table of analysis of DOY 328, Stonex receiver.

to the solution, but the Δx vector is still not null, hence, as precaution, another iteration has been done.

From Fig. 8.12, it is possible to notice that the first $\approx 500s$ the estimated errors are high, this is due to the *cold start* problem: the receiver when is switched on, could miss or estimate inaccurately its position, velocity and time, and also the visibility of any satellites; thus the receiver must systematically search for all possible satellites in the sky. After acquiring a signal, the receiver can begin to obtain approximate information on all the other satellites, called the almanac. This almanac is transmitted repeatedly every 12.5 minutes.[21]

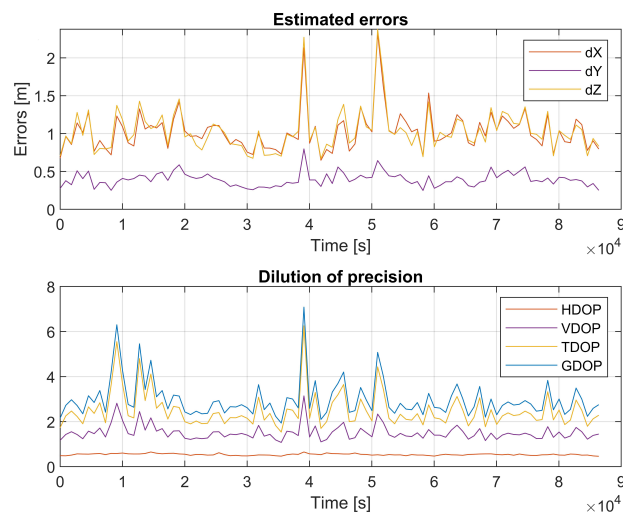


Figure 8.12: Estimated uncertainties on the position and Dilutions of precisions, DOY 328.

The accuracy and the precision of the STONEX S580 is expected to be worse than the one got with STONEX SC2200, because it is a mass market receiver; if the error prediction of Padua receiver is $\approx 1m$, in this case is $\approx 5m$ (when the DOP is acceptable). This is because the pseudoranges obtained during the measurement campaigns are noisy, hence, unless a smoothing procedure on pseudoranges is done, this is the best result achievable.

Fig. 8.13 shows the RMS of postfit residuals: it is high in the first epochs (because of the cold start process), this explains why, even if the DOPs are nearly acceptable, the error is high.

Speed values instead have an accuracy comparable with the one found from Padua station data; this because, as said before, the Doppler measures are really accurate, not

affected by atmospheric delays and less noisy.

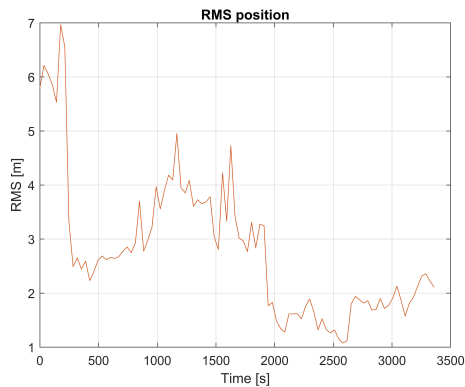


Figure 8.13: RMS postfit residuals of the positioning

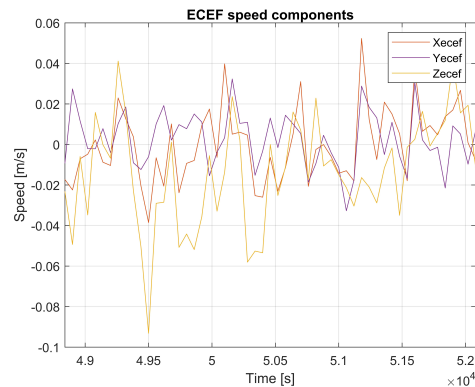


Figure 8.14: Speed components in ECEF, DOY 328.

In fact, looking at Fig. 8.14, the computed speed's components are still near zero, the average of postfit residuals is ≈ 5 mm/s and the RMS of postfit residuals is ≈ 2 cm/s.

In Fig. 8.16, the tropospheric error is shown; as the previous analysis, it is expected to be around 2.2 m, because the receiver didn't change its vertical position, but in this case, in the first 5 min of the analysis the tropospheric correction is quite variable, here too, because of the cold start procedure.

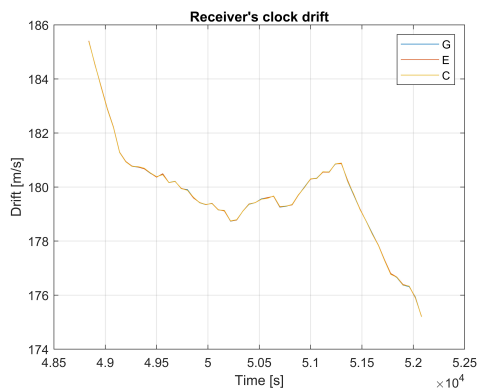


Figure 8.15: Receiver clock drift, DOY 328.

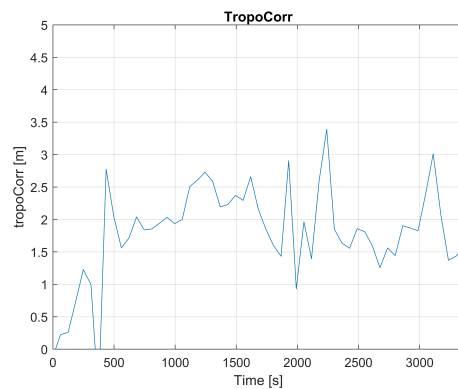


Figure 8.16: Tropospheric correction, DOY 328.

The receiver clock bias and clock drift are some orders of magnitude bigger than the values found for STONEX SC2200; STONEX S580 values are:

1. $dt_{GIUL} = 7$ ms
2. $\dot{dt}_{GIUL} = 600$ ns/s

this shows that the internal clock is less accurate and stable than the other; in particular, in Fig. 8.15, it can be noticed that the receiver drift is changing over time, in a quite linear way, thus the **jerk** of the receiver clock is $\neq 0$.

8.2 Dynamic positioning

In this Section the results obtained from the dynamic analysis are presented.

The first data set has been collected from the STONEX S580 receiver, used by a pedestrian user, while the second acquisition has been made by the same user, but driving a car.

DOY 298, STONEX S580 data

This experimental campaign has been done in Santa Maria di Sala (Venice) by a pedestrian user; the user walked along a street following a path as shown in the rendering in Fig. 8.19. A walking man generally has a speed of $\approx 1\text{-}1.5$ m/s (i.e. 5 km/h), the average-walk speed, thus the computed speed is expected to be in this range.

In Table 8.3 the setting parameters are itemized; in this analysis the check on the prefit residual (residual threshold) has been relaxed, because of the dynamics: the user's position is changing, hence the (x_0, y_0, z_0) a-priori coordinates are precise (near to the real position) only for the first epoch; for this reason many pseudorange and pseudodoppler would be rejected, because the prefit residuals are bigger than the residual threshold. To address the problem, the residual threshold should be lowered or the a-priori coordinate should change, (i.e. the previous epoch position fix becomes the a-priori (x_0, y_0, z_0) for the next epoch). The first option has been chosen for simplicity, while the second has been implemented for the PNT of a LEO satellite, because of the higher speed of the spaceborne receiver.

Analysis	used const	elev cutoff [°]	residual threshold [m]	sampling rate [s]	duration	iterations
Positioning	G R E C	5	1000	60	34 min	3
Speed	G E C	5	-	60	34 min	1

Table 8.3: Table of analysis of DOY 298.

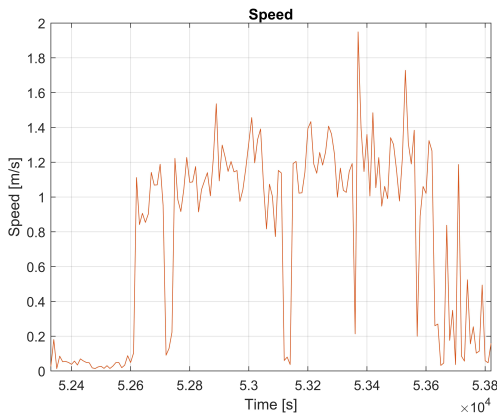


Figure 8.17: Speed norm, DOY 298.

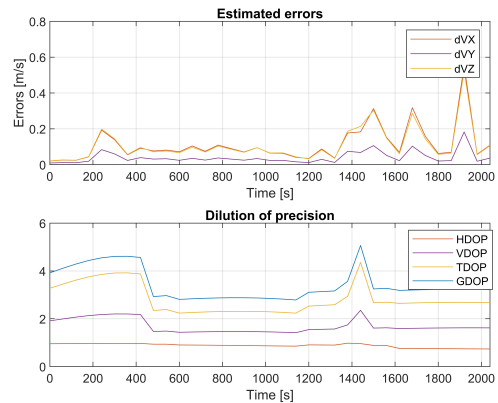


Figure 8.18: Estimated uncertainties on velocity and DOPs, DOY 298.

In Fig. 8.17, the speed variations over time are plotted; the mean walking speed of this man is ≈ 1.2 m/s. This plot has been done with sampled data on 10 s, hence a bigger sampling rate than the one declared on Table 8.3. The sharp variations on this plot can be caused by the highly noisy measures or the still too low sampling rate (in 10 second the man can vary his speed).

The man's speed is in the range of the average-walk speed; this is an appreciable result, but it cannot be compared with the real speed (because it wasn't measured), only the predicted uncertainties can give an idea of the precision on this esteem.

The predicted speed uncertainties are shown in Fig. 8.18; these are (< 0.1 m/s) in almost all the analysis duration, only in the last part they reach ≈ 0.5 m/s, because in that moment a little part of the path has been done driving a car, hence the speed was higher and consequently the imprecisions are bigger.

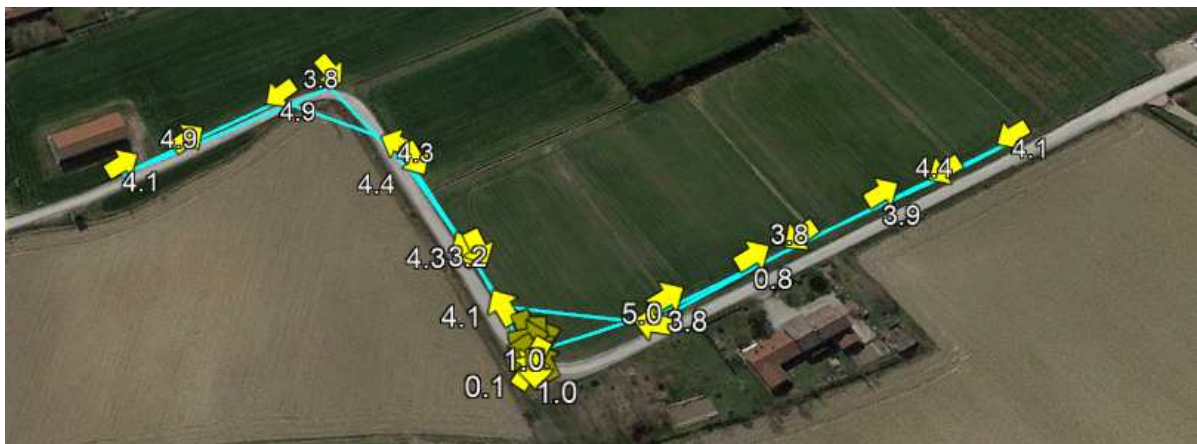


Figure 8.19: Google Earth rendering, DOY 298. The numbers near the yellow arrows are the speeds computed for each sample in km/h.

In Fig. 8.19, the Google Earth representation of the path done that day is drawn with light blue line; each yellow arrow is a sample and its heading specifies the speed direction; near each symbol, there is a number which indicates the speed norm computed in that moment for that sample.

In Fig. 8.20, the DOPs and the position errors are shown. It is important to notice that the DOPs are high during the first epochs, here too, because of the cold start process. In the speed determination, this problem causes a little bias (of the order of dm/s) that can be seen in particular on the vertical speed, which disappears after ≈ 5 min.

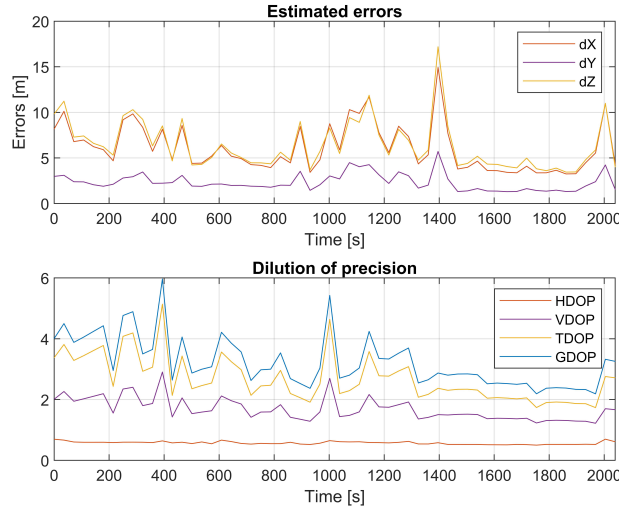


Figure 8.20: Estimated uncertainties on the position and Dilutions of precisions, DOY 298.

DOY 313, STONEX S580 data

In this paragraph results from a dynamic acquisition made by a receiver mounted in a car are presented.

The path done is displayed in Fig. 11.5; the last part of the circuit was covered on foot. During this test, the speed values were read on the speedometer (see Table 8.5) to compare them with the satellite determinate velocities.

As in the previous analysis, the settings are shown in Table 8.4: the residual threshold has been relaxed and the sampling rate decreased, because of the user's dynamic. The sampling rate has been selected higher than the previous, because in this case the speed was significant, hence to estimate the dynamics well, more samples have been taken.

Analysis	used const	elev cutoff [°]	residual threshold [m]	sampling rate [s]	duration	iterations
Positioning	G R E C	5	1000	30	58 min	3
Speed	G E C	5	-	30	58 min	1

Table 8.4: Table of analysis of DOY 313.

Fig. 11.5 shows the path done with the car, the DOY 313. The sampling rate used to create this image, is 1 sample every 60 s, a little less dense of the one declared on Table 8.4; this was done to get a clearer rendering, even if some parts of the circuit are not well represented (too low sampling rate causes some imprecision on the tracking). The last part was done on foot, for this reason the samples are closer, because the speed was lower.

In Table 8.5 are listed the speeds measured by the speedometer during the experimental campaign, while in Fig. 8.22 the velocities computed with the code are plotted (the red curve is the speed norm). As can be seen comparing the values, the obtained results fit quite well the measured ones, even if these are a little different: this is because

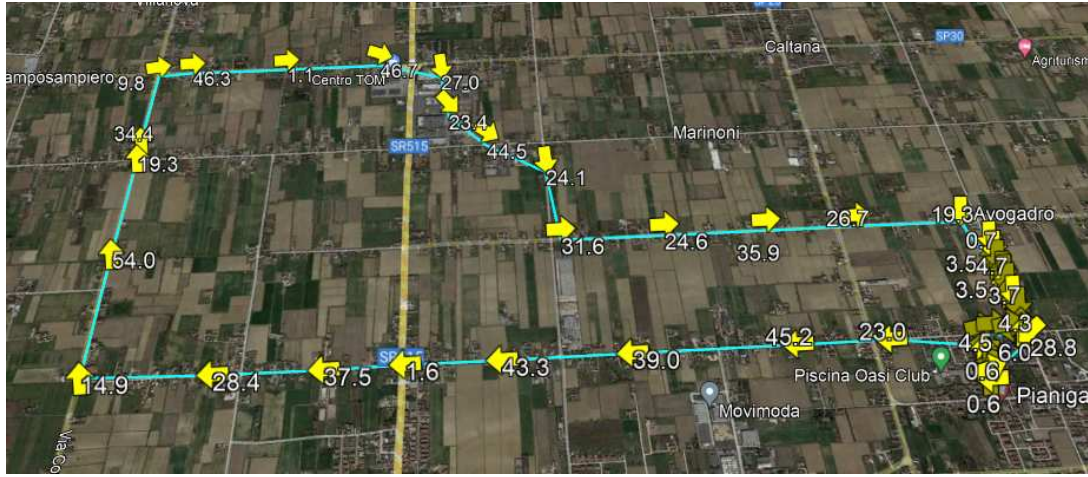


Figure 8.21: Google Earth rendering DOY 313, The numbers near the yellow arrows are the speeds computed for each sample in km/h.

Time	Speed [m/s]
18:27	00
18:30	6.9
18:31	9.7
18:32	11.1
18:33	13.3
18:35	13.3
18:37	8.3
18:38	12.5
18:39	13.9
18:40	16.7
18:41	00
18:42	6.9
18:43	00
18:44	13.8
18:45	11.1

Time	Speed [m/s]
18:46	8.3
18:47	5.6
18:48	5.6
18:49	8.3
18:50	11.4
18:51	8.3
18:52	5.6
18:53	8.3
18:54	9.7
18:56	12.5
18:57	8.3
18:58	00
18:59	00
19:02	on foot
19:35	on foot

Table 8.5: Table of measured speed with the speedometer, DOY 313.

car speedometers are not really precise instruments, usually give a bigger speed than the real one.

As in the previous analysis, the initial bias problem is detected; it is caused by the cold start procedure, in fact, looking at the different lines in Fig. 8.22, the v_{up} is not zero, but has a little bias. The Fig. 8.22 was done using a sampling rate of 1s, to detect every little variation of the speed.

From Fig. 8.23 the estimation of speed errors can be appreciated; in the first part, done driving the car, the errors are on the order of ≈ 0.5 m/s, while during the on foot, part they are < 0.05 m/s.

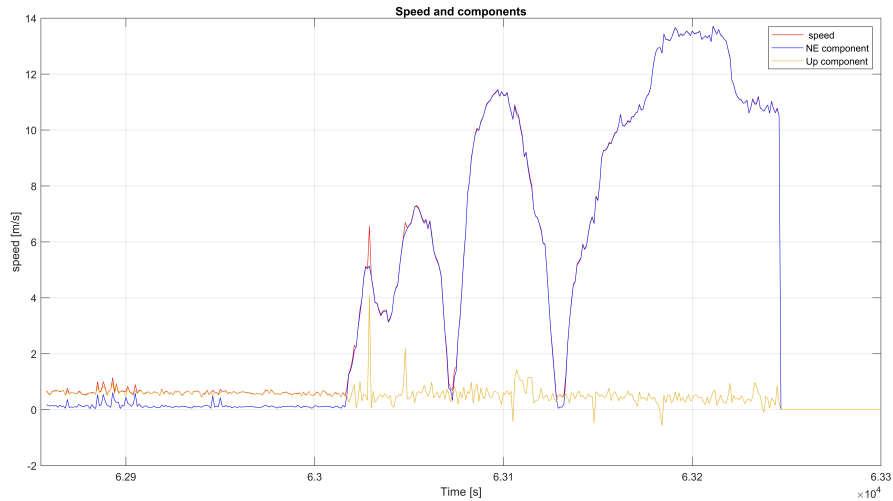


Figure 8.22: Speed norm and its NE and up components in m/s, DOY 313. N.B. This plot has been done with raw data, hence it contains also the very initial part of the test's data, in which the car was stationary.

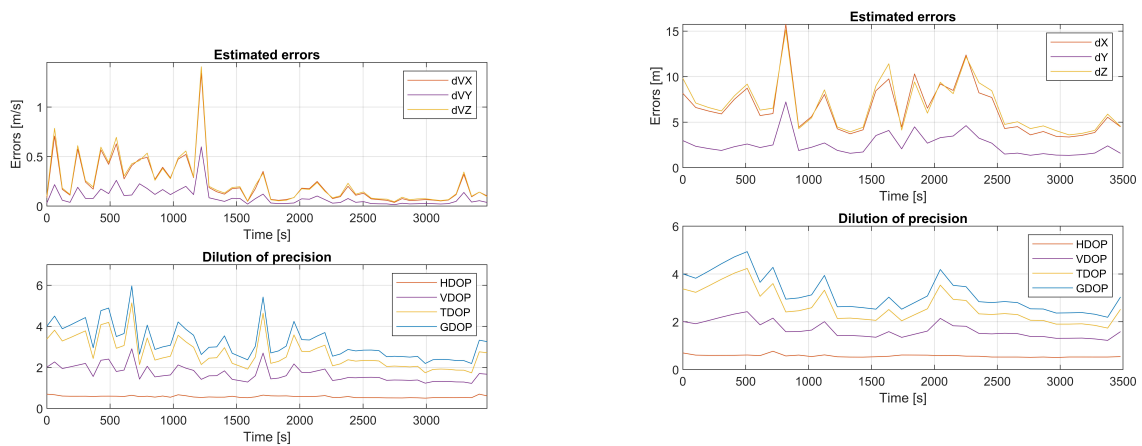


Figure 8.23: Estimated uncertainties on velocity and DOPs, DOY 313.

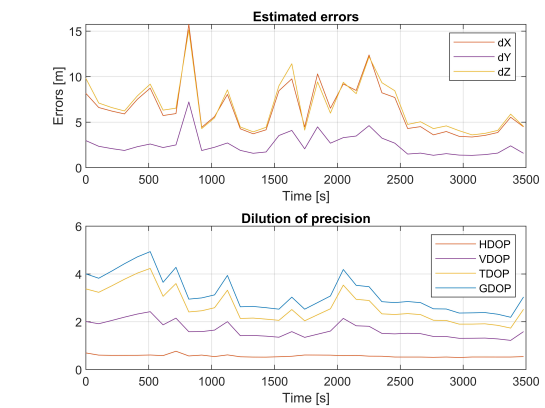


Figure 8.24: Estimated uncertainties on position and Dilutions of precisions, DOY 313.

During the test, the car passed near buildings, trees and streets, therefore the sky was quite covered, for this reason the DOPs are high; the part of the circuit done on foot was in a more free space, with no obstacle, across a cultivated field, in fact, the in last part of the plot, the DOPs are lower.

Chapter 9

PNT LEO satellite

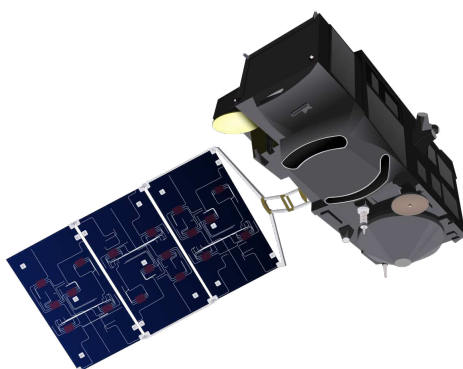


Figure 9.1: Sentinel 3A spacecraft.

In this Chapter the results obtained from the PNT of the Sentinel 3A are presented.

The modified versions of multiGNSS_v3 suite (described in Section 7.1.2) were used to retrace the orbital design. After that, a Google Earth rendering was plotted to verify the orbital shape and keplerian parameters were computed, writing a new code GoogleEarth-Coord.m.

The results obtained were consistent with the orbital design described in ESA website, but some deviations and fluctuations from these mean values were detected. Most of these fluctuations have a frequency equal to half the orbital period, hence a spectral analysis was done to prove that they are due to J_2 gravitational perturbation.

9.1 PNT and rendering

The RINEX data necessary for this PNT analysis were downloaded from the ESA data Hub (<https://scihub.copernicus.eu/gnss/#/home>). The data were collected on 22 November 2021, from the on board spaceborn receiver. It is capable of receiving the L1 C/A, L1P(Y) and the L2P(Y) signals of the GPS constellation, in RINEX version 3.03.

From these RINEX files, only pseudorange data were available, hence the speed determination with pseudodoppler analysis wasn't possible.

The multiGNSS_v3LEO has been executed using a sampling rate of 1 second, selecting the single frequency mode and with a relaxed check on profit residuals.



Figure 9.2: Sentinel 3A receiver.



Figure 9.3: Sentinel 3A antenna.

To get the keplerian parameters from the ECEF coordinates, expressed in terms of latitude, longitude and height, the code `GoogleEarthCoord.m` was written. Firstly, it reads the file `coordDOY0.log` to get the user's position, then it transforms them from the lla ECEF system (latitude, longitude, altitude) to the xyz ECEF system and computes the user's speed using gradient MATLAB function for **central differences**.

Then, it filters this data thanks to **moving average smoothing tool** of MATLAB. This tool (function `smooth.m`) uses a simple moving average with overlap and the span (number of data points for calculating the smoothed value) can be selected, in this case a span equal to 40 is used. This passage was essential to get processable signals in time.

The data in ECEF system of reference must be transformed in ECI system of reference, to obtain the Google Earth rendering and to get keplerian parameters. Hence a function `ECEFtoECI` (found in MATLAB central file exchange, and modified for this thesis purposes [22]) was used to do this; this function in input request the Julian date, the ECEF xyz vectors and the ECEF coordinates speed. At this point, the rendering is possible (using the function `cart2sph.m` to get (lat, lon, hgt) from $(x_{ECI}, y_{ECI}, z_{ECI})$) thanks to the function `kmlwrite.m` of MATLAB, which permits the conversion of a vector of coordinates to the file format Keyhole Markup Language (KML) of Google Earth. The results are shown in Fig. 9.4 and in Fig. 9.5.

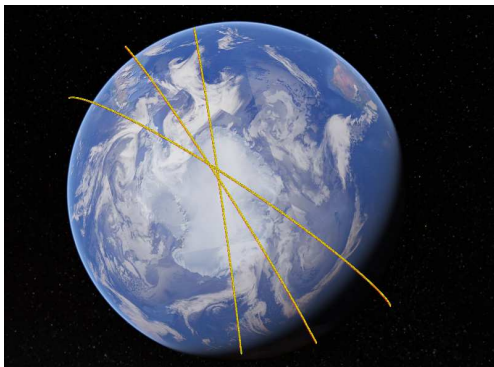


Figure 9.4: Sentinel 3A rendering, with ECEF coordinates.

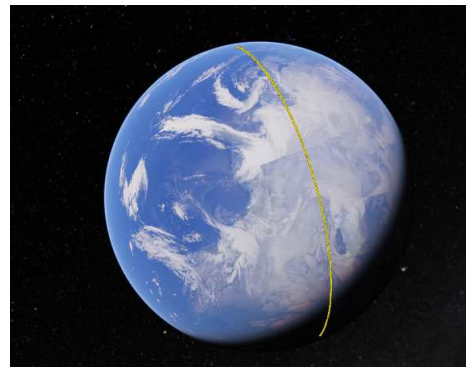


Figure 9.5: Sentinel 3A, rendering with ECI coordinates.

The results obtained have been given in input also to the software GMAT (General

Mission Analysis Tool), an open-source software developed by NASA and private industry for the orbital and general mission analysis, to verify again the orbit shape, the rendering obtained is in Fig. 9.6.

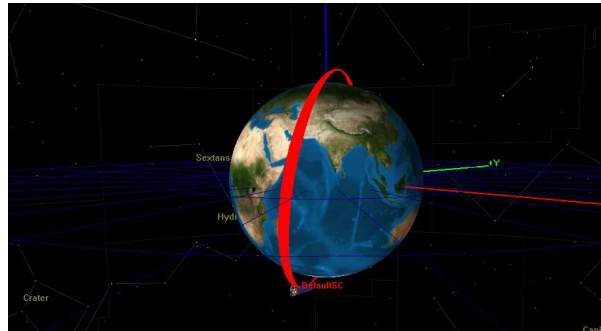


Figure 9.6: GMAT Sentinel 3A orbit rendering

This software also permits the groundtrack rendering as in Fig. 9.7.

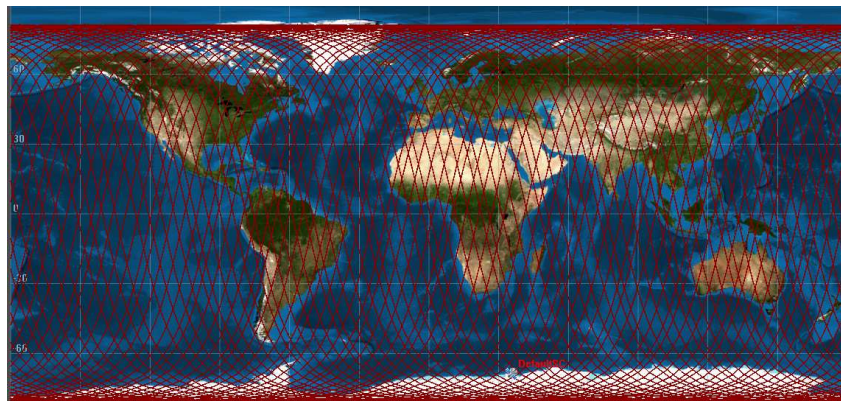


Figure 9.7: GMAT Sentinel 3A groundtrack

Finally, to get the keplerian parameters from $x_{ECI}, y_{ECI}, z_{ECI}$, another function has been written: `kepl_param.m`, it computes all the six keplerian parameters with the formulas 9.1.

$$\begin{aligned}
r &= \sqrt{\mathbf{r}_{\text{ECI}} \cdot \mathbf{r}_{\text{ECI}}} \\
v &= \sqrt{\mathbf{v}_{\text{ECI}} \cdot \mathbf{v}_{\text{ECI}}} \\
\mathbf{h} &= \mathbf{r}_{\text{ECI}} \times \mathbf{v}_{\text{ECI}} \\
h &= \sqrt{\mathbf{h} \cdot \mathbf{h}} \\
i &= \arccos\left(\frac{h_z}{h}\right) \\
\mathbf{n} &= \hat{\mathbf{k}} \times \mathbf{h}, \text{ where } \hat{\mathbf{k}} \text{ is the ECEF versor, aligned with the Earth's spin axis} \\
n &= \sqrt{\mathbf{n} \cdot \mathbf{n}} \\
\Omega &= \begin{cases} \arccos\left(\frac{n_x}{n}\right) & \text{for } n_y \geq 0 \\ 360^\circ - \arccos\left(\frac{n_x}{n}\right) & \text{for } n_y < 0 \end{cases} \\
\mathbf{e} &= \frac{1}{\mu} \left[\mathbf{v}_{\text{ECI}} \times \mathbf{h} - \mu \frac{\mathbf{r}_{\text{ECI}}}{\mathbf{r}} \right] \\
e &= \sqrt{\mathbf{e} \cdot \mathbf{e}} \\
\omega &= \begin{cases} \arccos\left(\frac{\mathbf{n} \cdot \mathbf{e}}{n \cdot e}\right) & \text{for } e_z \geq 0 \\ 360^\circ - \arccos\left(\frac{\mathbf{n} \cdot \mathbf{e}}{n \cdot e}\right) & \text{for } e_z < 0 \end{cases} \\
\theta &= \begin{cases} \arccos\left(\frac{\mathbf{e} \cdot \mathbf{r}_{\text{ECI}}}{e \cdot r}\right) & \text{for } \mathbf{r}_{\text{ECI}} \cdot \mathbf{v}_{\text{ECI}} \geq 0 \\ 360^\circ - \arccos\left(\frac{\mathbf{e} \cdot \mathbf{r}_{\text{ECI}}}{e \cdot r}\right) & \text{for } \mathbf{r}_{\text{ECI}} \cdot \mathbf{v}_{\text{ECI}} < 0 \end{cases}
\end{aligned} \tag{9.1}$$

[23] [24]

The results obtained are listed in Table 9.1; the little differences between the mean values found with the computation and the ESA website ones, are due to orbit variations between the beginning of life orbit and the actual orbit (data used in this work 22 November 2021, ESA data 17 February 2016, a day after the launch).

	Semi Major axis [km]	Inclination [°]	Eccentricity	RAAN [°/s]
ESA website	7185.5	98.65	0.0003	$1.14 \cdot 10^{-5}$
Obtained data	7175.1	98.62	0.002	$1.15 \cdot 10^{-5}$

Table 9.1: Table of keplerian parameters obtained in the analysis versus the actual ones present in ESA website. [25]

As expressed in the following paragraph (figures 9.10, 9.11, 9.12, 9.14 and 9.16), the time plots of keplerian parameters show that all of them oscillate harmonically with a period of ≈ 50 minutes (half of the orbital period) and some of them (the RAAN and the inclination) have a linear trend.

Therefore to investigate this phenomenon, a spectral analysis has been done, in particular to prove that these oscillations in time are due to gravitational perturbation, such as J_2 .

9.2 Perturbation analysis

In this Section a brief description of the Earth gravitational potential theory is done in order to introduce the orbital perturbation of J_2 and explain the variations of keplerian parameters.

Perturbation theory

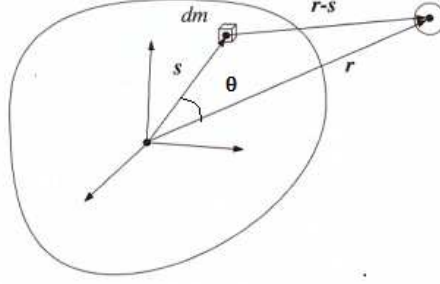


Figure 9.8: Earth potential computation.

The Earth gravitational potential U can be expressed as:

$$U = G \cdot \int_{Volume} \frac{\rho(s)}{|\mathbf{r} - \mathbf{s}|} ds^3 \quad (9.2)$$

where ρ is the density, G is the universal gravitational constant ($G = -6.67 \cdot 10^{11} \frac{N \cdot m^2}{kg^2}$), r is the distance from the infinitesimal volume of the Earth and s is the distance of it from the Earth's center (see Fig. 9.8).

The common approach for modeling the gravitational field of a planetary body is through the spherical harmonic representation:

$$U = \frac{\mu}{r} \sum_{l=0}^{\infty} \left(\frac{a_e}{r}\right)^l \sum_{m=0}^l P_{l,m}(\sin \phi) [C_{l,m} \cos m\lambda + S_{l,m} \sin m\lambda] \quad (9.3)$$

where μ is $G \cdot M_{Earth}$; a_e is the semi major axis of the Earth's reference ellipsoid; (r, ϕ, λ) are the satellite distance, latitude and longitude, respectively in a body-fixed coordinate system; $C_{l,m}$, $S_{l,m}$ are spherical harmonic coefficients of degree l and order m and $P_{l,m}$ are the *Associated Legendre Functions* of degree l and order m .

This representation of the geopotential can be thought of as the sum of three parts:

$$U = U_0 + U_1 + U_2 \quad (9.4)$$

The first part is simply the leading term of the expansion corresponding to the degree and order zero term. The *Associated Legendre Function* $P_{0,0}$ has a value of one, as the $C_{0,0}$ coefficient. This, the leading term is simply:

$$U_0 = \frac{\mu}{r} \quad (9.5)$$

This is the familiar potential resulting from treating the body as point mass.

The second part of the spherical harmonic representation are those terms which do not have a longitude dependence. These corresponds to $m = 0$ and are denoted as the *zonal contribution* to the potential:

$$U_1 = \frac{\mu}{r} \sum_{l=1}^{\infty} \left(\frac{a_e}{r}\right)^l P_{l,0}(\sin \phi) C_{l,0} \quad (9.6)$$

The degree 2 zonal term models the contribution due to the planetary oblateness (the well known J_2 term) and it is the second largest contributor to the overall potential, following the central body contribution. (The degree 1 term is zero assuming that the center of the Earth-fixed coordinate system coincides with the center of mass of the Earth). The notation J_l is often used for the zonal coefficients instead of the above $C_{l,0}$. The two notations simply differ in sign:

$$J_l = -C_{l,0} \quad (9.7)$$

so that the zonal part of the potential could also be written in the form:

$$U_1 = -\frac{\mu}{r} \sum_{l=1}^{\infty} \left(\frac{a_e}{r}\right)^l P_{l,0}(\sin \phi) J_l \quad (9.8)$$

The remaining part of the spherical harmonic representation is that part depending on longitude:

$$U_2 = \frac{\mu}{r} \sum_{l=0}^{\infty} \left(\frac{a_e}{r}\right)^l \sum_{m=0}^l P_{l,m}(\sin \phi) [C_{l,m} \cos m\lambda + S_{l,m} \sin m\lambda] \quad (9.9)$$

The largest longitudinal contributor to the potential is usually the degree 2 and order 2 terms. These terms represent the amount that the planet is “out of round” about the equator. (As with the degree zonal coefficient, the degree 1 and order 1 coefficients will be zero under the assumption that the center of the coordinate system coincides with the center of mass). Therefore, the spherical harmonic representation of the potential, eq. 9.3, can be written as:

$$\begin{aligned} U &= \frac{\mu}{r} \\ &- \frac{\mu}{r} \sum_{l=1}^{\infty} \left(\frac{a_e}{r}\right)^l P_{l,0}(\sin \phi) J_l \\ &+ \frac{\mu}{r} \sum_{l=0}^{\infty} \left(\frac{a_e}{r}\right)^l \sum_{m=0}^l P_{l,m}(\sin \phi) [C_{l,m} \cos m\lambda + S_{l,m} \sin m\lambda] \end{aligned} \quad (9.10)$$

[26]

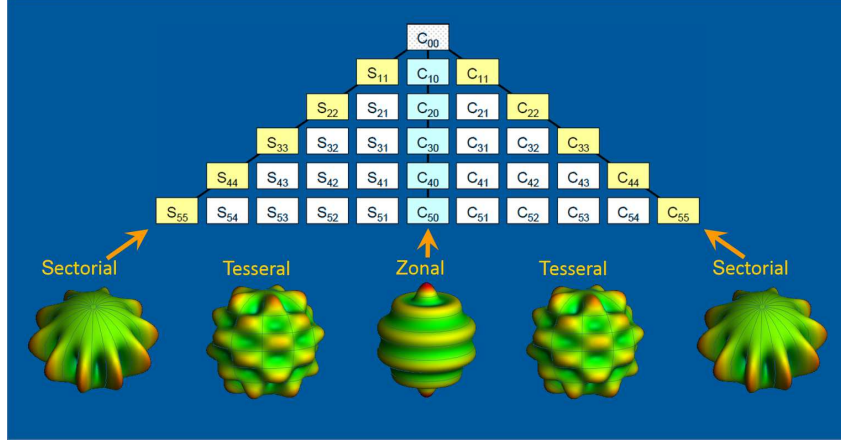


Figure 9.9: Earth gravitational harmonics and their coefficients.

These $J_{l,m}$, $C_{l,m}$ and $S_{l,m}$ follow the so called *Kaula's rule*, which says that the coefficients of expansion over spherical harmonics for the fluctuations of the gravitational field decrease as the number of the harmonic squared: $\frac{K}{l^2}$, where K depends on the planet (for the Earth $K = 10^{-5}$) and l is the order of the coefficient.

For this reason, the J_2 term is higher by 3 orders of magnitude with respect to J_3 , hence its influence is bigger. Therefore the expression of the potential U becomes:

$$U = \frac{GM}{r} - \frac{3\mu}{2r} J_2 \left(\frac{R_E}{r} \right)^2 \left(\sin^2 \phi - \frac{1}{3} \right) \quad (9.11)$$

where ϕ is the latitude, measured by the equator; writing $\sin \phi = \sin i \sin(\omega + \theta)$ (orbital relation), it is possible to express the perturbation part, now called R_2 , as:

$$\begin{aligned} R_2 &= -\frac{3\mu}{2r} J_2 \left(\frac{R_E}{r} \right)^2 \left[\sin^2 i \sin^2(\omega + \theta) - \frac{1}{3} \right] \\ R_2 &= -\frac{3\mu}{2r} J_2 \left(\frac{R_E}{r} \right)^2 \left[\frac{1}{2} \sin^2 i - \frac{1}{2} \cos 2(\omega + \theta) - \frac{1}{3} \right] \end{aligned} \quad (9.12)$$

where the $\sin^2(\omega + \theta)$ is written as $\frac{1 - \cos 2(\omega + \theta)}{2}$, thanks to bisection formulas. The second expression can be divided in two parts:

1. the secular variation: $R_{2,sec} = -\frac{3\mu}{2r} J_2 \left(\frac{R_E}{r} \right)^2 \left[\frac{1}{2} \sin^2 i - \frac{1}{3} \right]$
2. the periodic variation: $R_{2,per} = \frac{3\mu}{2r} J_2 \left(\frac{R_E}{r} \right)^2 \left[\frac{1}{2} \cos 2(\omega + \theta) \right]$

The periodic variation of the R_2 potential is proportional to $\cos 2(\omega + \theta)$; $\omega + \theta$ is the position of the satellite with respect to the line of ascending mode, because of that 2 factor, the period of this oscillation is *half of the orbital one*.

The term μ can be expressed by $\mu = n^2 a^3$ and the average on a orbit of $(a/r)^3$ is $(a/r)^3 = (1 - e^2)^{-3/2}$, hence the first equation can be rewritten as

$$\begin{aligned} R_{2,avg} &= -\frac{3}{2} n^2 R_E^2 J_2 \left(\frac{a}{r} \right)^3 \left[\frac{1}{2} \sin^2 i - \frac{1}{3} \right] = \\ R_{2,avg} &= -\frac{3}{2} n^2 R_E^2 J_2 \frac{1}{(1 - e^2)^{3/2}} \left[\frac{1}{2} \sin^2 i - \frac{1}{3} \right] \end{aligned} \quad (9.13)$$

From 9.13 it is possible to obtain the $\dot{\Omega}$, the right ascension ascending node rate of change in time due to J_2 perturbation, using the Lagrange's planetary perturbation equations for $\partial\Omega/\partial t$:

$$\begin{aligned}\frac{\partial\Omega}{\partial t} &= \frac{1}{n \cdot a^2 \sin i \sqrt{1-e^2}} \frac{\partial R_{2,avg}}{\partial i} \\ \frac{\partial\Omega}{\partial t} &= -\frac{3}{2} n J_2 \left[\frac{R_E}{a(1-e^2)} \right]^2 \cos i\end{aligned}\quad (9.14)$$

This last expression permits the computation of $\dot{\Omega}$ that for a sun synchronous orbit (as the Sentinel 3A) is equal to:

$$\dot{\Omega} = 1.991 \cdot 10^{-7} rad/s = 1.141 \cdot 10^{-5} deg/s \quad (9.15)$$

[17] [27]

Obtained results

To confirm what was said in the previous paragraphs, a spectral analysis on the semimajor axis, inclination and RAAN time variations has been done. First of all, the linear trend of the inclination and RAAN must be found to be removed before the Fourier transform process and to assess their cause.

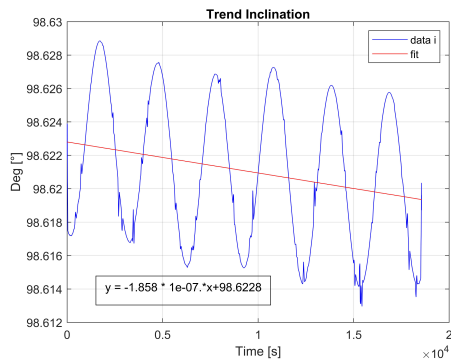


Figure 9.10: Trend inclination.

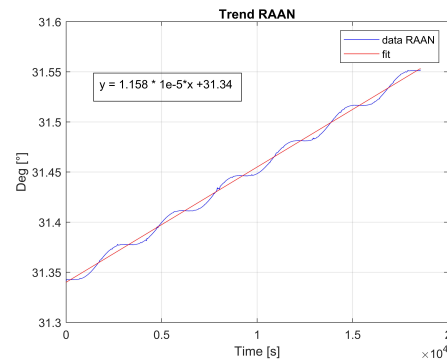


Figure 9.11: Trend RAAN

As Fig. 9.11 shows, the RAAN linear trend is:

$$RAAN(t) = 1.15 \cdot 10^{-5} \cdot t + 31.34deg \quad (9.16)$$

that is what was expected, from the previous discussion, because this orbit is sun synchronous (see 9.15). The time $t = 0s$ at the midnight of DOY 326.

While the inclination trend is:

$$i(t) = -1.858 \cdot 10^{-7} \cdot t + 98.6228deg \quad (9.17)$$

This secular variation of the inclination is not due to Earth gravitational potential, but to Moon and Sun third body effect.

After the trend analysis, the signals in time were reconstructed (in time domain) using the Taylor series expansions and compared with the filtered ones (as shown in Fig. 9.12, 9.14 and 9.16). The frequency used in reconstructed signals is the one expected from the theory: $f_0 = (\frac{T_{orb}}{2})^{-1} = 0.00033Hz$, with $T_{orb} = 100.97min = 6058.2s$.

After removing the trends and the mean from the signals, the fft has been done (using MATLAB tool `fft.m`) and the signals power has been computed.

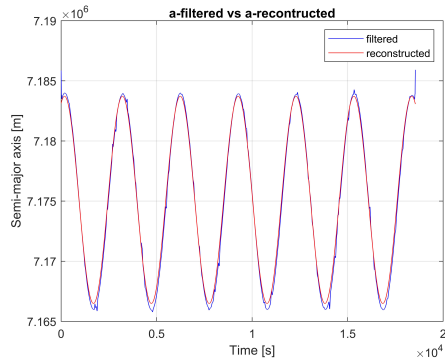


Figure 9.12: Semimajor axis time plot.

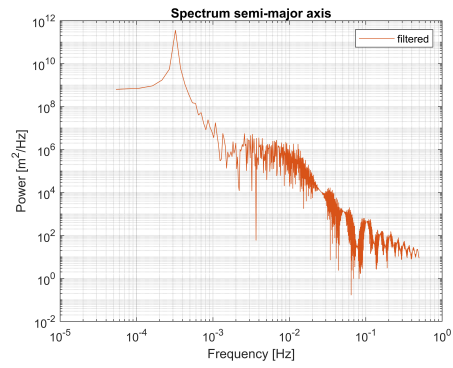


Figure 9.13: Spectrum semimajor axis

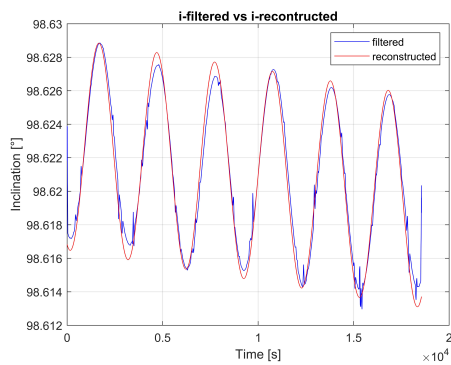


Figure 9.14: Inclination time plot.

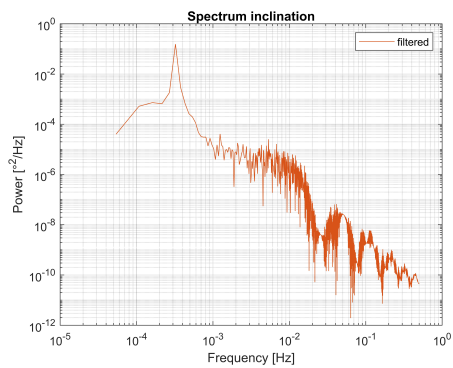


Figure 9.15: Spectrum inclination

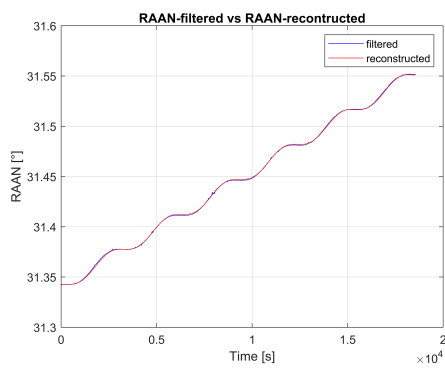


Figure 9.16: RAAN time plot.

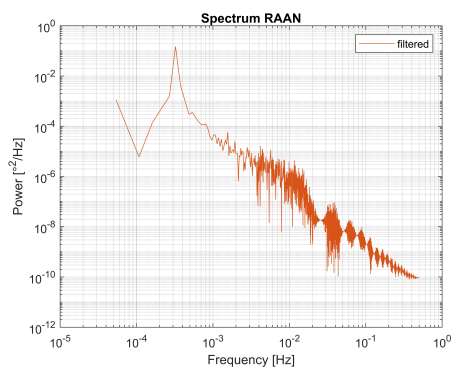


Figure 9.17: Spectrum RAAN

Then the signal power has been plotted on a double logarithmic graph, the results are shown in Fig 9.13, 9.15 and 9.17. The peak of the power is $\approx 0.00032Hz$ for all the spectra, hence very near to the expected one.

Chapter 10

Conclusion

The main aim of this thesis has been successfully achieved: the speed determination with pseudodoppler measures from multi-constellation data has been done reaching a good precision for every experimental campaign, both static and dynamic. The accuracy found is on the order of $\approx \mathbf{cm/s}$, when the receiver is static, and $\approx \mathbf{dm/s}$, when the receiver moves, which is really good result for a PVT done using code observations and Doppler shift (to get a better precision the Precise Point Positioning with phase measures and precise clock errors estimation must be implemented).

The existing positioning code has been studied and modified for this thesis purposes, using different data from a commercial receiver; the accuracy in this case is not as good as the speed, because the pseudoranges are more noisy and affected by atmosphere influences; the accuracy found is:

- STONEX SC2200 receiver (for professional use) $\approx \mathbf{1-2m}$ (depending on the DOPs);
- STONEX S580 receiver (for commercial use) $\approx \mathbf{5-10m}$ (depending on the DOPs).

Finally, the software for the PNT was tested with data from the spaceborne receiver of Sentinel 3A, from Copernicus constellation. The spacecraft was tracked and the **orbital design** was computed with a good precision, highlighting the orbital **perturbations's effects**.

The algorithms produced, as well as the physical technologies behind them, can be easily deployed for the common use, in devices and applications that can be created for the benefit of many businesses. The work done will be a useful starting point for many practical implementations in many scientific and manufacturing sectors.

Chapter 11

Misura della posizione, velocità e sincronismo con costellazioni GPS, Galileo, GLONASS e BeiDou

11.1 Introduzione

Il presente lavoro si propone di illustrare la teoria, il metodo e le modalità del calcolo della **PVT**, ovvero della posizione, della velocità e del sincronismo temporale, di un utente sulla Terra o di un satellite in orbita bassa (dotato di ricevitore multiGNSS), utilizzando un software integrato che sfrutti tutti i segnali provenienti da tutte le costellazioni a copertura globale in quel momento visibili. Nel caso presente si sono utilizzati i segnali da GPS, Galileo, GLONASS e BeiDou, rilevati grazie ad un ricevitore fornito dall'Università di Padova (STONEX S580), sia per la determinazione della posizione, sia per implementare il calcolo della velocità attraverso l'effetto Doppler.

Questo lavoro, in futuro, potrebbe portare a contributi nello sviluppo di tecnologie innovative in molti settori, quali: navigazione autonoma e trasporti, difesa e aerospazio, agricoltura e molti altri.

Per centinaia di anni la determinazione della posizione di un punto sulla superficie terrestre, è stata realizzata tramite misure di distanza da oggetti lontani: specchi riflettenti sulle cime delle montagne resero possibile l'uso di razzi ad alta quota; l'osservazione della sfera celeste, in particolare del Sole, delle stelle e pianeti, agevolò le prime navigazioni marittime e non solo. Tuttavia, è solo dall'avvento dell'Era Spaziale che si può cominciare a parlare di sistemi globali accurati per il posizionamento e per la navigazione. Questi sistemi vengono detti *space-based* e furono ideati tra gli anni Cinquanta e Sessanta.

Il primo sistema di posizionamento satellitare globale fu Transit, il quale si basava su misure di *Doppler shift* di un segnale radio; esso fu dismesso nel 1996, con l'inaugurazione del sistema GPS e delle sue più elevate prestazioni.

11.2 Principi di posizionamento multiGNSS

Il concetto di base che rende possibile il posizionamento satellitare è quello della *multi-laterazione* (si veda Fig. 11.1 e Fig. 11.2): dal momento che i segnali radio satellitari

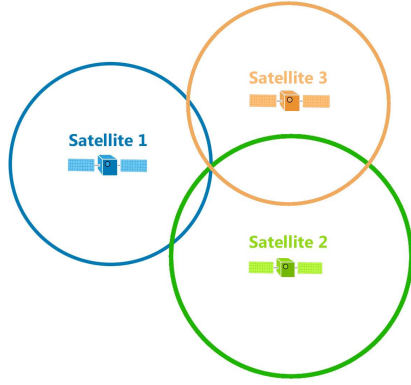


Figure 11.1: Posizionamento in due dimensioni.



Figure 11.2: Posizionamento in tre dimensioni.

viaggiano alla velocità della luce, è possibile ricavare la distanza tra l'utente sulla Terra e il satellite che trasmette il segnale come $p_i = \Delta t \cdot c$, ove p_i è detto *pseudorange* (ovvero pseudodistanza), poichè al suo interno contiene una serie di contributi; esso viene modellato come segue:

$$p_r^s = \rho_r^s + c(dt_r - dt^s + \delta t^{rel}) + I_r^s + T_r^s + \xi_r^s + c(d^s - d_r) + e_r^s \quad (11.1)$$

ove ρ_r^s è la distanza geometrica (da correggere con la rotazione terrestre ω_E); $c(dt_r - dt^s + \delta t^{rel})$ sono tutti gli errori temporali, che comprendono: errori di sincronizzazione degli orologi a bordo dei satelliti e interni al ricevitore e contributi della relatività ristretta e generale; I_r^s è l'errore dovuto al ritardo ionosferico (la ionosfera come mezzo carico elettricamente produce un ritardo nei segnali elettromagnetici che vi transitano) e T_r^s è il ritardo troposferico (la troposfera è l'ultima zona dell'atmosfera ed è caratterizzata da contenuti variabili di vapore acqueo, da variabili condizioni meteorologiche e variabili composizioni chimiche e fisiche); ξ_r^s è lo sfasamento del centro di fase dell'antenna; $c(d^s - d_r)$ sono i ritardi strumentali satellitari e del ricevitore e e_r^s è il contributo del *multipath* (ovvero riflessione multipla del segnale) e del rumore interno del ricevitore.

Con almeno 4 di queste misure di pseudo-distanza, si possono ricavare la posizione dell'utente (x_r, y_r, z_r) e il *clock bias* del ricevitore (ovvero la deviazione dell'orologio del ricevitore rispetto al tempo GPS); questo si può fare tramite un algoritmo ai minimi quadrati (*least squares algorithm*) che permette di trovare la posizione in termini di (x_r, y_r, z_r) che minimizza la somma degli scarti quadratici, in poche iterazioni.

Le misure di pseudo-doppler analogamente permettono il calcolo della velocità dell'utente, nota la velocità dei satelliti (ottenuta dalle effemeridi e da modelli orbitali): esse corrispondono allo spostamento in frequenza della portante del segnale satellitare generato dal moto relativo tra utente e satellite.

Esso è definito secondo il modello:

$$\dot{p}^s = (\mathbf{v}^s - \mathbf{v}_r) \cdot \mathbf{I}_{los} + \dot{dt}_r + \dot{\epsilon} \quad (11.2)$$

dove $(\mathbf{v}^s - \mathbf{v}_r) \cdot \mathbf{I}_{los}$ è la velocità relativa tra satellite e ricevitore proiettata lungo la linea di vista; \dot{dt}_r è la derivata del *clock bias* del ricevitore e $\dot{\epsilon}$ è l'errore composito più il rumore della misura. Si può dimostrare che la 11.2 è la derivata della 11.1.

Avendo dati da più costellazioni, si possono stimare diversi parametri ed ottenere la posizione dell'utente con maggiore precisione; il software opera una cosiddetta **PVTZ** multi-costellazione, ovvero avendo i dati di pseudo-range e di pseudo-doppler per più costellazioni, si può aumentare il numero delle incognite, calcolando con l'algoritmo del *weighted least squares clock bias* del ricevitore rispetto alle diverse scale dei tempi delle costellazioni e il ritardo troposferico.

Dunque, tramite un software scritto in MATLAB e in PERL (multiGNSS_v3 suite) fornito dall'Università di Padova, il posizionamento di una Stazione fissa (Padova, CISAS) e di un ricevitore commerciale portatile sono stati ottenuti con una precisione accettabile; questo software è stato integrato con un codice per la lettura e il calcolo dei dati di pseudo-doppler ottenendo un'ottima precisione per le velocità. Infine, una versione modificata di multiGNSS_v3 è stata utilizzata per ottenere la posizione e la velocità di un satellite in orbita bassa (Sentinel 3A, della costellazione Copernicus); dai vettori posizione e velocità, (x_s, y_s, z_s) e (v_x, v_y, v_z) , tramite calcoli orbitali, si sono calcolati i parametri kepleriani dell'orbita e sono stati confrontati con quelli presentati nel sito dell'ESA.

11.3 Risultati e conclusioni

Quattro campagne sperimentali sono state effettuate, due statiche (ovvero con il ricevitore fermo) e due dinamiche; vengono presentate le due più significative nelle Fig. 11.3 e Fig. 11.5.



Figure 11.3: Posizione CISAS, Padova, DOY 233.

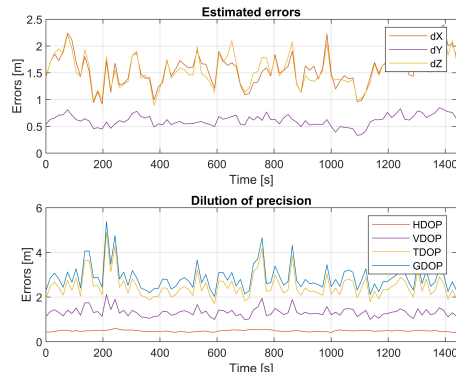


Figure 11.4: Incertezze stimate per il posizionamento e DOP.

La determinazione della velocità con misure pseudodoppler da dati multi-costellazione è stata portata a termine, raggiungendo una buona precisione per ognuna delle campagne sperimentali. La precisione trovata è dell'ordine di $\approx \text{cm/s}$, quando il ricevitore è statico, e $\approx \text{dm/s}$, quando il ricevitore si muove, che è davvero un buon risultato.

Il codice di posizionamento preesistente è stato studiato e modificato per questa tesi, utilizzando dati diversi da un ricevitore commerciale; la precisione in questo caso non è buona quanto la velocità, perché gli *pseudorange* sono più rumorosi e influenzati dall'effetto dell'atmosfera; la precisione riscontrata è:

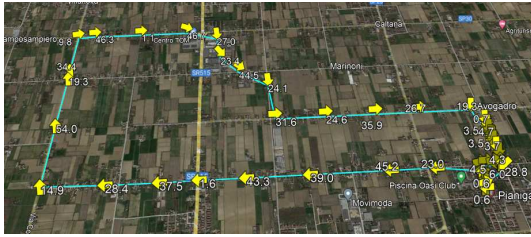


Figure 11.5: Percorso svolto in automobile, Pianiga, DOY 313.

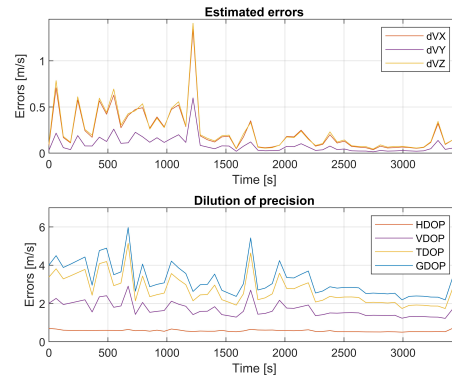


Figure 11.6: Incertezze stimate per la determinazione della velocità e DOP.

- Ricevitore STONEX SC2200 (per uso professionale) \approx **1-2m**(a seconda della disposizione dei satelliti nel cielo);
- Ricevitore STONEX S580 (per uso commerciale) \approx **5-10m** (a seconda della disposizione dei satelliti nel cielo).



Figure 11.7: *Google Earth rendering* dell'orbita ricostruita di Sentinel 3A.

Infine, il software per il posizionamento di un satellite in LEO è stato testato con i dati del ricevitore spaziale di Sentinel 3A, dalla costellazione di Copernicus. Il veicolo spaziale è stato tracciato e il **disegno orbitale** (in Fig. 11.7) è stato calcolato con una buona precisione, evidenziando gli effetti delle **perturbazioni** orbitali.

Chapter 12

List of figures

In this Chapter the figures and their credits are listed, divided by chapter.

Chapter 1:

- Fig. 1.1: Transit 2A; source: NRO Archive, Author: Bruce Carlson;
- Fig. 1.2: Transit's measurement concept; source: JHU/APL;
- Fig. 1.3: GNSS' orbits; source: Presentation of Public ESA Multi-GNSS Products.

Chapter 2:

- Fig. 2.1: GNSS and RNSS overview; source: "Springer Handbook of Global Navigation Satellite Systems "[1]
- Fig. 2.2: SBAS overview; source: "Springer Handbook of Global Navigation Satellite Systems "[1]
- Fig. 2.3: GNSSs' orbital design; source: <https://spacenews.com/modern-civilization-would-be-lost-without-gps/>
- Fig. 2.4: GPS evolution; source: "GPS III: Building on 200 years of On-Orbit PNT Excellence", Mark Stewart, Vice President Navigation Systems, Lockheed Martin
- Fig. 2.5: GPS Control Segment; source: <https://www.gps.gov/systems/gps/control/>
- Fig. 2.6: Baikonur Cosmodrome; source: <https://fineartamerica.com/featured/baikonur-cosmodrome-granger.html>
- Fig. 2.7: GLONASS Ground Segment; source: https://gssc.esa.int/navipedia/index.php/GLONASS_Ground_Segment
- Fig. 2.8: Galileo Ground Segment; source: https://gssc.esa.int/navipedia/index.php/Galileo_Ground_Segment
- Fig. 2.9: Experimental Study on the Precise Orbit Determination of the BeiDou Navigation Satellite System - Scientific Figure on ResearchGate; source: https://www.researchgate.net/figure/Ground-tracks-of-the-BeiDou-satellites-and-distribution-of-the-experimental-tracking_fig1_236080831
- Fig. 2.10: QZSS orbits and ground tracks; source: "Springer Handbook of Global Navigation Satellite Systems" [1]
- Fig. 2.11: QZSS Control Segment; source: Quasi-Zenith Satellite System (QZSS), First Quasi-Zenith Satellite System 'MICHIBIKI' Quasi-Zenith Satellite System Project Team Space Application Mission Directorate Japan Aerospace Exploration Agency;
- Fig. 2.12: IRNSS Ground track; source: K. Rajaiah, K. Manamohan, S. Nirmala, S.C. Ratnakara, "Modified empirical Solar Radiation Pressure model for IRNSS

constellation”

- Fig. 2.13: List of IRNSS satellites; source: <https://www.isro.gov.in/spacecraft/list-of-navigation-satellites>
- Fig. 2.14: Coverage SBAS map; source: https://gssc.esa.int/navipedia/index.php/SBAS_Systems

Chapter 3:

- Fig. 3.1: GPS signal modulation; source: “Springer Handbook of Global Navigation Satellite Systems” [1]
- Fig. 3.2: BPSK chip shape; source: “Springer Handbook of Global Navigation Satellite Systems” [1]
- Fig. 3.3: BOC chip shape; source: “Springer Handbook of Global Navigation Satellite Systems” [1]
- Fig. 3.4: BPSK modulation; source: https://commons.wikimedia.org/wiki/File:Phase_modulation_BPSK_GPS.svg
- Fig. 3.5: Multiple access techniques; source: “Springer Handbook of Global Navigation Satellite Systems” [1]
- Fig. 3.6 and Fig. 3.7: GPS L1 Signal Plan; source: https://gssc.esa.int/navipedia/index.php/GPS_Signal_Plan
- Fig. 3.8 and Fig. 3.9: GPS L2 Signal Plan; source: https://gssc.esa.int/navipedia/index.php/GPS_Signal_Plan
- Fig. 3.10 and Fig. 3.11: GPS L5 Signal Plan; source: https://gssc.esa.int/navipedia/index.php/GPS_Signal_Plan
- Fig. 3.12: GLONASS antipodal satellites strategy; source: https://gssc.esa.int/navipedia/index.php/GLONASS_Signal_Plan
- Fig. 3.13 and Fig. 3.14: GLONASS L1 Signal Plan; source: https://gssc.esa.int/navipedia/index.php/GLONASS_Signal_Plan
- Fig. 3.15 and Fig. 3.16: GLONASS L2 Signal Plan; source: https://gssc.esa.int/navipedia/index.php/GLONASS_Signal_Plan
- Fig. 3.17 and Fig. 3.18: Galileo E1 Signal Plan; source: https://gssc.esa.int/navipedia/index.php/Galileo_Signal_Plan
- Fig. 3.19 and Fig. 3.20: Galileo E6 Signal Plan; source: https://gssc.esa.int/navipedia/index.php/Galileo_Signal_Plan
- Fig. 3.21 and Fig. 3.22: Galileo E5 Signal Plan; source: https://gssc.esa.int/navipedia/index.php/Galileo_Signal_Plan
- Fig. 3.23: BeiDou Signal Plan; source: https://gssc.esa.int/navipedia/index.php/BeiDou_Signal_Plan

Chapter 4:

- Fig. 4.1: Receiver’s architecture scheme; source: “GNSSs, Signals, and Receivers, Mohamed Tamazin and Malek Karaim and Aboelmagd Noureldin” [8]
- Fig. 4.2: Down conversion scheme; source: “GNSSs, Signals, and Receivers, Mohamed Tamazin and Malek Karaim and Aboelmagd Noureldin” [8]
- Fig. 4.3: Acquisition process; source: Acquisition of Weak Signals in Multi-Constellation Frequency Domain Receivers - Scientific Figure on ResearchGate. Available from: https://www.researchgate.net/figure/Recorded-live-GPS-L1-C-A-acquisition-search-grid-for-PRN-14_fig2_263329794
- Fig. 4.4: Correlation process within BaseBand processing; source: GMV for Navipedia

- Fig. 4.5: Correlation process; source: https://gssc.esa.int/navipedia/index.php/GNSS_Basic_Observables
- Fig. 4.6: RINEX Obs 3.04; source: STONEX S580 receiver

Chapter 5:

- Fig. 11.1 and Fig. 11.2: Bidimensional and Tridimensional multilateration; source: <https://gisgeography.com/trilateration-triangulation-gps/>
- Fig. 5.3: GPS signal modulation; source: Professor E. Lorenzini's slides [17]
- Fig. 5.4: Different time references; source: Precise time scales and navigation systems: mutual benefits of timekeeping and positioning - Satellite Navigation, Authors: Tavella Patrizia and Petit Gérard
- Fig. 5.5: Maser clock; source: https://www.esa.int/ESA_Multimedia/Images/2004/07/Hydrogen_maser_clock
- Fig. 5.6: Sketch of atmospheric delay; source: <https://www.e-education.psu.edu/geog862/node/1719>, GPS for Land Surveyors
- Fig. 5.7: Propagation of a modulated signal; source: "Springer Handbook of Global Navigation Satellite Systems" [1]
- Fig. 5.8: Ionospheric layers; source: <http://sidstation.loudet.org/ionosphere-en.xhtml>
- Fig. 5.9: Sketch of propagation length through ionosphere; source: by the author
- Fig. 5.10: Multipath in a city; source: <https://www.e-education.psu.edu/geog862/node/1721>, GPS for Land Surveyors
- Fig. 5.11: Choke ring antenna; source: GPS Vulnerabilities in the Transportation Sector - Scientific Figure on ResearchGate. Available from: https://www.researchgate.net/figure/1-Choke-Ring-Antenna-Source-Leicacom_fig4_311062249

Chapter 6:

- Fig. 6.1: Least Squares algorithm; source: Professor E. Lorenzini slides [17]
- Fig. 6.2: ECEF and NEU reference systems; source: Posizionamento Satellitare e Determinazione orbitale, Alessandro Caporali [16]
- Fig. 6.3: Kalman filter algorithm; source: by the author

Chapter 7:

- Fig. 7.1 and Fig. 7.2: RINEX observation files before and after decomposition process; source: STONEX S580 receiver
- Fig. 7.4: multiGNSS_v3 suite scheme; source: Software multiGNSS: architettura del sistema e manuale utente, Luca Nicolini [20]
- Fig. 7.5: multiGNSS_v3 scheme, original version; source: by the author
- Fig. 7.6: multiGNSS_v3 scheme, modified version for STONEX data and Doppler reading; source: by the author
- Fig. 7.7: multiGNSS_v3 scheme, modified version for spaceborne receiver data; source: by the author
- Fig. 7.8: multiGNSSvelocity input scheme; source by the author
- Fig. 7.9: multiGNSSvelocity output file; source: multiGNSSvelocity code, by the author

Chapter 8:

- Fig. 8.1: STONEX SC2200 receiver; source: <https://www.stonex.it/project/sc2200-gnss-receiver/>

- Fig. 8.2: CISAS Padua, DOY 233, Google Earth rendering; source: Google Earth rendering, by the author
- Fig. 8.3: Estimated uncertainties DOY 233; source: MATLAB plot, by the author
- Fig. 8.4: Receiver clock drift, DOY 233; source: MATLAB plot, by the author
- Fig. 8.5: Tropospheric correction; source: MATLAB plot, by the author
- Fig. 8.6: ECEF speed DOY 233; source: MATLAB plot, by the author
- Fig. 8.7: RMS postfit residuals; source: MATLAB plot, by the author
- Fig. 8.8 STONEX S580 receiver, source: <https://www.stonex.it/it/project/s580-ricevitore-gnss/>
- Fig. 8.9: Pianiga (VE), DOY 328, Google Earth rendering; source: Google Earth rendering, by the author
- Fig. 8.10: Skyplot DOY 328, Pianiga; source: STONEX S580 receiver
- Fig. 8.11: Position given by SONEX S580; source: STONEX S580 receiver
- Fig. 8.12: Estimated uncertainties and DOP, DOY 328; source: MATLAB plot, by the author
- Fig. 8.13: RMS postfit residuals, DOY 328; source: MATLAB plot, by the author
- Fig. 8.14: Speed components in ECEF, DOY 328; source: MATLAB plot, by the author
- Fig. 8.15: Receiver clock drift, DOY 328; source: MATLAB plot, by the author
- Fig. 8.16: Tropospheric correction, DOY 328; source: MATLAB plot, by the author
- Fig. 8.17: Speed norm, DOY 298; source: MATLAB plot, by the author
- Fig. 8.18: Estimated uncertainties on velocity and DOP, DOY 298; source: MATLAB plot, by the author
- Fig. 8.19: Santa Maria di Sala (VE), DOY 298, Google Earth rendering; source: Google Earth rendering, by the author
- Fig. 8.20: Estimated uncertainties on position and DOP, DOY 298; source: MATLAB plot, by the author
- Fig. 11.5: Pianiga (VE), DOY 313, Google Earth rendering; source: Google Earth rendering, by the author
- Fig. 8.22: Speed norm and components, DOY 313; source: MATLAB plot, by the author
- Fig. 8.23: Estimated uncertainties on velocity and DOP, DOY 313; source: MATLAB plot, by the author
- Fig. 8.24: Estimated uncertainties on position and DOP, DOY 313; source: MATLAB plot, by the author

Chapter 9:

- Fig. 9.1: Sentinel 3A spacecraft; source: SkywalkerPL, via Wikimedia Commons <https://creativecommons.org/licenses/by/4.0>
- Fig. 9.2: <https://sentinels.copernicus.eu/web/sentinel/technical-guides/sentinel-3-altimetry/instrument/gnss>
- Fig. 9.3: <https://sentinels.copernicus.eu/web/sentinel/technical-guides/sentinel-3-altimetry/instrument/gnss>
- Fig. 9.4: Google Earth rendering, DOY 326, Sentinel 3A ECEF system of reference; source: Google Earth rendering, by the author
- Fig. 9.5: Google Earth rendering, DOY 326, Sentinel 3A ECI system of reference; source: Google Earth rendering, by the author

- Fig. 9.6: GMAT rendering of Sentinel 3A orbit; source: GMAT, by the author
- Fig. 9.7: GMAT rendering of Sentinel 3A ground track; source: GMAT, by the author
- Fig. 9.8: Earth potential computation; source: Professor E. Lorenzini slides [17]
- Fig. 9.9: Earth gravitational harmonics; source: Ince, Elmas Sinem & Barthelmes, Franz & Reißland, Sven & Elger, Kirsten & Foerste, Christoph & Flechtner, F. & Schuh, H.. (2019). “ICGEM -15 years of successful collection and distribution of global gravitational models, associated services, and future plans”
- Fig. 9.10: Trend Inclination plot; source: MATLAB plot, by the author
- Fig. 9.11: Trend RAAN plot; source: MATLAB plot, by the author
- Fig. 9.12: Semimajor axis time plot; source: MATLAB plot, by the author
- Fig. 9.13: Spectrum semimajor axis; source: MATLAB plot, by the author
- Fig. 9.14: Inclination time plot; source: MATLAB plot, by the author
- Fig. 9.15: Spectrum inclination; source: MATLAB plot, by the author
- Fig. 9.16: RAAN time plot; source: MATLAB plot, by the author
- Fig. 9.17: Spectrum RAAN; source: MATLAB plot, by the author

Chapter 13

Acknowledgements

Un ringraziamento sincero al Professor Alessandro Caporali, relatore di questa tesi, per il suo impegno, la sua pazienza e la sua infinita disponibilità.

Un gigantesco grazie ai miei genitori, Alessandro e Manuela, per avermi supportato (e sopportato) in questi mesi e a mio zio Massimo (alias *SuperMino*) sempre pronto a farsi in quattro e a camminare alla velocità della luce per aiutarmi.

Ringrazio Davide, il mio ragazzo, per avermi portato via dai libri “perché quando è troppo, è troppo...” ed essermi sempre stato vicino nei momenti più difficili di questi due anni di magistrale, di pandemia e di cambiamento con saggi consigli, affetto inesauribile e sconsiderata spensieratezza.

Vorrei ringraziare tutti i miei amici (in particolare Nello, Luigi, Chiara, Laura e Ambra) per avermi ascoltato quando ero in dubbio e in crisi, o semplicemente per avermi fatto scordare le mie ansie e paure per qualche ora.

Infine un ringraziamento al Centro Educativo Karaté Pianiga, ormai una seconda famiglia, e specialmente al Maestro Fiorenzo, per avermi offerto non solo una valvola di sfogo di tutte le frustrazioni della vita, ma anche una finestra su un universo nuovo e completamente diverso dal mio, dal quale ho imparato tantissimo.

I would like to express my gratitude to my thesis supervisor, Professor Alessandro Caporali, for his commitment, his patience and his dedication.

Thanks also to my parents, Alessandro and Manuela, for supporting me in these months and to my uncle Massimo (alias *SuperMino*), my “logistic manager”.

Davide, my boyfriend, deserves endless gratitude for watching me over these difficult two years of pandemic and changings with wise advices and love.

To all my friends (especially Nello, Luigi, Chiara, Laura and Ambra) thank you for listening to my doubts and thanks for distracting me from my anxieties, even for a little while.

Finally, I cannot forget the “Centro Educativo Karate Pianiga”, another family to me, and especially to Sensei Fiorenzo, for offering me the possibility of discovering another universe, completely different from mine, from which I have learnt so much.

References

- [1] P. Teunissen and O. Montenbruck, eds., *Springer Handbook of Global Navigation Satellite Systems*, vol. XXXI. Springer, 2017.
- [2] “How satellite navigation works.” https://www.esa.int/Applications/Navigation/How_satellite_navigation_works. ESA website.
- [3] P. Misra and P. Enge, *Global Positioning System: Signals, Measurements, and Performance*. Ganga-Jamuna Press, Lincoln MA, 2nd edition ed., 2006.
- [4] “Navipedia: The reference for Global Navigation Satellite Systems.” <https://gssc.esa.int/navipedia/index.php>. ESA and GSSC.
- [5] “BeiDou Navigation Satellite System.” <http://en.beidou.gov.cn/>.
- [6] “Department of Space, Indian Space Research Organisation.” <https://www.isro.gov.in/irnss-programme>.
- [7] “Binary Offset carrier modulation, Spirent blogs.” https://www.spirent.com/blogs/2011-05-31_what_is_boc_modulation.
- [8] M. Tamazin, M. Karaim, and A. Noureldin, *GNSSs, Signals, and Receivers*. 2018.
- [9] “Navipedia: RINEX files.” https://gssc.esa.int/navipedia/index.php/Interfaces_and_Protocols.
- [10] R. W. G. International GNSS Service (IGS) and R. T. C. for Maritime Services Special Committee 104 (RTCM-SC104), “Rinex 3.04.igs.rtcn.doc,”
- [11] “Navipedia: Nequick Ionospheric model.” https://gssc.esa.int/navipedia/index.php/NeQuick_Ionospheric_Model.
- [12] “Navipedia: Ionospheric delay.” https://gssc.esa.int/navipedia/index.php/Ionospheric_Delay.
- [13] “Navipedia: Tropospheric delay.” https://gssc.esa.int/navipedia/index.php/Tropospheric_Delay.
- [14] “Navipedia: Fundamental Physics.” https://gssc.esa.int/navipedia/index.php/Fundamental_Physics#cite_note-1.

- [15] A. Dalla Torre and A. Caporali, “An analysis of intersystem biases for multi-gnss positioning,” *Gps Solutions*, vol. 19, no. 2, pp. 297–307, 2015.
- [16] A. Caporali, *Posizionamento satellitare e determinazione orbitale*. Scienza della terra, CLEUP, 2018.
- [17] “E. Lorezini’s slides (course of *Astrodinamica* Università di Padova).” <https://elearning.unipd.it/dii/>. Astrodynamics for Aerospace engineering.
- [18] “Navipedia: Weighted Least Squares.” [https://gssc.esa.int/navipedia/index.php/Weighted_Least_Square_Solution_\(WLS\)](https://gssc.esa.int/navipedia/index.php/Weighted_Least_Square_Solution_(WLS)).
- [19] “GNSS Compare documentation.” https://gnss-compare.readthedocs.io/en/latest/user_manual/implemented_algorithms.html.
- [20] L. Nicolini, “Software multignss: architettura del sistema e manuale utente,”
- [21] “Time to the first fix.” https://en.wikipedia.org/wiki/Time_to_first_fix.
- [22] M. Meysam, “ECEFtoENI function.” <https://www.mathworks.com/matlabcentral/fileexchange/61957-eci2ecef-ecef2eci-transformations>.
- [23] H. Curtis, *Orbital Mechanics: For Engineering Students*. Aerospace Engineering, Elsevier Science, 2015.
- [24] D. Vallado, *Fundamentals of Astrodynamics and Applications*. Space Technology Library, Springer New York, 2007.
- [25] “Sentinel Online, ESA.” <https://sentinels.copernicus.eu/web/sentinel/missions/sentinel-3/satellite-description/orbit>.
- [26] NASA, “Spherical Harmonic Representation of the Gravity Field Potential,”
- [27] V. Chobotov, *Orbital Mechanics*. AIAA education series, American Institute of Aeronautics and Astronautics, 2002.